UNCLASSIFIED

DTIC FILE COPY (2)

AD-A217 827

REPORT DOCUMENTATION PAGE

	1b RESTRICTIVE MARKINGS
	3 DISTRIBUTION/AVAILABILITY OF REPORT Approved for public release: distribution is unlimited
2b DECLASSIFICATION/DOWNGRADING SCHEDULE	
4 PERFORMING ORGANIZATION REPORT NUMBER(S) TELAC 88-14	5 MONITORING ORGANIZATION REPORT NUMBER(S) AFOSR-TR- 89 1321 AFOSR 90-0082
6a NAME OF PERFORMING ORGANIZATION TELAC, Massachusetts Institute of Technology	6b OFFICE SYMBOL (If applicable)
7a NAME OF MONITORING ORGANIZATION AFOSR/NA	
6c ADDRESS (City, State and ZIP Code) M.I.T., Room 33-309 77 Massachusetts Avenue Cambridge, MA 02139	7b ADDRESS (City, State and ZIP Code) Building 410 Bolling Air Force Base Washington, DC 20332-6448
8a NAME OF FUNDING/SPONSORING ORGANIZATION AFOSR/NA	8b OFFICE SYMBOL (If applicable) NA
9 PROCUREMENT INSTRUMENT IDENTIFICATION NUMBER AFOSR-85-0206	
8c ADDRESS (City, State and ZIP Code) Building 410 Bolling Air Force Base Washington, DC 20332-6448	10 SOURCE OF FUNDING NOS

PROGRAM ELEMENT NO	PROJECT NO	TASK NO	WORK UNIT NO
61102F	2302	B2	

11 TITLE (Include Security Classification) (U) Fracture and Longevity of Composite Structures, (CON'T OVER)

12 PERSONAL AUTHOR(S)
Paul A. Lagace

13a TYPE OF REPORT	13b TIME COVERED	14 DATE OF REPORT (Yr., Mo., Day)	15 PAGE COUNT
Final	FROM 8JUN85 TO 31AUG87	1988, June	85

16 SUPPLEMENTARY NOTATION

17 COSATI CODES			18 SUBJECT TERMS (Continue on reverse if necessary and identify by block number)
FIELD	GROUP	SUB GR	Delamination, fracture, longevity, composites, graphite/epoxy

19 ABSTRACT (Continue on reverse if necessary and identify by block number)

The results of several investigations into the fracture and longevity of composite structures are reported. During this year, the work has concentrated on the phenomena of delamination and final failure. Work is reported on the initiation of delamination under tensile and compressive loading. Work on the growth of delamination and the final failure of the specimen under tensile load is also reported.

20 DISTRIBUTION/AVAILABILITY OF ABSTRACT	21 ABSTRACT SECURITY CLASSIFICATION
UNCLASSIFIED/UNLIMITED ☑ SAME AS RPT ☐ DTIC USERS ☐	UNCLASSIFIED

22a NAME OF RESPONSIBLE INDIVIDUAL	22b TELEPHONE NUMBER (Include Area Code)	22c OFFICE SYMBOL
George Haritos, Lt. Col.	202-767-4937 0465	NA

DD FORM 1473, 83 APR EDITION OF 1 JAN 73 IS OBSOLETE UNCLASSIFIED
SECURITY CLASSIFICATION OF THIS PAGE

(CONTINUATION OF BLOCK #11)

(U) "QUADRATIC STRESS CRITERION FOR INITATION OF DELAMINATION"

(U) "AN ELASTIC FOUNDATION MODEL TO PREDICT THE GROWTH OF DELAMINATIONS"

(U) "THE SANDWICH COLUMN AS A COMPRESSIVE CHARACTERIZATION SPECIMEN FOR THIN LAMINATES"

(U) "EFFECTS OF PLY DROPOFFS ON THE TENSILE BEHAVIOR OF GRAPHITE/EPOXY LAMINATES"

TELAC REPORT 88-14

FRACTURE AND LONGEVITY OF COMPOSITE STRUCTURES

Final Report for Period 15 June 1985 - 14 June 1987
Grant No. AFOSR-85-0209

Paul A. Lagace

Technology Laboratory for Advanced Composites
Department of Aeronautics and Astronautics
Massachusetts Institute of Technology
77 Massachusetts Avenue
Cambridge, Massachusetts 02139

JUNE 1988

FOREWORD

This report describes work done at the Technology Laboratory for Advanced Composites (TELAC) of the Department of Aeronautics and Astronautics at the Massachusetts Institute of Technology for the Air Force Office of Scientific Research under grant number AFOSR-85-0206. Lt. Col. George Haritos was the contract monitor.

The work report herein was performed during the period from 15 June 1986 to 14 June 1987. The work represents the efforts of several graduate and undergraduate students under the direction of the faculty in the laboratory and is reported as such.

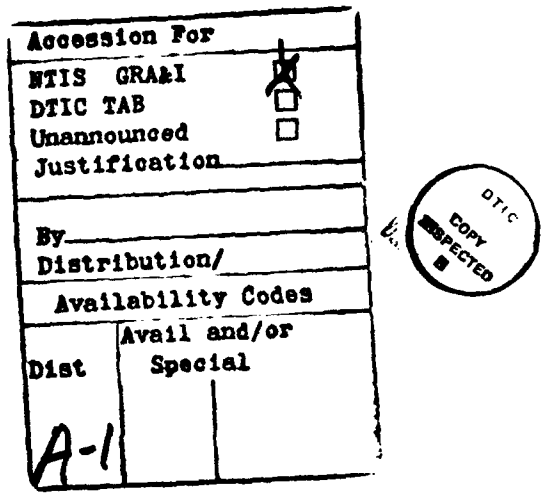

TABLE OF CONTENTS

LIST OF TABLES

1. INTRODUCTION

The Technology Laboratory for Advanced Composites (TELAC) of the Department of Aeronautics and Astronautics at M.I.T. has performed research for several years, with the cooperation and support of the Air Force Office of Scientific Research (AFOSR), on the properties of composite materials and their structures with particular emphasis on the fracture and longevity of such. During the past year covered by this report (June 15, 1986 to June 14, 1987), the students and faculty of TELAC have conducted research in a number of problem areas in a continuing effort to understand the fracture and longevity of composite structures. The work during the past year has concentrated on delamination and resulting final failure. Both graduate and undergraduate students have been involved in this experimental and analytical work with an aim at developing design methodologies for composite structures.

The primary objective of this ongoing research continues to be to gain understanding of the fundamental mechanisms involved in the failure of filamentary composite materials so that the methodologies for predicting fracture and longevity can be developed and enhanced. In addition, via this research, needed data bases can be identified and partially provided. This latter objective does not imply the establishment of the data base within the scope of this effort. Rather, through both analysis and directed experimentation, the critical parameters can be identified and studied in order to gain an understanding of the

fundamental fracture and damage mechanisms of composites so that proper engineering data bases and methodologies can be established.

Delamination plays an important role in the failure of composite structures [e.g. 1]. Interlaminar stresses which arise in gradient fields can trigger the failure of the interply resin layer. It is necessary to study and understand the initiation and growth of delamination and the interaction of this mode with in-plane damage which leads to final failure of the composite piece. Thus, the major objective in this effort is to investigate the phenomena which occur between the initiation of delamination and final failure in order to lay the groundwork to provide a design methodology to bridge an existing technology gap in the design of composite structures. This will include refining techniques to predict the initiation of delamination.

The projects which were completed during the past year under the auspices of this AFOSR grant will be summarized herein. All of the work is fully documented in laboratory reports and/or published papers. These documents have been submitted to AFOSR and may be obtained there or through the laboratory. Therefore, only technical summaries of the major highlights of the work and the findings are presented for the projects herein. Interested personnel may refer to the individual reports for a more thorough description. In addition, a list of all reports generated under this grant during the grant year are listed in Appendix A.

2. BASIC EXPERIMENTAL TECHNIQUES

The general experimental procedures are summarized in this section. Important variations are noted in the individual subsections.

2.1 Specimen Fabrication

The specimens manufactured in this work were constructed using the basic procedures developed at TELAC [2]. The unidirectional and fabric graphite/epoxy used throughout arrive from the manufacturer in rolls of preimpregnated tape or "prepreg". The unidirectional rolls are 305 mm wide and the fabric graphite/epoxy rolls are 990 mm wide. Unless otherwise noted, the materials utilized are Hercules AS4/3501-6 unidirectional tape and A370-5H/3501-6 fabric. The prepreg is stored at or below -18°C.

The prepreg is cut into individual plies and laid up into laminates with the use of razor knives and templates. Rectangular laminates, 305 mm by 350 mm in dimension, are laid up and cured in an autoclave utilizing the manufacturer's recommended cure cycle illustrated in Figure 1. The laminates are postcured in an oven for eight hours at 177°C. Following the postcure, the laminates are cut to the desired final dimensions utilizing a water-cooled diamond grit cutting wheel mounted on a specially outfitted milling machine. Each laminate yields five standard specimens which are illustrated in Figure 2. Glass/epoxy loading tabs manufactured from 3M Scotchply type SP-1002 precured glass/epoxy

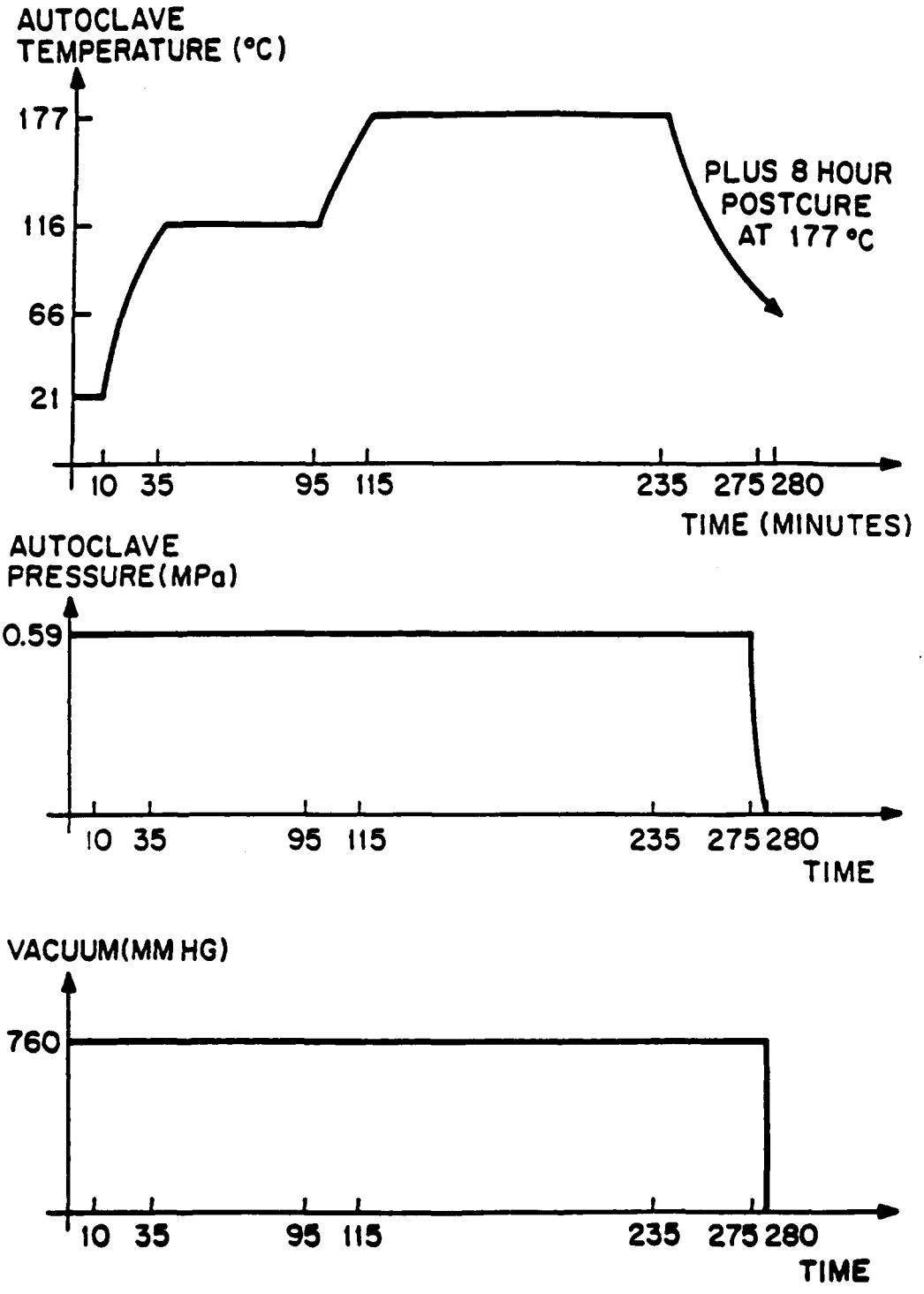

Figure 1 Cure cycle for AS4/3501-6 unidirectional graphite/epoxy and A370-5H/3501-6 woven graphite/epoxy fabric.

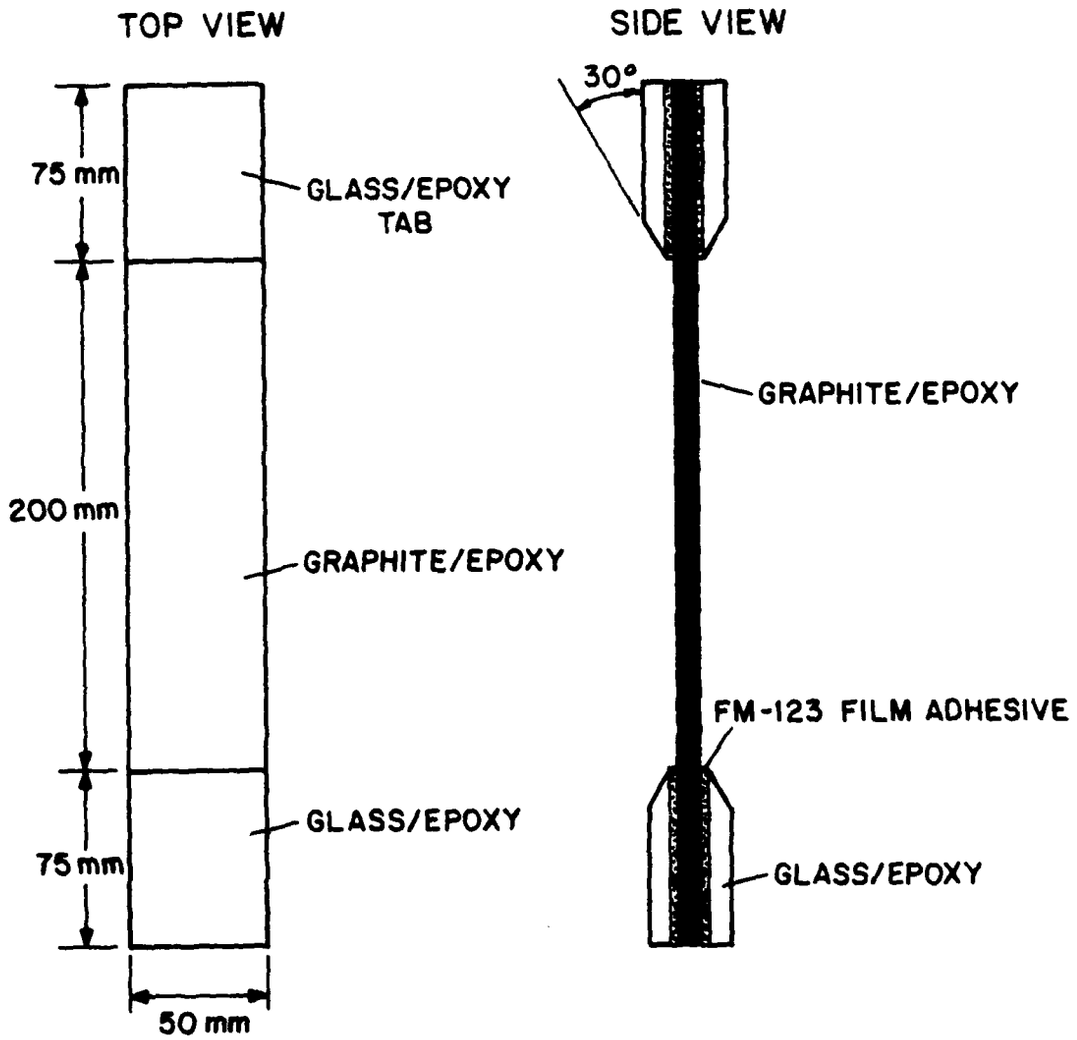

Figure 2 Geometry of standard tensile coupon test specimen.

are applied to the ends of the graphite/epoxy in a secondary bond operation with American Cyanamid FM123-2 film adhesive.

A strain gage is mounted on each specimen to monitor longitudinal strain level during testing. In many of the specimens, the free edges are examined via edge replication. In order to improve the quality of edge replicas, the specimen edges were polished with a 25 mm diameter felt bob soaked in a colloidal solution of Kaopolite SF, a mild abrasive.

All specimens were loaded in an MTS 810 test machine in stroke control with the aid of hydraulic grips. The nominal strain rate in the test section was approximately 5000 microstrain per minute. Load, strain, and stroke data were recorded by a PDP-11/34 computer at a rate of 3 to 6 Hz.

2.2 Detection of Delamination Initiation

In order to detect the initiation of delamination, the load-displacement approach first proposed by O'Brien [3] was used and modified. When delamination initiates, strain continuity is no longer applicable in the delaminated region since the delaminated sublaminates are no longer rigidly bonded. O'Brien suggested that the modulus of this region is the average modulus of the remaining sublaminates weighted by thickness. Energy considerations suggest that this modulus will always be less than the original modulus. When this decrease in modulus is a result of instantaneous delamination in a laminate which is quasistatically loaded under stroke control, the result is an instantaneous drop in load. Hence, a drop in load may be indicative of delamination

initiation. However, even for a moderate amount of delaminated area, the change in modulus of the test section is small. Thus, the point of change in modulus can be difficult to detect in the stress-strain data. In contrast, a drop in load can be pinpointed as long as data are taken with sufficient frequency that the load drop is not obscured by the increase in load resulting from normal specimen loading. A computer program was written for specimen testing which allowed the automatic termination of a test when a drop in load was detected. The ability of the computer to detect a drop in load was dependent on several factors. First, the size of the load drop is a function of the size of the delaminated area. Second, the parameters of the data acquisition system and the strain rate at which the test is conducted are important. And third, the data acquisition time increment must be considered. If the time increment is too short, the inherent noise of the system can be larger than the expected rise in load per time increment. When this occurs, the test can be stopped erroneously. Previous work [12] indicated the necessary values of these parameters. In all cases, it was decided to err on the side of choosing a time increment which is "too short" since it is more desirable to obtain "false positives" than to miss the occurrence of delamination initiation.

For these tests, the testing machine was run under computer control such that data acquisition and load application would start simultaneously. A test was stopped when the detected load at one data point was lower than the value at the previous point.

This apparent load drop was taken as an indication of possible delamination initiation.

Once the test was stopped, the stroke was decreased by a factor of two and two edge replicas taken of each edge of the specimen using the basic method described by Klang and Hyer [5]. The replicas were carefully examined under a microscope at magnifications ranging from 7X to 40X. Backlighting the replicas enhanced the contrast and facilitated identification of features. Replicas were taken of the specimen edges before testing to serve as *initial comparisons*. When a replica showed a delamination that was not in a previous replica, the test was considered to have detected an initiation point. If no such feature was discovered, the specimen was retested. When a specimen was retested, the computer program ignored any perceived load drop which occurred before the specimen reached its previous maximum load since these load drops were artifacts of the procedure and not indicative of delamination initiation.

2.3 Damage Growth Detection

The study of delamination growth and final failure requires that the damage state be nondestructively monitored over a series of tests, The method used for monitoring delamination growth is dye penetrant-enhanced x-radiography. The dye penetrant used is di-iodobutane (DiB). DiB is applied to the free edge of a specimen with a cotton swab while a specimen is at half the maximum stroke level. The DiB has a low viscosity and can seep into delaminated regions via capillary action.

After DiB is applied, the specimen is removed from the testing machine. The location of the DiB can be detected with x-radiography. A Scanray Torrex 150D X-ray Inspection Device was utilized with Polaroid PolaPan instant sheet film type 52.

The resulting X-radiograph essentially shows three shades of gray. The region of the film which is not shielded by any portion of the specimen is for all practical purposes white. The region under the undelaminated section of the laminate is a medium gray. This results from the fact that the specimen absorbs a portion of the X-rays passing through it. Delaminated regions and angle ply splits where the DiB has seeped in show up as dark gray as the DiB absorbs nearly all the X-rays.

3. DELAMINATION INITIATION

The work on delamination initiation is divided into four separate project areas and is reported as such.

3.1 Effect of Interlaminar Normal Stress

Excellent correlation of the delamination initiation stress for the various laminates tested in Reference 4 has been achieved using the Quadratic Delamination Criterion proposed there:

$$\left(\frac{\bar{\sigma}_{1z}}{Z^{s1}}\right)^2 + \left(\frac{\bar{\sigma}_{2z}}{Z^{s2}}\right)^2 + \left(\frac{\bar{\sigma}^{c}_{zz}}{Z^{c}}\right)^2 + \left(\frac{\bar{\sigma}^{t}_{zz}}{Z^{t}}\right)^2 = 1 \qquad (1)$$

where the overbar indicates that the stresses are averaged over a dimension determined from the experimental data, x_{avg}:

$$\bar{\sigma}_{ij} = \frac{1}{x_{avg}} \int_0^{x_{avg}} \sigma_{ij}\, dx \qquad (2)$$

The Z terms are the interlaminar strengths in shear and extension. One averaging dimension gives excellent correlation for all laminates and ply thicknesses, suggesting that the averaging dimension is a material parameter. However, two issues remain with regard to the use of this criterion for general prediction of delamination initiation. The criterion was tested only on laminates in which delamination initiation was controlled primarily by the interlaminar shear stress, σ_{1z}, and the contributions of thermally-induced interlaminar stresses were relatively small. The average value of the other interlaminar

shear stress σ_{2z}, will normally be negligible in these cases since it is required by the boundary conditions to be zero both in the laminate interior and at the free edge. However, there are laminates in which the interlaminar normal stress, σ_{zz}, can be important. The Quadratic Delamination Criterion can be further verified by isolating the effects of the interlaminar normal stress as well as by choosing laminates with large contributions of interlaminar stresses induced in manufacturing due to thermal considerations.

Kassapoglou and Lagace [6] have shown that in uniaxially loaded specimens, σ_{1z} is mainly a function of the in-plane shear stress σ_{12}. In cases where the in-plane shear stress is zero throughout the laminate, the σ_{1z} component will be identically zero [7]. Only if all the plies have extensional-shear coupling terms equal to zero can the in-plane shear stress be avoided. The only plies of orthotropic fibrous materials with this behavior are those with angular orientations of the fibers of 0° and 90° to the longitudinal axis. A cross-ply laminate could therefore potentially have significant σ_{zz} and no σ_{1z}.

Conventional cross-ply laminates have an unacceptable disadvantage in the context of this investigation. As has been noted in the literature [e.g. 8], 90° plies in laminates are often susceptible to transverse cracking. The points where the transverse cracks meet the interlaminar interface are potential sites of "premature" delamination initiation. The effects of these transverse cracks on the local interlaminar stress state or the strain energy release rate would have to be evaluated before

the presently available delamination initiation models could be properly applied. Solutions for this effect are not available. It is therefore desirable to avoid 90° plies.

A manner in which to do this is to utilize a woven graphite/epoxy fabric material along with unidirectional tape. Although there are 90° fiber tows in the fabric, splitting of these tows before delamination initiation is likely to be inhibited by the weave of the fabric.

Three laminate types were chosen for this experiment. They are $[0_{5U}/0_F]_s$, $[0_{5U}/0_F/0_U]_s$, and $[0_{10U}/0_F]_s$, where the subscripts "U" and "F" denote unidirectional and fabric plies, respectively. These gave reasonable values of the interlaminar normal stress. The mechanically-induced components of the interlaminar normal stress were calculated using the method of Kassapoglou and Lagace [6] and are shown in Figure 3 while the thermally-induced components were calculated using the method of Lagace, Kassapoglou, and Brewer [9] and are shown in Figure 4. The change in temperature used to calculate these values is -156°C which is the difference between the set temperature of the epoxy matrix during cure (177°C) and room temperature (21°C). The influence of thermally-induced stresses can thus be evaluated. The material parameters used in the calculations are given in Table 1. Note that the interlaminar stresses are plotted only for the critical interfaces. Since only the interlaminar normal stress is significant in these laminates, the critical interface is the one with the highest value of this component of interlaminar stress. The critical interface is the $0_F/0_U$ interface for the $[0_{5U}/0_F/0_U]_s$

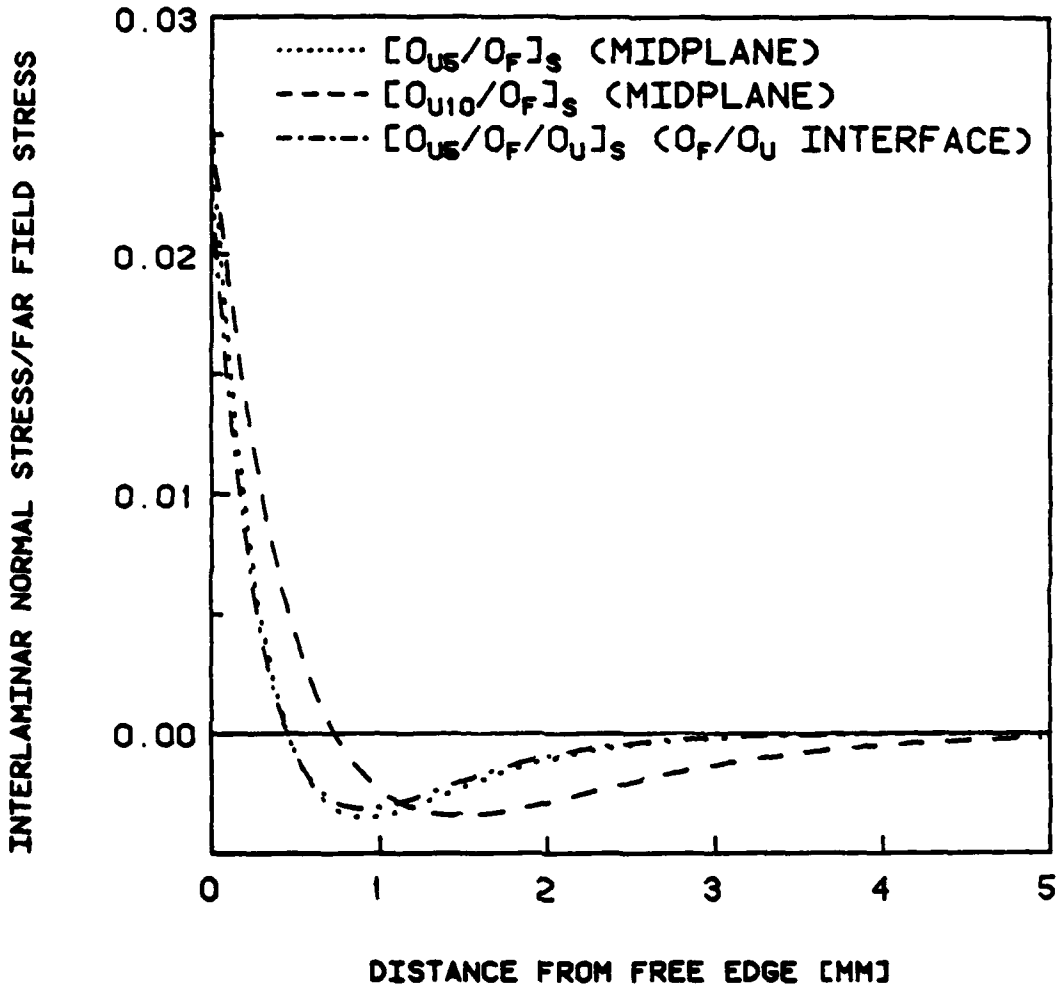

Figure 3 Mechanically-induced interlaminar normal stress for $[0_{U5}/0_F]_S$, $[0_{U10}/0_F]_S$, and $[0_{U5}/0_F/0_U]_S$ laminates.

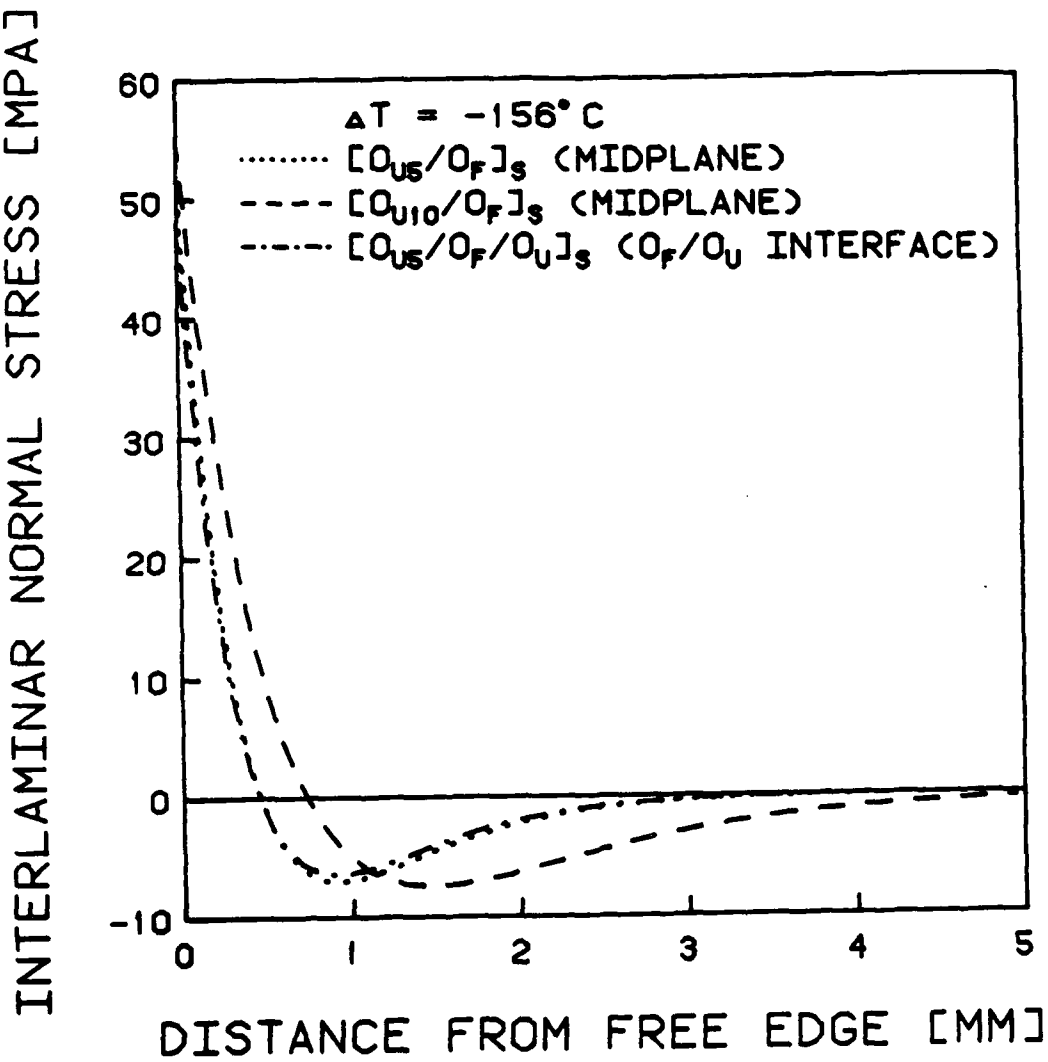

Figure 4 Thermally-induced interlaminar normal stress for $[0_{U5}/0_F]_S$, $[0_{U10}/0_F]_S$, and $[0_{U5}/0_F/0_U]_S$ laminates.

Table 1 Material parameters of Hercules AS4/3501-6 unidirectional graphite/epoxy and Hercules A370-5H/3501-6 fabric Graphite/epoxy

	AS4/3501-6	AW370-5H/3501-6
t_{ply}	0.134 mm	0.35 mm
E_{11}	142 GPa	72.5 GPa
E_{22}	9.81 GPa	72.6 GPa
E_{33}	9.81 GPa	10 GPa
G_{12}	6.0 GPa	4.43 GPa
G_{13}	6.0 GPa	4.43 GPa
G_{23}	4.8 GPa	4.43 GPa
ν_{12}	0.3	0.059
ν_{13}	0.3	0.3
ν_{23}	0.34	0.3
α_{11}	-0.2 μstrain/°F	1.29 μstrain/°F
α_{22}	16.0 μstrain/°F	1.29 μstrain/°F

laminates and the midplane for the other two laminate configurations.

Five specimens of each laminate were constructed. This results in the test matrix outlined in Table 2.

Delamination initiation was detected before final failure in all of the specimens. In the $[0_{10U}/0_F]_s$ specimens, delamination initiated before any mechanical loading had been applied. This implies that thermally-induced interlaminar stresses can be important in initiating delamination. The initiations occurred along the fill fiber tows and were generally closer to the midplane than the unidirectional plies. The $[0_{5U}/0_F]_s$ specimens had delamination initiation at an average applied stress of 528 MPa with a coefficient of variation of 2.6%. All these delaminations initiated along the fill fiber tow close to the midplane. A difficulty was encountered in finding the delamination initiation point for the $[0_{5U}/0_F/0_U]_s$ specimens in that the magnitude of the load drops associated with the initiation of delamination in these specimens was apparently below the resolution of the testing equipment and computer program and the tests were stopped manually when visible damage was observed at the free edge by the naked eye. Thus, only a range of values can be specified. The average lower bound of this range is 451 MPA and the average upper bound is 744 MPa. The delamination initiations were detected along fill fiber tows near the $0_F/0_U$ interface closer to the midplane.

The delamination initiation data was compared to predictions made using the Quadratic Delamination Criterion with an averaging

Table 2 Test matrix for tape/fabric delamination initiation specimens

Laminate Type[a]	Number of Specimens
$[0_{5U}/0_F]_s$	5
$[0_{5U}/0_F/0_U]_s$	5
$[0_{10U}/0_F]_s$	5

[a]Subscript "U" refers to plies of unidirectional graphite/epoxy tape. Subscript "F" refers to plies of woven graphite/epoxy fabric.

dimension of 0.178 mm which was the value determined for AS1/3501-6 unidirectional graphite/epoxy [4]. Since delamination is mainly dependent on matrix properties, it is not expected that this value will change with the change in fiber from AS1 to AS4. The interlaminar normal stress is the only nonzero interlaminar stress in these three lamination sequences, considering both mechanically-induced and thermally-induced stresses. The interlaminar normal strength parameter, Z^t, used is 43 MPa. This is the value measured for AS4/3501-6 graphite/epoxy via direct through-the-thickness tests [10].

The thermally-induced interlaminar stresses were dominant in all three lamination sequences. The contributions of the mechanically-induced stresses were relatively small at delamination initiation. For example, thermally-induced interlaminar normal stresses accounted for 79% of the average interlaminar normal stress at delamination initiation in $[0_{5U}/0_F]_s$ specimens. The thermally-induced components of the interlaminar normal stress at the delamination initiation stress are depicted for this laminate type in Figure 5. The relatively small contribution allows for a precise experimental determination of the average interlaminar normal stress at initiation. This can be regarded as a calculated value for the interlaminar strength parameter which can be compared with the interlaminar normal strength measured from direct testing. The predicted delamination initiation stress, the measured delamination initiation stress, and the calculated interlaminar normal strength are given in Table 3.

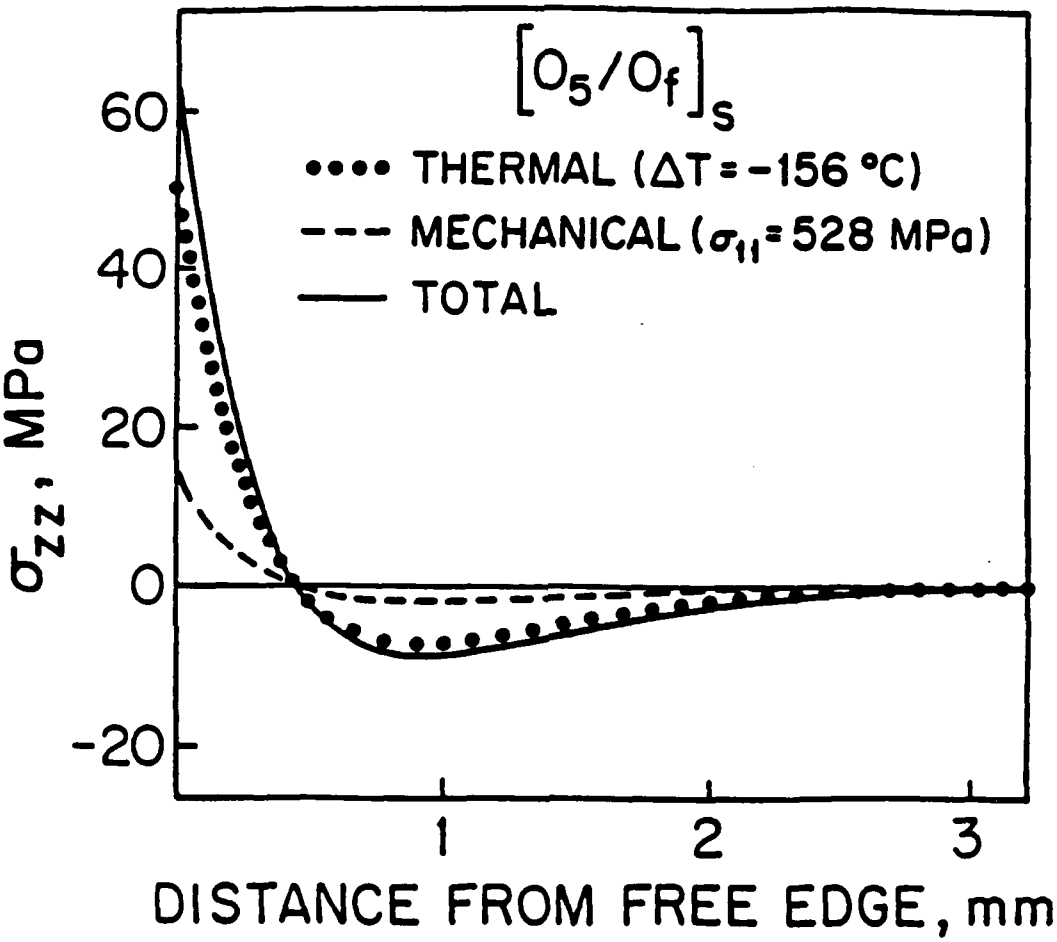

Figure 5 Thermal and mechanical components of interlaminar normal stress at delamination initiation stress at the midplane of a $[0_{U5}/0_F]_s$ specimen.

Table 3 Predicted and measured delamination initiation stress and calculated interlaminar normal strength for tape/fabric specimens

Lamination Sequence	Predicted Initiation Stress [MPa]	Actual Initiation Stress [MPa]	Calculated Interlaminar Normal Strength[a] [MPa]
$[0_{5U}/0_F]_s$	436	528	44.6
$[0_{5U}/0_F/0_U]_s$	681	451-744	39.4-44.0
$[0_{10U}/0_F]_s$	0	0	$\leq$43.4

[a]Calculated at experimental initiation stress.

This methodology correlates the delamination initiation stress for all three lamination sequences using an interlaminar normal strength parameter which was measured directly. Thus, the importance of thermally-induced interlaminar stresses and interlaminar normal stress in particular are demonstrated. The good correlation is further evidence that the averaging dimension, x_{avg}, is a material parameter. The fact that the delaminations initiated at the boundary of fabric plies is an indication that the averaging dimensions may be independent of the form of the material system (i.e. unidirectional versus fabric).

The initiations occurred at the interfaces predicted by the Quadratic Delamination Criterion. These initiations tend to form along fill fiber tows on the boundary of the fabric ply. The criterion and the supporting interlaminar stress analysis assume smeared homogeneous plies. Micromechanical effects play a role in the exact position of the delamination initiation, but important parameters such as delamination initiation stress and critical interface can be predicted without relaxing the smeared homogeneous ply assumptions.

It should be noted that the simplified strain energy release rate approach as proposed by O'Brien [3] cannot be used to predict delamination at the midplane as was observed in two of the three cases. The simple rule of mixtures approach used for determining the modulus of the delaminated region predicts no loss of modulus for a delamination at the midplane of a symmetric laminate. This implies no energy would be available for formation of a fracture surface. The energy for delamination results from the fact that

the bending-stretching parameters become nonzero when the delamination divides the specimen into two unsymmetric halves. This is not accounted for in O'Brien's approach and thus delamination initiation would not be predicted in these two particular laminates whereas it occurs in reality.

This work is reported in detail in Reference 11.

3.2 Delamination under Uniaxial Compression

To date the Quadratic Delamination Criterion, equation (1), has been utilized for specimens loaded under uniaxial tension. A test program was carried out to see the applicability of this criterion to specimens loaded in uniaxial compression. Since no assumptions were made as to the type of loading in formulating the criterion, the applied loading type should not matter. In addition, this opportunity was used to further investigate the role of interlaminar normal stresses in initiating delamination.

The $[0_n/\pm 15_n]_s$ laminate family, with the normalized effective ply thickness, n, varying from 2 to 4, was chosen for this work. This laminate family was chosen for two reasons. One, it has been shown [12] that these laminates delaminate under tensile loading mainly due to the interlaminar shear stress, σ_{1z}, at the +15/-15 interface. Two, under uniaxial compressive loading, the interlaminar normal stress will be tensile at the free edge at the +15/-15 interface. If, as has been hypothesized, tensile interlaminar normal stresses are an important contributor to delamination, versus compressive interlaminar normal stresses, then the delamination initiation stress of a $[0_n/\pm 15_n]_s$ laminate

should differ under tensile and compressive applied loading. To further test this hypothesis, $[0_3/\pm15_3]_s$ specimens were also tested under uniaxial tensile loading. The interlaminar stress state, normalized by the far-field applied stress, at the +15/-15 interface for this laminate family is shown in Figure 6 as calculated via the method of Reference 6.

In addition, the $[\pm45_4/90_4]_s$ laminate was also investigated under both tensile and compressive loads. This laminate, under applied compressive load, has a high compressive interlaminar normal stress at the free edge which is predicted to cause delamination initiation. This thus serves as a further test case as to the role of interlaminar normal stresses.

Five specimens of each laminate were constructed. The tensile coupons are of the same geometry as previously shown in Figure 2. The specimens tested in uniaxial compression need to have a configuration such that they resist global buckling. The specimen designed for relatively thin laminates [13] was utilized. This consists of the test laminates bonded to a honeycomb substructure as illustrated in Figure 7.

All specimens were tested in the appropriate load form utilizing the same procedures previously described including the load drop technique and edge replication. Specimens were tested until indications of the initiation of delamination were present.

The results of the experiments are summarized in Table 4 including the predicted delamination initiation stresses utilizing the Quadratic Delamination Criterion. It is clear from looking at the results of the $[0_n/\pm15_n]_s$ specimens loaded in compression that

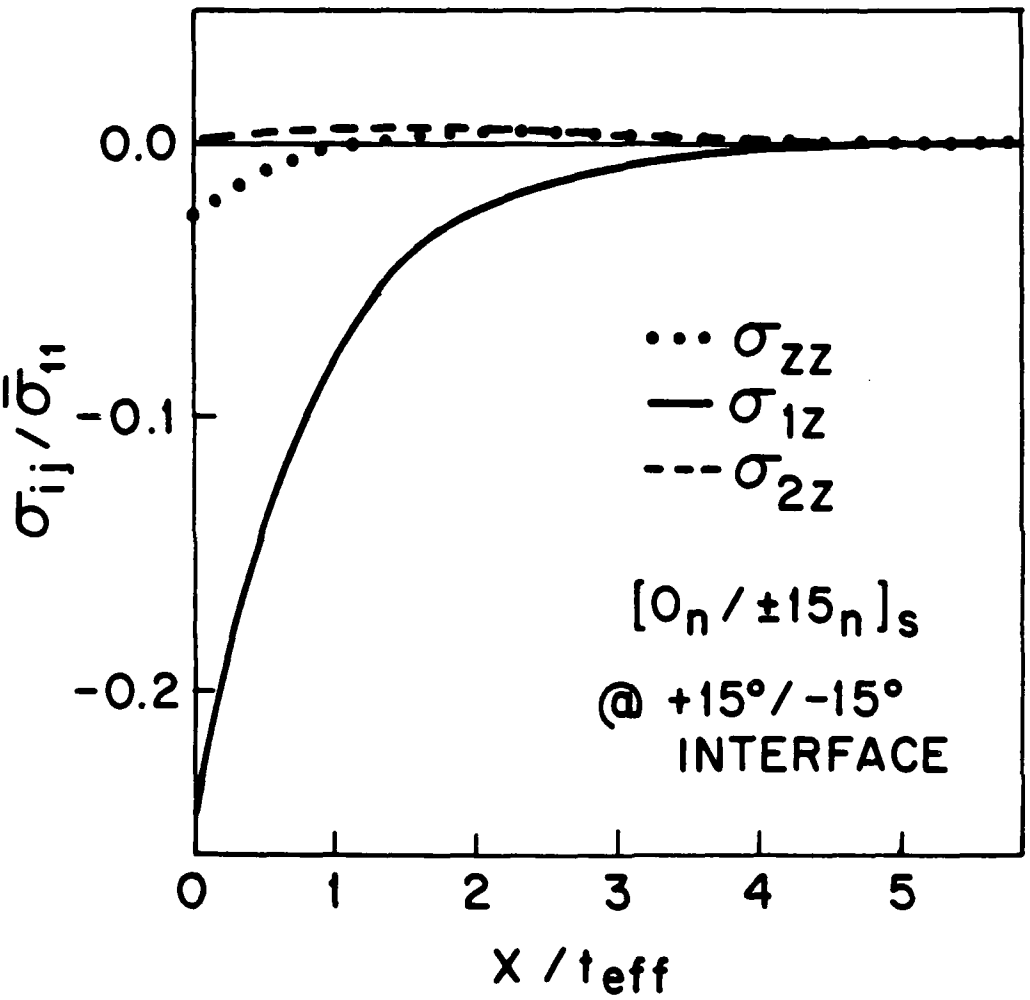

Figure 6 Interlaminar stresses at +15/-15 interface of $[0_n/\pm 15_n]_s$ laminate under uniaxial load.

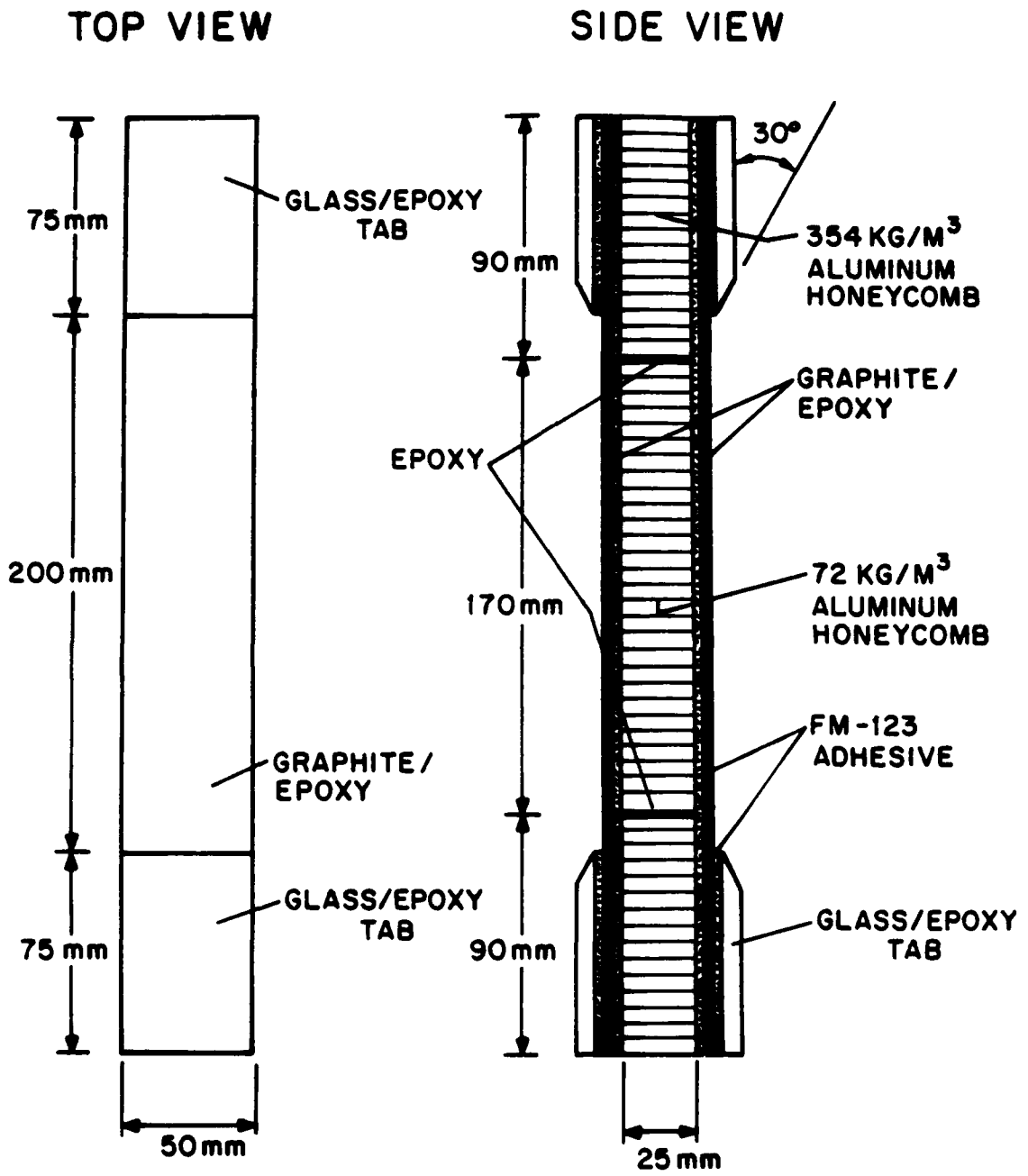

Figure 7 Geometry of standard compressive column test specimen.

Table 4 Experimental and predicted delamination initiation stresses for compressive specimens

Laminate	Applied Force	Delamination Initiation Stress, MPa	
		Experimental	Theoretical
$[0_2/\pm15_2]_s$	Compression	-485 (5.9%)[a]	-412
$[0_3/\pm15_3]_s$	Tension	700 (1.4%)	+644
	Compression	-367 (2.9%)	-353
$[0_4/\pm15_4]_s$	Compression	-360 (2.3%)	-324
$[\pm45_4/\pm90_4]_s$	Tension	b	+83
	Compression	-147 (4.5%)	-321

[a] Numbers in parentheses are coefficients of variation.

[b] Transverse cracking in 90° plies occurred prior to delamination initiation

the effective ply thickness has a similar effect under compressive loads as previously observed under tensile loads [14]. Furthermore, the Quadratic Delamination Criterion, utilizing the previously determining averaging dimension of 0.178 mm [4] works well in predicting these delamination initiation stresses.

The significant difference in delamination initiation stress for the $[0_3/\pm15_3]_s$ laminate between tensile and compressive applied loads, 700 MPa versus -367 MPa, indicate that, indeed, tensile interlaminar normal stresses play an important role in delamination initiation while compressive interlaminar normal stresses do not. Again, the Quadratic Delamination Criterion is successfully able to predict this effect. It should be noted that in all cases the delamination initiates at the +15/-15 interface as predicted.

The results from the final laminate tested, $[\pm45_4/90_4]_s$, are rather inconclusive. The specimens tested under uniaxial tension showed transverse cracks prior to any delamination in all cases. Once these cracks appear, the stress state calculated at the free edge is no longer valid as interlaminar stresses now arise at the tips of these cracks. These results thus cannot be compared to theoretical predictions. In the case of uniaxial compressive loading, the delamination initiated at the +45/-45 interface as opposed to the midplane as predicted. This may further indicate that compressive interlaminar stresses do not contribute to delamination. However, the initiation at the +45/-45 interface, where interlaminar shear stresses are more dominant, occurred much

earlier than predicted (-147 MPa versus -321 MPa). This discrepancy requires further investigation.

This work is described in detail in Reference 15.

3.3 Delamination at Ply Dropoffs

In order to make a structural configuration efficient, the thickness of the structure is often tapered as the requirement to carry load decreases. In structures made of composite materials, this is accomplished by terminating, or "dropping off", individual plies. These ply dropoffs are essentially a discontinuity which acts as a stress riser both in-plane and out-of-plane, even with strictly in-plane loading.

The work to date has concentrated on delamination at straight free edges and has led to a criterion and methodology to predict when delamination will initiate at a straight free edge. The work now progresses to a gradient stress field where interlaminar stresses arise due to the gradient in structural configuration. Relatively little work has been done to study the effect of ply dropoffs, and much of this has been design-specific [e.g. 16]. The current work looks at the basic effects of ply dropoffs and specifically determines, via experimentation, the propensity for delamination to initiate at such dropoffs.

A number of factors were isolated and studied by varying the layups considered in this work. These factors include the number of plies dropped off, the orientation of the plies dropped off, the arrangement of the dropped plies within the laminate, and the effective ply thickness. This led to five different classes of

ply dropoffs being considered in order to isolate these factors. These classes are (1) a single 0° ply dropped off; (2) two 0° plies dropped off symmetrically; (3) angle plies (±45°, ±15°) dropped off symmetrically; (4) 0° and angle plies dropped off symmetrically; and (5) an entire symmetric sublaminate ($[\pm 45/0]_s$) dropped off. These seven test laminates, divided into these categories, are listed in Table 5.

The majority of these laminates are based on the $[\pm 45/0]_s$ stacking sequence configuration. This is a relatively well understood layup which does not delaminate due to free edge effects [14]. Thus, the effects of the ply dropoffs can be isolated from those of the free edge. No 90° plies were included in order to reduce the likelihood of transverse crack formation before the effects of the ply dropoff become substantial. An alternative layup using ±15° plies rather than the ±45° plies was chosen specifically for its tendency to delaminate at the free edge [14]. This allowed for comparison between laminates with a tendency toward in-plane and out-of-plane failure, and the effects of ply dropoffs on each.

The basic tensile coupon was modified as shown in Figure 8 for these experiments. In specimens with ply dropoffs, the appropriate plies were terminated at the specimen midline as indicated. These plies are notated by a subscript 'D' in Table 5. The specimen is thus divided into "undropped" and "dropped" sections. In addition to the ply dropoff configuration, flat laminates (without ply dropoffs) were studied. The configurations of these laminates are the same as the various configurations of

Table 5 Summary of test laminates for work on ply dropoffs

Laminate[a]	Undropped Section	Dropped Section
$[\pm 45/0_D/0/-+45]_T$	$[\pm 45/0]_S$	$[\pm 45/0/-+45]_T$
$[\pm 45_2/0/0_D]_S$	$[\pm 45_2/0_2]_S$	$[\pm 45_2/0]_S$
$[+45/+45_D/-45/-45_D/0/0_D]_S$	$[\pm 45_2/0_2]_S$	$[\pm 45/0]_S$
$[\pm 45/\pm 45_D/0_2]_S$	$[\pm (45)_2/0_2]_S$	$[\pm 45/0_2]_S$
$[+15/+15_D/-15/-15_D/0/0_D]_S$	$[\pm 15_2/0_2]_S$	$[\pm 15/0]_S$
$[\pm 45/\pm 45_D/0/0_D]_S$	$[(\pm 45)_2/0_2]_S$	$[\pm 45/0]_S$
$[\pm 45/0/(\pm 45/0)_D]_S$	$[\pm 45/0]_{2S}$	$[\pm 45/0]_S$

[a] subscript 'D' indicates ply dropped off at centerline.

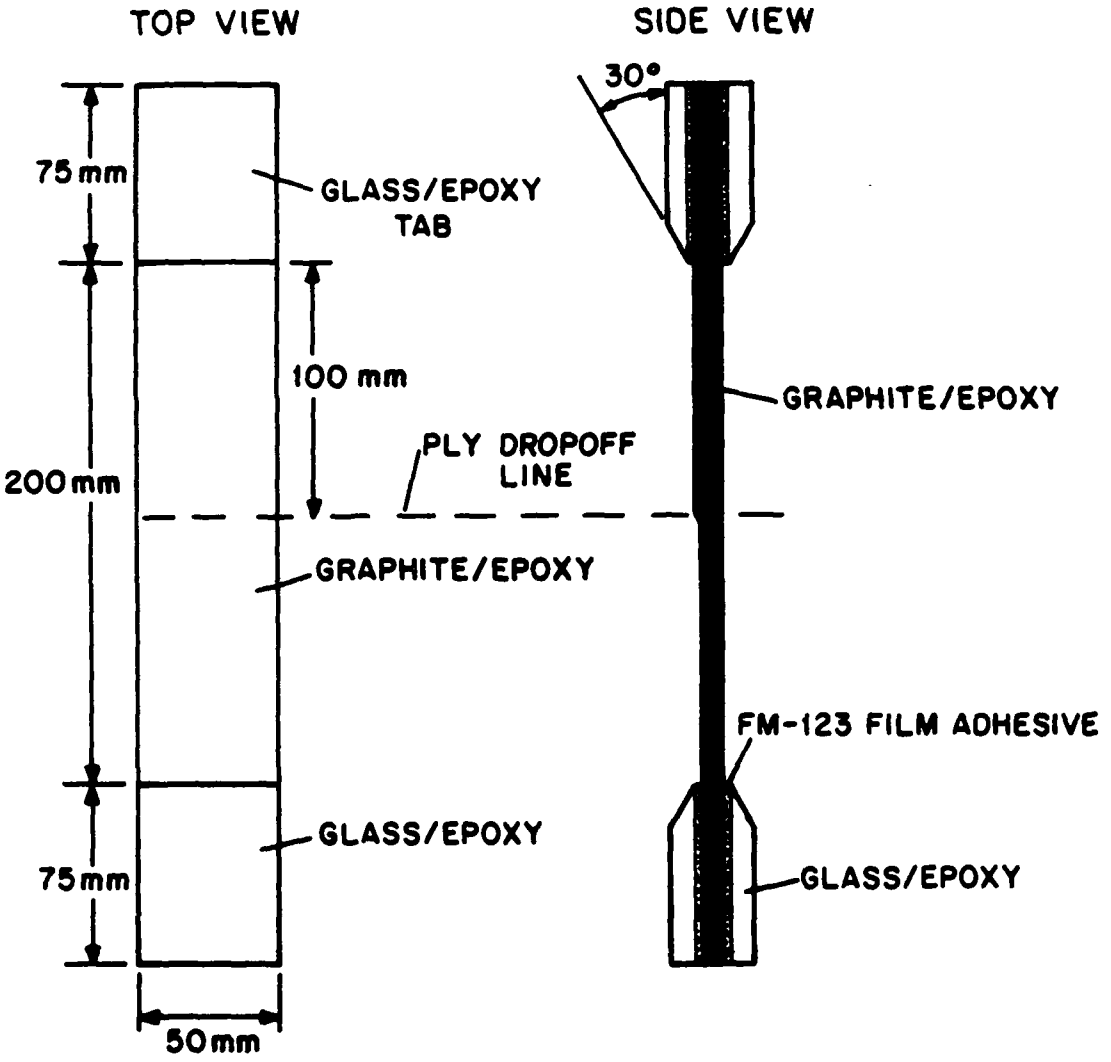

Figure 8 Geometry of coupon specimen with ply dropoffs.

the undropped and dropped sections of the ply dropoff laminates as noted in Table 5. Five specimens of each laminate were manufactured and tested. As before, Hercules AS4/3501-6 graphite/epoxy was used throughout.

All plies were dropped off internally. That is the plies which are dropped off have covering contoured plies over them such that the dropped ply is not exposed. This was done for realism as most structural designs using ply dropoffs have internal ply dropoffs. Furthermore, most of the specimens with ply dropoffs were constructed with one side flat as would be done in actual applications. The other side is not flat due to the ply dropoffs. The plies laid up on top of the terminating plies curve over the ply dropoff and then become flat again over the dropped section of the coupon. Although the specimens are laid up symmetrically, with both the dropped and undropped sections having symmetric layups, the entire specimen is not geometrically symmetric as the midplanes of the dropped and undropped sections do not coincide. Thicker loading tabs were used on the dropped end of the specimen to minimize loading eccentricity. In order to separate out this influence, the $[\pm 15/0]_s$ type specimens with dropoffs were layed up in a geometrically symmetric manner as compared to the geometrically unsymmetric manner. This had no discernible effect on the results.

Special care was taken in manufacturing the specimens with ply dropoffs. A preliminary study was conducted to determine the best means to drop off the plies without causing voids at the ply dropoffs. This study showed that plies should be dropped off with

a spacing of 1.5 mm (for a 0.134 mm thick ply) and that overlaid plies should carefully conform to the dropped area. This was accomplished with a plastic smoothing tool Specific procedures are summarized in Reference 17. Tests were conducted in uniaxial tension. The load drop technique was not utilized in this case. Specimens were examined carefully after failure to determine whether delamination had occurred and taken part in the final failure process.

The ply dropoffs did not have a significant effect on the global stress-strain behavior of the specimens. An analysis [17] indicated that bending effects due to the local geometric eccentricity would die out, to 1% of their maximum effect, within 25 to 70 mm of the ply dropoff line depending on the layup. Strain gages, located 50 mm from the ply dropoff line, did not show any discernible bending in any of the specimens.

The average fracture loads of all the laminates are listed in Table 6 along with the corresponding average stresses in the dropped and undropped sections of the laminates. The data in the table are best examined by comparing the failure load of a specimen with a ply dropoff to the corresponding flat laminates of the dropped and undropped sections. Observations of the failure modes indicate that failure always occurs in the dropped section, thus the failure load of the corresponding laminate with the stacking sequence of the dropped section is most important.

To better illustrate this comparison, the failure load of the dropped laminate and the corresponding flat laminate with the undropped section layup is shown in bargraph format for all

Table 6 Summary of fracture loads and stresses for specimens with ply dropoffs

Laminate	Maximum Load, kN	Fracture Stress[a], MPa	
		Undropped Section	Dropped Section
$[\pm 45/0_D/0/-+45]_T$	18.1 (3.1%)[b]	451	541
$[\pm 45_2/0/0_D]_S$	28.9 (18.8%)	359	431
$[+45/+45_D/-45/-45_D/0/0_D]_S$	29.0 (10.3%)	361	722
$[\pm 45/\pm 45_D/0_2]_S$	64.4 (4.2%)	801	1202
$[+15/+15_D/-15/-15_D/0/0_D]_S$	37.6 (2.8%)	468	935
$[\pm 45/\pm 45_D/0/0_D]_S$	32.2 (13.6%)	401	801
$[\pm 45/0/(\pm 45/0)_D]_S$	29.8 (9.6%)	371	741
$[\pm 45/0]_S$	32.3 (12.3%)	804	
$[\pm 45/0/-+45]_S$	18.4 (9.9%)	548	
$[\pm 45_2/0_2]_S$	64.2 (6.2%)	799	
$[\pm 45_2/0]_S$	33.8 (5.4%)	505	
$[\pm 15_2/0_2]_S$	57.2 (7.5%)	712	
$[\pm 15/0]_S$	35.3 (1.6%)	878	
$[(\pm 45)_2/0_2]_S$	63.0 (6.9%)	783	
$[\pm 45/0_2]_S$	59.5 (6.5%)	1110	
$[\pm 45/0]_{2S}$	70.4 (1.4%)	876	

[a] Stress based on thickness of dropped or undropped section.

[b] Numbers in parentheses are coefficients of variation.

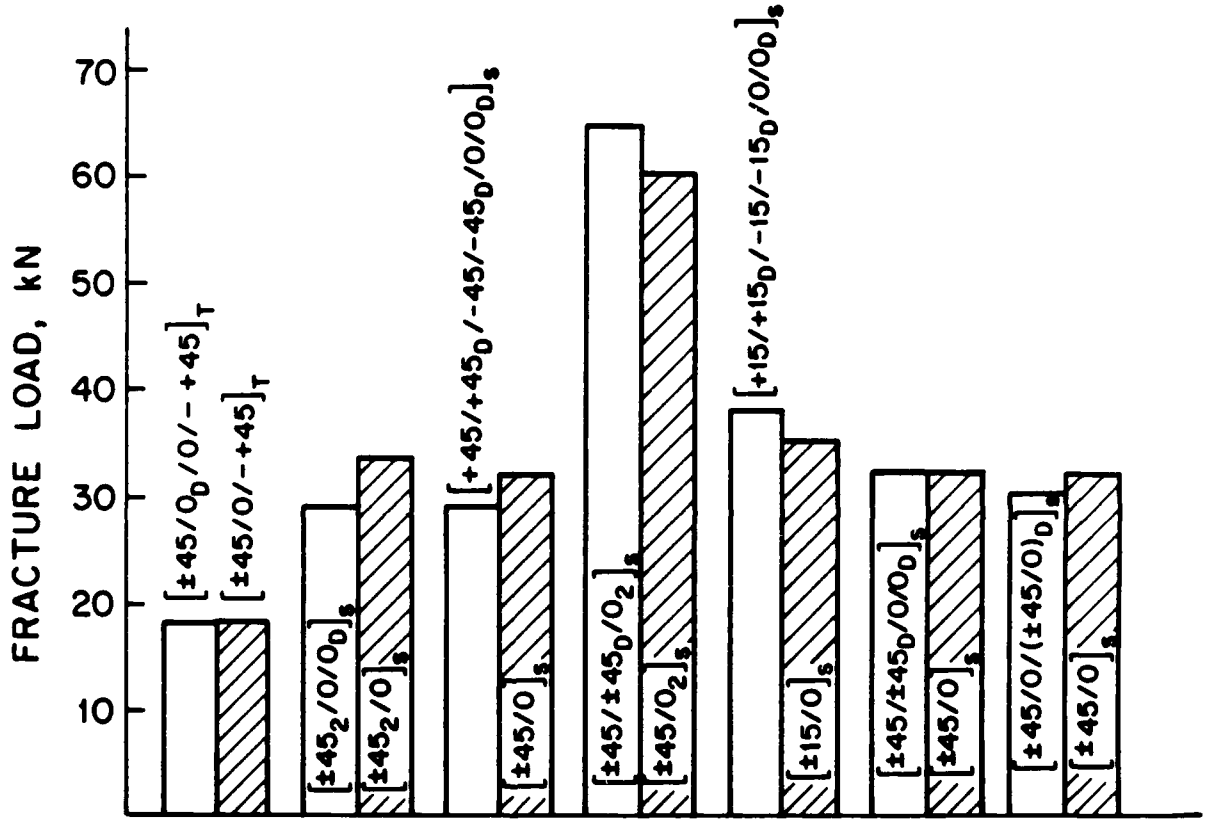

Figure 9 Bargraph representation of fracture loads comparing ply dropoff specimen with flat specimen configuration of section with ply dropoffs.

laminates in Figure 9. It is clear that in all cases, the ply dropoff has not affect the ultimate load-carrying capability of the basic laminate. The ultimate load-carrying capability can thus be calculated from the fracture stresses of the basic layup of each section and determining the minimum load-carrying capability of the two sections.

The presence of the ply dropoffs did not appear to have any effect on the failure modes in all but one case. Failure in the laminates with ply dropoffs generally originated at the area of the ply dropoff and extended into the dropped section of the laminate. In some cases, damage was observed in the undropped section. In these cases, calculations show that the stresses were nearly critical in this section when failure occurred. Failure modes of the ply dropoff laminates generally approximated that of the flat specimen with a layup equal to that of the dropped section of the laminate. Most notably, in-plane failure occurred in those laminates in which in-plane failure was observed to occur in the base flat laminates and out-of-plane failure occurred in the $[+15/+15_D/-15/-15_D/0/0_D]_s$ laminate where out-of-plane (delamination) failure was observed to occur in the base laminate: $[\pm 15/0]_s$.

The one exception noted is the $[\pm 45/0/(\pm 45/0)_D]_s$ laminate which failed with considerable delamination as the sublaminate consisting of the inner six dropped plies would normally delaminate away from the rest of the undropped sections and then in-plane failure would occur. The basic flat laminates of this configuration both failed in an in-plane mode. A possible cause

of this difference in failure modes is that this laminate is laid up with all of the plies dropped off consecutively as a single sublaminate for a total of six consecutive ply dropoffs. It appears that dropping these plies off all at once rather than spreading them throughout the laminate is more delamination critical. However, although delamination did initiate, it did not appear to have an effect on the final strength as this configuration failed only about 8% lower than the flat laminate modeling the dropped section.

In summary, the tests conducted indicate that the presence of ply dropoffs has little effect on the tensile global stress-strain or fracture behavior of graphite/epoxy laminates when compared to the base laminate behavior of the "undropped" and "dropped" sections of the laminate configurations. Only in the case where several plies are dropped off consecutively does delamination initiate. This indicates that the local particulars of the manner in which the plies are dropped off will determine whether delamination will occur and it further shows that care in dropoff placement and manufacture can prevent delamination due to ply dropoffs.

This work is described in detail in Reference 17.

3.4 Delamination at Holes

Just as the work reported in the last section looks at delamination in a gradient stress field, this work also progresses from the basic straight free edge delamination case to one encountered in actual structures: holes. As was the case in the

earlier work on delamination at straight free edges, the initial objective is to experimentally observe the possible effects of delamination and various parameters on delamination behavior at holes in composite laminates. The main focus was to duplicate, somewhat, the work on the effect of ply thickness on delamination [14], but to now do this with various hole diameters.

Two base layups of the AS4/3501-6 graphite/epoxy were utilized in this work: $[\pm 15/0]_s$ and $[+45/0/-45]_s$. The former laminate exhibits delamination at the straight free edge [14] as well as some delamination in the final failure mode with holes [18]. The latter laminate does not show delamination at the free edge or at holes for the case of n equal to 1 [18]. Both the ply thickness and overall laminate thickness were varied independently. The former was accomplished by grouping plies of the same angular orientation: $[\pm 15_n/0_n]_s$ and $[+45_n/0_n/-45_n]_s$; while the laminate thickness was only changed independently in the former laminate: $[\pm 15/0]_{ns}$. The value of n ranged up to 3. Three different hole sizes were used: 3.18 mm, 6.35 mm, and 12.7 mm. In each case, three specimens were made. This laminates which were tested are summarized in Table 7. A total of sixty-three specimens were tested in this program. The same specimen illustrated in Figure 2 was used in this work except that a hole was drilled through the specimen center.

This variation of ply and laminate thickness was done to check whether thickness variations induced changes in delamination behavior due to overall laminate changes or due to changes to the ply thickness as observed in the case of straight free edges [14].

Table 7 Summary of fracture loads and modes for specimens with holes

	Fracture Stress, MPa						
Hole Diameter, mm	$[\pm 15/0]_S$	$[\pm 15_2/0_2]_S$	$[\pm 15_3/0_3]_S$	$[\pm 15/0]_{2S}$	$[\pm 15/0]_{3S}$	$[+45/0/45]_S$	$[+45_2/0_2/-45_2]_S$
3.18	1009[b]	670[c]	675[c]	984[b]	921[b]	541[a]	545[a]
6.35	877[b]	660[c]	613[c]	794[b]	804[b]	465[a]	458[a]
12.7	656[b]	637[c]	566[c]	672[b]	660[b]	320[a]	389[a]

[a] indicates in-plane failure only.

[b] indictes in-plane failure with some delamination.

[c] indicates major delamination in failure mode.

It should be noted that the existence of the hole may complicate this issue.

The ultimate objective of such work is to determine the stress at which delamination initiates at the hole edge. However, in this preliminary work, the objective was to test the specimens to failure and observe effects on final failure stress and on delamination exhibited in postmortem failure examinations. However, strain gages were placed around the hole to detect any deviations in linear strain behavior which may be indicative of delamination. Furthermore, some tests were conducted in incremental load fashion with dye penetrant wiped onto the hole edge at each interval and an X-ray taken. These techniques did indicate the existence of delamination, but the results were not sensitive enough to discern quantitative results. This indicates the need to develop an edge-replicating technique for the hole edge as is done for straight free edges. These results using the X-rays and strain gages are reported in Reference 19.

The results are summarized in Table 7. The average fracture stresses are presented along with the assessment of the failure mode observed in the post-mortem examinations. Very similar trends are seen as were observed for the case of coupons without holes. As the ply thickness is increased, that is the value of n increases from 1 to 3, more delamination is observed in the final failure and the failure stress goes down. This is especially obvious for the smallest hole size where notch sensitivity effects are not as pronounced as in the 12.7 mm diameter hole. In marked contrast, the laminates which only have laminate thickness

increased, i.e. $[\pm 15/0]_{ns}$, do not show any significant change in the fracture stress or the failure mode as the thickness increases. This indicates that, again, the ply thickness is a major controlling factor in the interlaminar stress state at the hole edge and that increased effective ply thickness reduces the resistance to delamination.

The $[+45_n/0_n/-45_n]_s$ laminates also do not show any appreciable difference in fracture stress for the two effective ply thicknesses tested. In fact, no delamination is visible in the postmortem examinations.

These results indicate that similar experiments and calculation methods should be pursued for the case of a hole in a specimen as was done for the straight free edge coupon.

A full description of this work is provided in Reference 19.

4. DELAMINATION GROWTH AND FINAL FAILURE

The work on delamination growth and final failure is divided into six separate sections and is reported as such. The variables investigated as to their effect on delamination growth and final failure are specimen width, effective ply thickness, lamination sequence, character of the ply interface, and implantation of simulated delamination and angle ply splits.

4.1 Finite Width Effects

The first variable investigated was specimen width. This was selected to evaluate the hypothesis that a critical delamination area may exist for unstable delamination growth or in-plane failure. The results from the specimens with nonstandard widths can be used to determine if such a critical size exists and if this size is a function of specimen width. For example, the critical delamination area could be a percentage of test section area or an absolute value independent of specimen width.

The $[\pm 15_3]_s$ laminate was chosen for these experiments because it has been shown to delaminate in a previous investigation [4]. As throughout most of this work, AS4/3501-6 was utilized. The specimens used were standard specimens as illustrated in Figure 2 except in width. The widths used in these tests are 10 mm, 20 mm, 30 mm, 50 mm, and 70 mm. These widths range from approximately seven to 50 times the width of the interlaminar stress boundary region.

To determine the appropriate loads to which to test these specimens, it was necessary to know the delamination initiation stress and final failure stress of the laminate. An additional two 10 mm wide specimens and two 30 mm wide specimens were manufactured and tested to determine these values. Five specimens of each width were then tested using constant stress increments from approximately 90% of the observed delamination initiation stress to final failure. Damage was assessed by dye penetrant-enhanced x-radiography after each test increment. The test matrix is summarized in Table 8.

Failure in all these specimens was accompanied by massive splitting and delamination of the outer plies across the entire width of the specimen. In some cases, the specimen did not break into two separate pieces although, for all practical purposes, it could not carry load. The stress-strain behavior of the specimens was not affected by the specimen width. Average values of specimen modulus and failure stresses and strains are reported in Table 9.

The delaminated area and intrusion for the specimens of nonstandard width were determined after each incremental load from x-radiographs. The shape of the delamination during growth was usually triangular. The triangle was always bounded on one side by the free edge and on another by a split in the +15° ply. The third side of the triangle was the delamination front. The delamination front usually extended from the angle ply split toward the free edge at approximately a right angle. This delamination shape is depicted schematically in Figure 10.

Table 8 Test matrix for $[\pm 15_3]_s$ specimens of nonstandard width

Specimen Width [mm]	Number of Specimens Tested for Delamination Initiation and Final Failure	Number of Specimens Tested to Incremental Load Levels and Monitored with Dye Penetrant-Enhanced X-Radiography
10	2	5
20	0	5
30	2	5
50	0	5
70	0	5

Table 9 Average modulus, failure stress, and failure strain for $[\pm 15_3]_s$ specimens of nonstandard width

Width [mm]	Modulus [GPa]	Failure Stress [MPa]	Failure Strain [μstrain]
10	115 (8.8%)[a]	508 (4.1%)	4336 (5.8%)
20	116 (2.5%)	502 (3.3%)	4318 (2.7%)
30	116 (4.0%)	515 (3.6%)	4348 (3.5%)
50	110 (1.2%)	505 (2.8%)	4600 (3.2%)
70	110 (5.3%)	488 (7.3%)	4687 (13.5%)

[a]Numbers in parentheses are coefficients of variation.

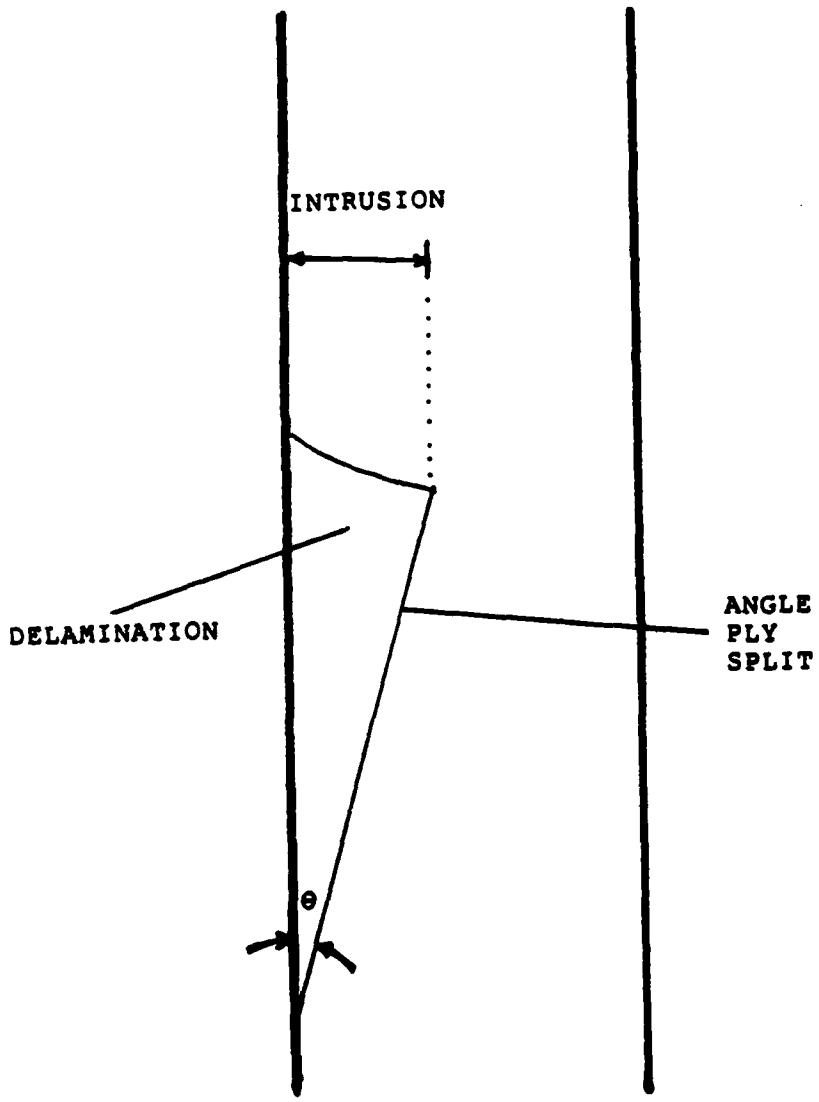

Figure 10 Schematic of observed delamination damage.

The average failure stress for these five sets of specimens of nonstandard width are within experimental scatter of one another. Thus, failure stress is independent of specimen width for these specimens even though delamination is the controlling mechanism. This indicates that the mechanism controlling failure is also independent of specimen width.

Once a delamination starts to grow, the plies decouple and the local strength drops rapidly. Since the failure stress is approximately the same for all specimen widths, the failure of these specimens appears to be controlled by the strength of the decoupled sublaminates. Apparently, local in-plane failure of the delaminated sublaminate causes stress gradients which can trigger further delamination and the corresponding sublaminate failure.

The only dependency on width was that larger delaminated areas were detected before final failure. The delaminations are apparently better able to start and stop in the wider specimens. There are a number of possible explanations for this. There may be finite width effects on the strain energy release rate curves that may affect growth. There may be other mechanisms at work that are related to the probability of arresting a delamination as a function of amount of growth. Nonetheless, when the sublaminates started to fail, total delamination and final failure followed.

Within the resolution of these experiments, there does not appear to be a definitive critical delamination size for unstable delamination growth or final failure. This set of experiments shows that unstable growth and final failure can coincide.

However, these experiments do not prove that the two necessarily do coincide. For example, it is possible that the final failure of similar specimens would not coincide with unstable delamination growth if the in-plane strength of the delaminated sublaminates were higher.

This work is fully reported in Reference 11.

4.2 Effect of Thickness and Lamination Sequence

In this phase of the work, two similar laminates types were used: $[\pm 15_n/0_n]_s$ and $[0_n/\pm 15_n]_s$. In previous work, delamination initiated at the +15/-15 interface as is predicted here. The two laminate types have nearly identical interlaminar stress states at this interface except that the interlaminar normal stress at the free edge is tensile in the former case and compressive in the latter case as previously discussed in section 3.2. Another significant difference between the two laminate types is that the 0° plies can constrain delamination and damaged angled plies in the $[0_n/\pm 15_n]_s$ case. The plies can then be loaded through friction. In contrast, the $[+15_n]$ sublaminate in the $[\pm 15_n/0_n]_s$ case is prone to out-of-plane peeling. That is, the delaminated portion of the sublaminate between the angle ply split and the free edge peels away from the specimen. No load can be carried by this portion of the sublaminate.

Varying the effective ply thickness has distinct effect on the interlaminar stress state as it "spreads out" the distributions of the interlaminar stress components while not altering the free edge magnitude [14]. The strain energy release

rate curve is also scaled upward and outward by the effective thickness factor n. This is the result of two effects. First, the energy available per unit delaminated area is directly proportional to the laminate thickness and, thus, n. Second, the interlaminar stress boundary region which influences the shape of the strain energy release rate curve near the free edge is shifted outward.

When the Quadratic Delamination Criterion, discussed in section 3.1, is applied to interlaminar stress solutions with a finite free edge value, it gives an asymptotic limit for delamination initiation stress. This limit results from the fact that as the effective ply thickness becomes large, the calculated average interlaminar stress components approach the free edge values [6].

The effects of effective ply thickness on the strain energy release rate and delamination initiation stress have significant consequences. Thin laminates require a high strain level for delamination growth to be energetically feasible. Since the strain energy release rate is proportional to effective ply thickness, delamination growth is energetically feasible at much lower strain levels in thick laminates. Since delamination initiation stress may have an asymptotic lower limit, delamination growth in thick laminates may be energetically feasible before delamination initiation. Thick laminates can therefore be used to determine if delamination growth can occur before the Quadratic Delamination Criterion predicts delamination initiation. To allow for a wide range of possible behavior, the values of the effective

ply thickness factor, n, used in this set of experiments were 1, 2, 3, 5, and 8.

Five specimens of each type were manufactured. The first three were tested monotonically to failure. The remaining two were tested incrementally from approximately 75% of the failure stress to final failure in 5% increments. The damage state was evaluated after each loading increment by dye penetrant-enhanced x-radiography. Table 10 is a summary of this test program.

Failure in these cases was usually accompanied by the delamination and in-plane failure of the angled plies and splitting of the 0° plies. All stress-strain curves were relatively linear to failure. The summary of specimen modulus and failure stress and strain is presented in Table 11.

Two trends are evident in the failure data. First, failure stress and strain decrease as effective ply thickness increases. Second, the values for $[0_n/\pm 15_n]_s$ specimens are consistently higher than those for the $[\pm 15_n/0_n]_s$ specimens. These trends have previously been observed [14]. In addition, the range when delamination was first detected via the x-radiography is indicated in Table 12.

Although the general behavior of the two laminate types are similar in that the failure stress decreases with increasing ply thickness, there is a difference in the failure stress of the two laminate configurations for the same effective ply thickness. It is unlikely that the interlaminar stress state prior to initiation is the controlling factor in this case since the delamination has initiation before final failure. The difference in behavior after

Table 10 Test matrix for $[\pm 15_n/0_n]_s$ and $[0_n/\pm 15_n]_s$ specimens with different effective ply thicknesses

Lamination Sequence	Number of Specimens Tested Monotonically to Failure	Number of Specimens Tested to Incremental Load Levels and Monitored with Dye Penetrant-Enhanced X-Radiography
$[\pm 15/0]_s$	3	2
$[\pm 15_2/0_2]_s$	3	2
$[\pm 15_3/0_3]_s$	3	2
$[\pm 15_5/0_5]_s$	3	2
$[\pm 15_8/0_8]_s$	3	2
$[0/\pm 15]_s$	3	2
$[0_2/\pm 15_2]_s$	3	2
$[0_3/\pm 15_3]_s$	3	2
$[0_5/\pm 15_5]_s$	3	2
$[0_8/\pm 15_8]_s$	3	2

Table 11 Average modulus, failure stress, and failure strain for $[\pm 15_n/0_n]_s$ and $[0_n/\pm 15_n]_s$ specimens

Laminate Type	Modulus [GPa]	Failure Stress [MPa]	Failure Strain [μstrain]
$[\pm 15/0]_s$	125 (3.2%)[a]	1003 (4.1%)	7935 (6.5%)
$[\pm 15_2/0_2]_s$	122 (5.7%)	747 (8.1%)	6312 (10.7%)
$[\pm 15_3/0_3]_s$	123 (5.0%)	642 (6.6%)	5997 (19.5%)
$[\pm 15_5/0_5]_s$	117 (8.0%)	618 (10.5%)	5626 (17.0%)
$[\pm 15_8/0_8]_s$	115 (6.1%)	541 (2.5%)	5137 (11.5%)
$[0/\pm 15]_s$	124 (3.1%)	1160 (3.3%)	9028 (5.5%)
$[0_2/\pm 15_2]_s$	123 (6.4%)	863 (4.7%)	7463 (9.4%)
$[0_3/\pm 15_3]_s$	123 (8.1%)	760 (8.8%)	6570 (19.1%)
$[0_5/\pm 15_5]_s$	119 (10.5%)	669 (7.1%)	6289 (15.1%)
$[0_8/\pm 15_8]_s$	114 (14.1%)	618 (5.9%)	5371 (6.3%)

[a] Numbers in parentheses are coefficients of variation.

Table 12 Average first growth stress range for $[\pm 15_n/0_n]_s$ and $[0_n/\pm 15_n]_s$ specimens

Laminate Type	Average First Growth Stress Range [MPa]
$[\pm 15/0]_s$	785-837
$[\pm 15_2/0_2]_s$	629-666
$[\pm 15_3/0_3]_s$	512-541
$[\pm 15_5/0_5]_s$	<495[a]
$[\pm 15_8/0_8]_s$	<414[a]
$[0/\pm 15]_s$	1001-1059
$[0_2/\pm 15_2]_s$	733-772
$[0_3/\pm 15_3]_s$	<540[a]
$[0_5/\pm 15_5]_s$	<502[a]
$[0_8/\pm 15_8]_s$	<484[a]

[a]Delamination occurred in the first test of both specimens.

initiation can be attributed to the physical characteristics of the lamination sequence. The angle plies in the $[0_n/\pm15_n]_s$ specimens are constrained from out-of-plane deformation after damage due to the 0° plies. The difference in energy directly attributable to bending was evaluated in a simple experiment. Several small masses were placed on a peeled sublaminate. The deflection of the ply gave an indication of the energy needed to restore it to its original position. This was found to be negligible when compared to other quantities of energy. However, even if a region of a ply is completely debonded from the neighboring plies, frictional loads can still be applied. In contrast, the surface plies of the $[\pm15_n/0_n]_s$ specimens are free to peel away and unload. The net effect is that more strain energy is available for delamination growth in these latter specimens at any stress level. Hence these specimens experience delamination growth earlier which in turn subjects them to redistribution of in-plane stresses and the associated in-plane failure at lower stresses.

The thinnest specimens, with n equal to 1, exhibited failure modes which could be associated with in-plane failure. The delamination initiation stress for these specimens is quite high. When a significant area of the specimen delaminated, there was a sudden increase in local compliance. The local stresses and strains apparently exceeded the level necessary for local in-plane failure of the remaining sublaminates. When this occurred, the compliance in the local region increased. The local stresses and strains at the edge of the failing region apparently exceeded the

level necessary for in-plane failure of the laminate and failure propagated across the specimen width.

Failure of a laminate appears to be governed by in-plane strength. When delamination is involved, the relevant in-plane strength is the local in-plane strength of the delaminated sublaminates.

If growth is governed by an energy consideration, then there should be a general trend toward earlier growth for thicker specimens. This is because the available energy is directly proportional to laminate thickness. Details may vary as a result of effects of the interlaminar stress boundary region and finite dimensions. Since strain energy is proportional to the square of the strain (or stress) level, then these variations should be roughly inversely proportional to effective ply thickness. However, the fact that delamination growth is energetically feasible is not a sufficient condition for growth to occur. Delamination initiation appears to be a necessary prerequisite. Hence no growth occurs before delamination initiation.

The data from this work can be used to verify some of these premises. The average first growth range and final failure stress are plotted as a function of effective ply thickness for the $[\pm 15_n/0_n]_s$ specimens in Figure 11 and for the $[0_n/\pm 15_n]_s$ specimens in Figure 12. Also plotted are three theoretical curves. The first is the delamination initiation stress predicted by the Quadratic Delamination Criterion as discussed in section 3.1. The second is the failure stress predicted for the damaged specimens using the Tsai-Wu in-plane failure criterion [20]. The damage to

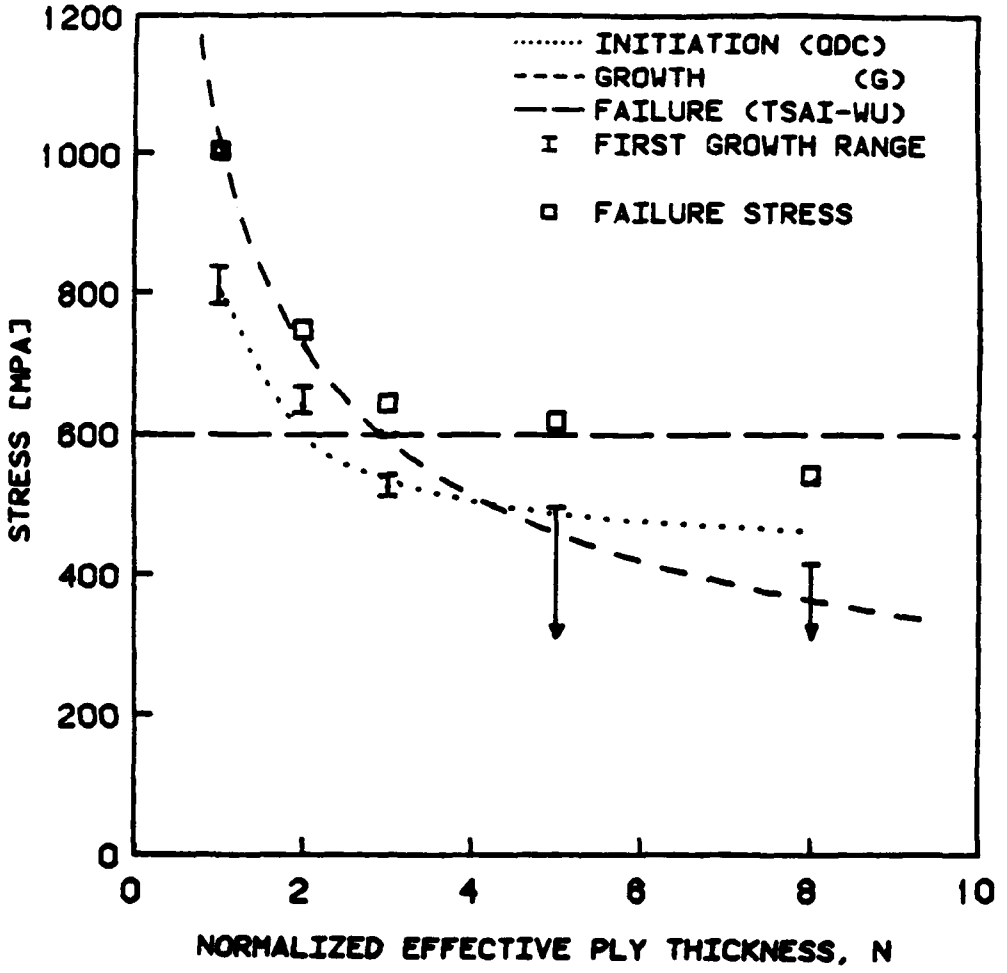

Figure 11 Experimental values and analytical curves for delamination initiation, growth, and final failure of $[\pm 15_n/0_n]_s$ specimens.

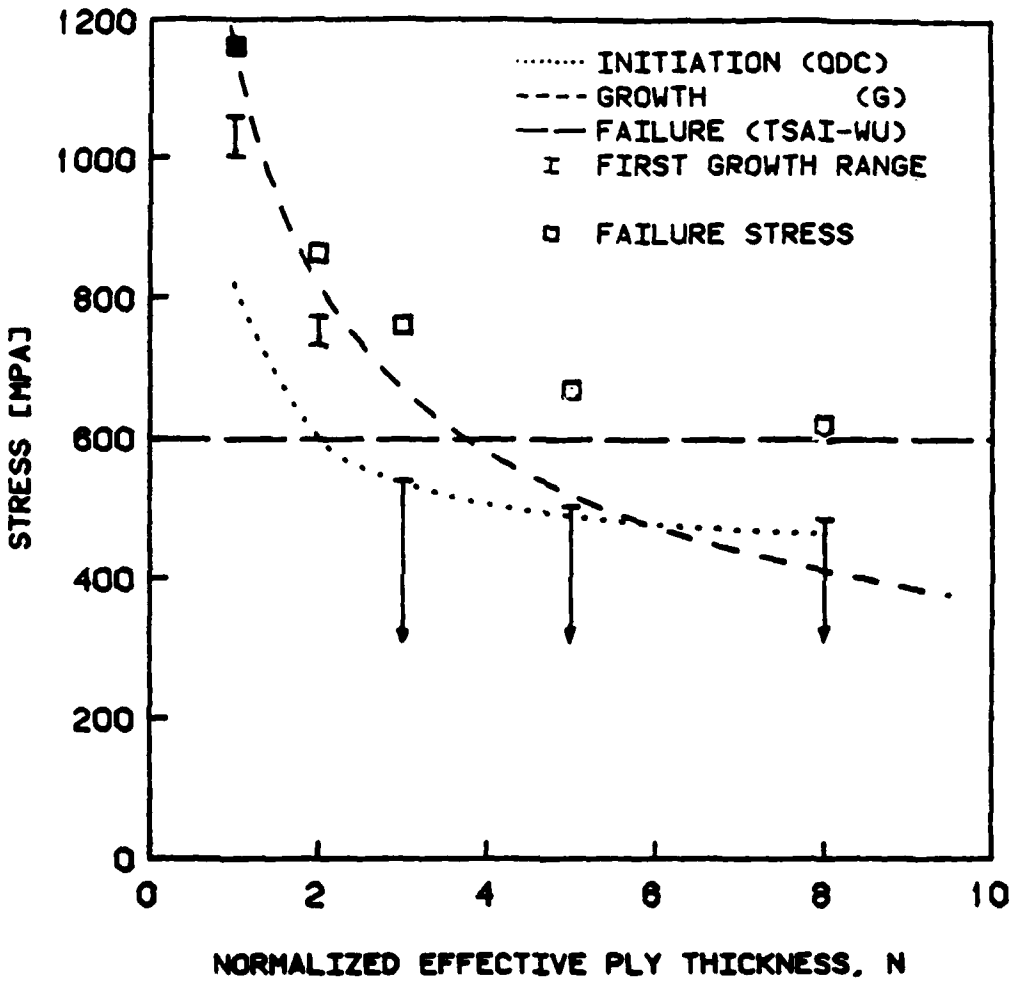

Figure 12 Experimental values and analytical curves for delamination initiation, growth, and final failure of $[0/\pm 15_n]_s$ specimens.

the specimens was assumed to be complete delamination at the +15/-15 interface and in-plane failure (in the form of splitting) of the isolated angle ply sublaminates. The failed sublaminate was assumed to carry no load and therefore contribute no strength or stiffness to the specimen. The third curve is generated by a constant strain energy release rate as predicted by the O'Brien method [3].

These two figures clearly indicate that there was no delamination growth until approximately the predicted delamination initiation stress, even when significant delamination growth was theoretically possible as determined by the strain energy release rate curve. This shows conclusively that initiation must occur before any growth can occur and that the strain energy release rate criterion is a necessary but not a sufficient condition for delamination growth. However, strain energy release rate is a necessary condition for certain types of damage growth. It can also be seen that failure occurs soon after growth as long as the stress is near or above the post first ply failure stress predicted via the in-plane criterion.

The work is discussed in detail in Reference 11.

4.3 Delamination at Fabric Ply Interfaces

A set of experiments was performed to attempt to ascertain the role of angle ply split propagation in delamination growth. By utilizing fabric plies, A370/3501-6, angle ply splitting is limited and delamination propagation in the absence of angle ply splitting can be observed. The laminates chosen for this were

nominally $(\pm 20)_s$ laminates where the () indicate fabric rather than the [] which indicate unidirectional tape. Thus, the warp fiber tows were angled at ±20° to the longitudinal axis of the specimen. All the components of the interlaminar stress state at the midplane of an angle ply laminate are identically zero [7]. Therefore, any delamination would initiate and grow at the +20/-20 interface. The 20° angle was chosen because of the high interlaminar shear stress, σ_{1z}, obtained in this configuration and the resulting low predicted delamination initiation stress.

The difference between the experimental laminates was the character of the ply surfaces at the +20/-20 interface. A five-harness satin weave has an "over four - under one" weave of the fiber tows as shown in Figure 13. This means that 80% of the exposed fibers on one face of the ply are warp fibers while 80% of the exposed fibers on the other face are fill fibers. These are referred to as the "warp face" and "fill face" of the ply, respectively. One laminate was made with only warp faces at the +20/-20 interfaces while the other was made with only fill faces at the +20/-20 interfaces.

Splits are observed to form within plies in association with delamination initiation. The delamination initiation is believed to be the primary damage mode since delamination initiations have been observed without splits in fabric plies, but not vice versa. It is reasoned that splits in the warp fiber tows emanating from the +20/-20 interface at the free edge could be inhibited from growing at the point where the tows crossed "under" the fill tows. In contrast, splits in the fill fiber tows could grow farther from

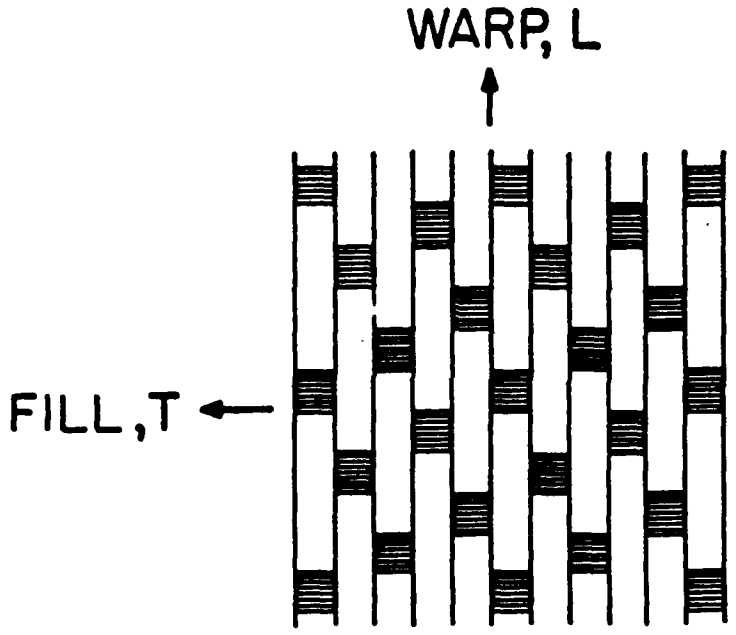

Figure 13 Schematic of five-harness satin weave fabric.

the free edge before crossing under a tow. The two types o specimens therefore allow for the direct comparison of specimens with essentially the same in-plane behavior and interlaminar stress state, but a different character of the splitting state of the fiber tows closest to the delaminating interface.

Five standard coupon specimens, as in Figure 2, were tested. As in the work reported in section 4.2, the first three of each group were tested to failure and the remaining two were tested incrementally to failure from 75% of the failure stress to failure in 5% increments. The damage state was evaluated after each loading increment by dye penetrant-enhanced x-radiography.

The average modulus and failure stress and strain values for these specimens are given in Table 13. There is indeed 13% difference in the failure stress between specimens with a fill/fill versus warp/warp interface. The delamination growth behavior also varied for the two specimen types. The specimens with only fill faces at the +20/-20 interface exhibited delaminations detectable from the x-radiographs at lower stresses. These delaminations are most likely not formed concurrently with delamination initiation, which should be the same for both specimen types. The delamination tended to be triangular shaped and were bounded on one side by the free edge and on the other two sides by lines at ±20° to the longitudinal axis. The lines were apparently splits in warp fiber tows. The boundaries of the delaminated region did not coincide exactly with these splits. The specimens with only warp faces at the +20/-20 interface exhibited smaller, more clearly defined delaminations. These

Table 13 Average modulus, failure stress, and failure strain for $(\pm 20)_s$ fabric specimens

Interface Type	Modulus [GPa]	Failure Stress [MPa]	Failure Strain [μstrain]
Fill/Fill	56 (3.8%)[a]	470 (2.7%)	9291 (8.9%)
Warp/Warp	55 (5.3%)	530 (4.0%)	9895 (5.2%)

[a]Numbers in parentheses are coefficients of variation.

delaminations were bounded on one side by a line at 20° to the longitudinal axis and on the other side by a line roughly perpendicular to that.

Light lines at ±70° to the longitudinal direction were visible in most x-radiographs in which delaminations were visible. These lines indicate splits in the fill fiber tows of all the plies. They apparently formed after the delaminations.

It is clear that delamination occurred in all these specimens and that the delaminations contributed to the final failure and, furthermore, that there is a significant effect of the character of the ply interface on delamination growth and thus final failure stress.

The differences in character of the interface were manifested in the character of the delaminations. In the specimens with warp faces at the +20/-20 interfaces, the boundaries of the delamination were delineated by splits in the warp fiber tows on one side and the fill fiber tows on the other side. The splits had the effect of "blunting" the delamination front. This affects the energy required for extension of the delamination front. It appears that when growth beyond the splits become energetically feasible, the delaminated region grows across the specimen width. Once this occurs, the in-plane strength of the specimen decreases and the specimen fails.

In specimens with fill faces at the +20/-20 interfaces, the delamination growth seems to have been unrestricted by any splits in the fill fiber tows. Only when splits in the warp fibers caused a disturbance in the stress field did these delaminations

appear to be arrested. This apparently either increased the energy needed to extend the delaminated region (perhaps by inducing small cracks at the +20/-20 interface which blunted the delamination front) or decreased the energy available on a local level. The difference between the two specimen types seems to have affected the stress at which delamination grows across the width and therefore the final failure stress.

Although not successful in studying delamination in the absence of splitting, these specimens did show only local splitting due to the woven nature of the fabric and indicated how this splitting does interact with the delamination in terms of growth and final failure.

These results and procedures are described in detail in Reference 11.

4.4 Importance of Angle Ply Splits in Final Failure

The work has clearly indicated that splits in the angle plies adjacent to the delaminated interface play an important role in the delamination growth and eventual failure of the specimen. In order to isolate the effect of angle ply splits, a method was develop to implant angle ply splits in otherwise undamaged specimens. This involved utilizing a teflon filament which was placed between a cut running along the fiber direction in the angle ply during layup. This filament was about two ply thicknesses (0.27 mm) in diameter and thus an effective ply thickness of two or increments of two is necessary so that the teflon filament is the same thickness as the effective ply. This

teflon filament is left in the laminate after cure and simulates a split in that ply.

For the experimental program, $[0_2/\pm 20_2]_s$ specimens were utilized. Once again, AS4/3501-6 graphite/epoxy was utilized. A 20° angle was selected so that the filament could be put in and still protrude from each end of the 50 mm wide specimen of Figure 2 without the filament passing under the loading tabs. This could not be done with a 15° ply. This configuration is type A. A second configuration where the filament was placed so that it did run under the tab is type B. Ten of each type were manufactured and tested. Specimens were tested in uniaxial tension to failure in load increments. Edge replicas and x-radiographs were taken at each interval to monitor the initiation and growth of delamination. In addition, five virgin specimens were manufactured and tested.

No difference was observed in the behavior of the type A, type B, or unflawed specimens in growth or final failure. The failure stresses are 909 MPa for the type A specimens, 857 MPa for the type B specimens and 919 MPa for the unflawed specimens. Coefficients of variation are 9.2%, 10.1% and 3.0%, respectively. However, in specimens with implanted angle ply splits, delamination did always initiate at the split.

These results conclusively show that it is the interaction of the delamination and angle ply split(s) which lead to final failure. The existence of the angle ply split by itself, as implanted herein, does not change the behavior of the specimen.

This work is described in detail in Reference 21.

4.5 Implanted Delaminations and Angle Ply Splits

Based on the work reported in the previous section, the interaction of the delamination front and angle ply splits was investigated. The tests specimens contained "implanted" delaminations and angle ply splits. These features were achieved by implanting thin teflon film between and within the plies of a specimen before curing. The nonstick property of the teflon caused the plies to decouple at a relatively low load in a prescribed shape simulating the delamination shape observed in other experiments. This approximates a naturally occurring delamination.

The delamination shape investigated is triangular, bounded by the free edge, an angle ply split, and a delamination front approximately perpendicular to the split as illustrated in Figure 10. This is the configuration generally observed to naturally occur. The relative importance of the split and the delamination front were evaluated by manufacturing one set of specimens with no angle ply split and one set with an angle ply split extending beyond the delamination front as illustrated in Figure 14. No specimens were made with the angle ply split extending exactly to the delamination front because that would be equivalent to the naturally occurring damage.

Six specimens of each type were made. The lamination sequence is $[0_3/\pm 15_3]_s$. This sequence was chosen because it was observed to delaminate at the +15/-15 interface with an associated angle ply split in the $[-15_6]$ sublaminate. This laminate has an

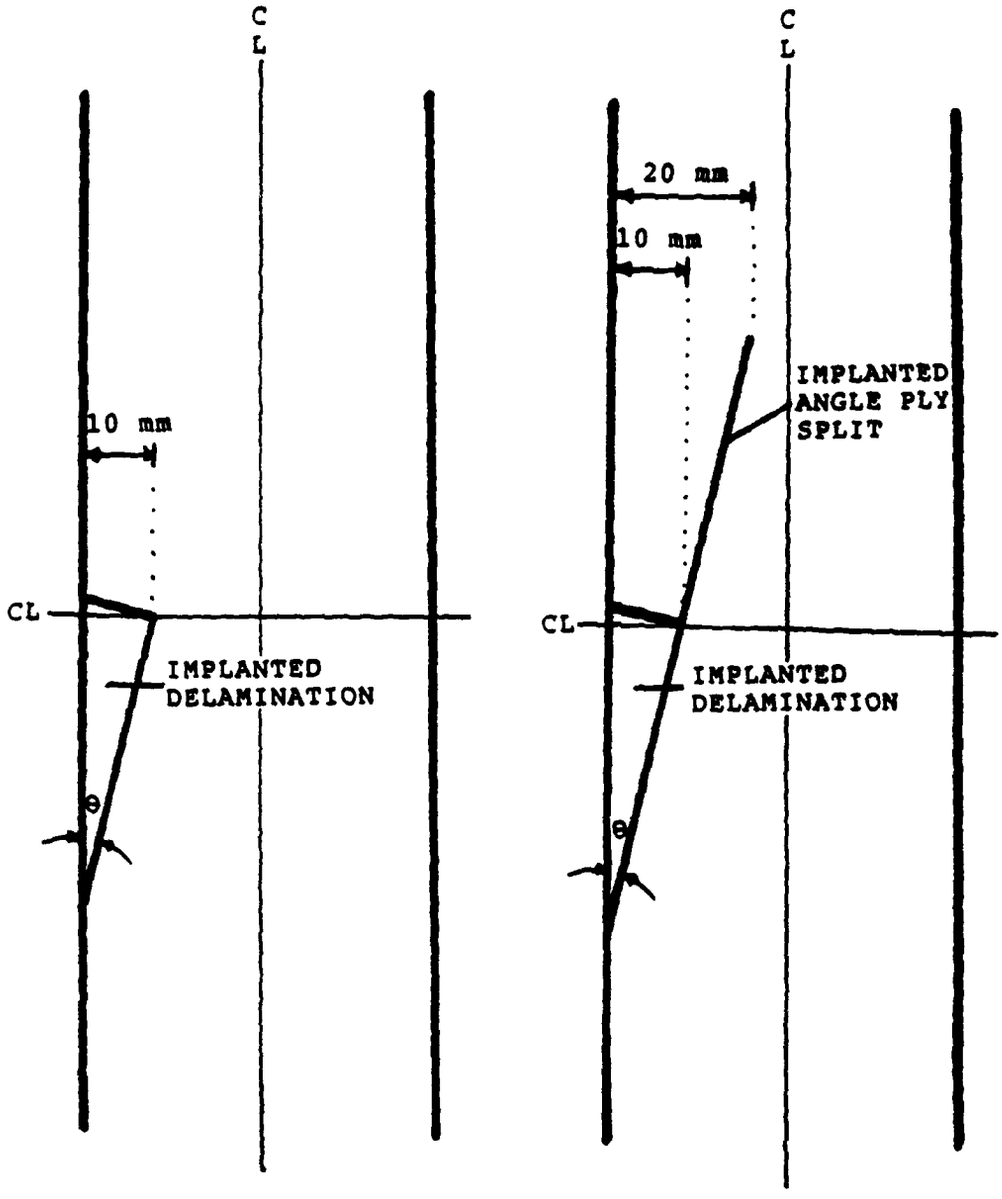

Figure 14 Schematic of specimens with implanted delaminations.

advantage over comparable $[\pm 15_n/0_n]_s$ laminate types because the angle ply split is confined to one sublaminate. Having one relatively thick sublaminate with an angle ply split instead of two thinner ones simplified the manufacturing process. An implanted delamination was positioned at each +15/-15 interface. These delaminations were aligned through the thickness so as to be symmetric with respect to the midplane of the specimen.

The size of a delamination can be characterized by the maximum distance from the free edge or "intrusion" as illustrated in Figure 10. The intrusion of the delamination in both cases was nominally 10 mm. The intrusion of the angle ply split was 20 mm.

These experiments were designed to give information about the progression of damage in delamination growth. The specimens were tested to the same load levels as similar specimens with no implanted damage were as described in section 4.2. The damage state was monitored after each test with dye penetrant-enhanced x-radiography. The specimens were eventually tested to final failure. The summary of failure stresses and strain are provided in Table 14. There does not appear to be any experimentally significant difference in the final failure stress of these two implanted damage types versus such specimens without implanted damage.

There was usually little delamination growth seen in either specimen type before failure. Angle ply splits did form in the $[+15_3]$ and $[-15_6]$ sublaminates in the delaminated region. In some instances, the splits in the $[+15_3]$ sublaminates extended between the region of the implanted delamination and the free edge. In

Table 14 Modulus and failure data for $[0_3/\pm15_3]_s$ specimens with implanted delaminations

Nominal Intrusion of the Implanted Delamination [mm]	Nominal Intrusion of the Implanted Angle Ply Split [mm]	Modulus [GPa]	Failure Stress [MPa]	Failure Strain [μstrain]
10	0	114 (3.1%)[a]	775 (1.8%)	6708 (2.5%)
10	20	112 (5.2%)	697 (2.4%)	6253 (5.9%)

[a]Numbers in parentheses are coefficients of variation.

these cases, the delamination front advanced slightly to include this region.

Angle ply splits did form spontaneously at the edge of the delaminated region in specimens with implanted delaminations alone. Thus, the state of stress in the vicinity of that edge of the delamination must be conducive to such formation. The fact that the splits did not extend beyond the edge of the implanted delamination indicates that the splits cannot extend arbitrarily beyond the delaminations and that the split growth is not independent of the growth of the delamination.

The interaction of the delaminations and the angle ply splits appears quite strong in these specimens. Under tanding the details of what occurs at their intersection may be instrumental to understanding how growing delaminations can be arrested and how arrested delaminations can reinitiate. A study of this interaction is warranted.

A complete description of this effort is presented in Reference 11.

4.6 Analysis of Delamination Growth

The delamination shapes observed in the previous parts of this work are significantly different from those reported and modeled in the literature. The currently observed shapes are more representative of those which would be encountered in multidirectional laminates. Although the strain energy release rate models work well for some cases in the literature, they do not work well for the damage observed in this investigation. In

the literature, the delaminations are generally modeled as strips along the free edge. The laminates investigated in the literature usually contain 90° plies.

The differences in these shapes are important. Since the delamination shape is triangular, the width is in no sense constant as is often assumed in the literature. Most of the delamination is bounded by an angle ply split meaning that a portion of the ply near the split may be partially or totally unloaded and that interaction with in-plane damage is taking place.

A finite element model equivalent to a virtual crack closure method was formulated to provide baseline information about the strain energy available for release near the free edge and then incorporated into a more general model. The details of this formulation and the results are presented in Reference 11. These are not presented here due to the fact that the model was not successful in capturing the intricacies of the physical situation. The model was a two-dimensional representation and the work clearly indicates that a full three-dimensional model must be pursued in order to analyze the interaction of the in-plane and out-of-plane damage modes. This was beyond the scope of the current work.

5. SUMMARY

Jamison's statement regarding the failure of advanced composites [22] is an eloquent summary of the problem: "Failure can be preceded by a complex and interacting global ensemble of discrete damage modes." Delamination of graphite/epoxy composites is a complicated process which has defied numerous attempts at simple explanation. Research has shown that it has several stages, each of which appears to reveal additional intricacies with every investigations. The work over the past contract year has attempted, with some success, to resolve issues of delamination initiation, growth, and final failure.

5.1 Delamination Initiation

Delamination initiation is a critical stage in the failure of graphite/epoxy induced by delamination. Delamination initiation, like any event, is controlled to some extent by energy considerations. Nonetheless, energy criteria are in general necessary rather than sufficient conditions. Fracture mechanics methodologies, such as the strain energy release rate, are derived in terms of crack tip stress fields. The delamination initiation occurs, by definition, without a preexisting interlaminar crack. Local stress levels may be insufficient over large enough areas to form the initiation even though initiation and growth may be energetically feasible.

The existence of high stress gradients and possible weak singularities near free edges makes point stress criteria

inappropriate. Inhomogeneity and initial flaw distribution become potentially important micromechanical issues. The use of an average stress approach mitigates these effects by considering a large enough region that these issues effectively become unimportant. Thus, an average stress approach can be used to characterize this complex behavior.

The Quadratic Delamination Criterion has been shown to be an acceptable criterion for delamination initiation for several reasons. First, it gives excellent agreement of the data as reported herein and in other sources [e.g. 4]. Second, the experimentally determined averaging dimension appears to be a material parameter. Third, the interlaminar normal strength parameter determined by direct experiment works well. Fourth, the potential importance of thermally-induced interlaminar stresses and interlaminar normal stresses have been demonstrated. It appears that, with the additional work reported herein, that the Quadratic Delamination Criterion is sufficient to describe the initiation of delamination in graphite/epoxy composites. Care must be taken, however, to include the effects of thermally-induced stresses and interlaminar normal stresses as well as the interlaminar shear stress.

With its applicability proven for the case of the straight free edge, the criterion should be utilized for more complicated cases such as ply dropoffs and holes in laminates. The work during the past year has shown that, at least for holes, the issues and some parameters are similar as for the case of the straight free edge. Work should progress to calculate the

interlaminar stress state at the edge of the hole and careful experiments be done to measure the experimental delamination initiation stress and location and compare this to predictions. Work can then proceed to other loading types, shear, bending, and the like. Furthermore, work should commence on cyclic loading to determine whether the strength of materials approach is also applicable for the initiation of delamination under cyclic loading.

5.2 Delamination Growth and Final Failure

Energy criteria are necessary but insufficient conditions for delamination growth as well as delamination initiation. The data presented herein show that there must be delamination initiation before there can be delamination growth. Thus, the difference between initiation and growth is that an interlaminar crack is already present. This makes fracture mechanics methodologies such as the strain energy release rate more likely to apply once the delamination initiation has formed.

Laminates with greater effective ply thicknesses were shown to be susceptible to delamination initiation at lower stresses. These laminates have larger regions of high interlaminar stress near the free edge. Thus, they are susceptible to delamination initiation, growth, and final failure at lower stresses.

The work clearly indicates that the growth of delamination and the contribution of delamination to final failure is not an isolated one but is an effect which interacts with in-plane damage modes, specifically angle ply splitting. The key to understanding

the growth of delamination and final failure due to delamination is in understanding the interaction of these damage modes. Depending on the orientation with respect to the delamination front, splits that form ahead of the delamination front can blunt it and hinder its advance. The details of this interaction should thus be investigated both analytically and experimentally. The analytical investigation must include a full three-dimensional analysis, most likely finite element, to properly model the delamination and the angle ply splits. A number of effects must be considered when developing such a model. These issues have been shown herein: the constraint of intact sublaminates, the nature of the ply interface, and others.

It is recommended that work continue on the straight free edge coupon before proceeding to more complicated, and real-life, situations. It is necessary to first understand the physics and mechanisms involved in this very simple case before introducing the added complexity of a hole or other configuration.

REFERENCES

1. A.C. Jackson, "Testing of the L-1011 Advanced Composite Vertical Fin", *Proceedings of the Sixth Conference of Fibrous Composites in Structural Design*, AMMRC-MS-83-2, Army Materials and Mechanics Research Center, 1983.

2. P.A. Lagace, J.C. Brewer, and C.F. Varnerin, "TELAC Manufacturing Course Notes", Edition 0-3, TELAC Report 88-4, Massachusetts Institute of Technology, September, 1987.

3. T.K. O'Brien, "Characterization of Delamination Onset and Growth in a Composite Laminate", *Damage in Composite Materials, ASTM STP 775*, American Society for Testing and Materials, 1982, pp. 140-167.

4. J.C. Brewer and P.A. Lagace, "Quadratic Stress Criterion for Initiation of Delamination", *Journal of Composite Materials*, Vol. 22, December, 1988, pp. 1141-1155.

5. E.C. Klang and M.W. Hyer, "Damage Initiation at Curved Free Edges: Application to Uniaxially Loaded Plates Containing Holes and Notches", *Recent Advances in Composites in the United States and Japan, ASTM STP 864*, American Society for Testing and Materials, 1985, pp. 62-90.

6. C. Kassapoglou and P.A. Lagace, "An Efficient Method for the Calculation of Interlaminar Stresses in Composite Materials", *Journal of Applied Mechanics*, Vol. 53, December, 1986, pp. 744-750.

7. C. Kassapoglou and P.A. Lagace, "Closed Form Solutions for the Interlaminar Stress Field in Angle-Ply and Cross-Ply Laminates", *Journal of Composite Materials*, Vol. 21, 1987, pp. 292-308.

8. F.W. Crossman, W.J. Warren, A.S.D. Wang, and G.E. Law, "Initiation and Growth of Transverse Cracks and Edge Delamination in Composite Laminates. Part 2. Experimental Correlation", *Journal of Composite Materials*, Vol. 14 Supplement, 1980, pp. 88-108.

9. P.A. Lagace, C. Kassapoglou, and J.C. Brewer, "An Efficient Method for the Calculation of Interlaminar Stresses in Composite Materials Due to Thermal and Mechanical Effects", *Proceedings of the International Symposium on Composite Materials and Structures*, Beijing, China, June, 1986, pp. 777-783.

10. P.A. Lagace and D.B. Weems, "A Through-the-Thickness Strength Specimen for Composites", *Test Methods for Design Allowables for Fibrous Composites, 2nd Volume, ASTM STP 1003*, American Society for Testing and Materials, 1989, pp. 197-207.

11. J.C. Brewer, "Failure of Graphite/Epoxy Induced by Delamination", TELAC Report 88-6, Massachusetts Institute of Technology, May, 1988.

12. J.C. Brewer, "The Effect of Ply Thickness on the Free Edge Delamination of Graphite/Epoxy Laminates", TELAC Report 85-9, Massachusetts Institute of Technology, May, 1985.

13. P.A. Lagace and A.J. Vizzini, "The Sandwich Column as a Compressive Characterization Specimen for Thin Laminates", *Composite Materials: Testing and Design (8th Conference), ASTM STP 972*, American Society for Testing and Materials, 1988, pp. 143-160.

14. P. Lagace, J. Brewer, and C. Kassapoglou, "The Effect of Thickness on Interlaminar Stresses and Delamination in Straight-Edged Laminates", *Journal of Composites Technology & Research*, Vol. 9, Fall, 1987, pp. 81-87.

15. K. Scribner and T. Wilson, "Delamination of Graphite/Epoxy Laminates under Compressive Loading", TELAC Report 87-19, Massachusetts Institute of Technology, December, 1987.

16. G.C. Grimes and E.G. Dusablon, "Study of Compressive Properties of Graphite/Epoxy Composites with Discontinuities", *Composite Materials: Testing and Design, ASTM STP 787*, American Society for Testing and Materials, 1982, pp. 513-538.

17. R.K. Cannon, "The Effects of Ply Dropoffs on the Tensile Behavior of Graphite/Epoxy Laminates", TELAC Report 87-12, Massachusetts Institute of Technology, May, 1987.

18. P.A. Lagace, "Static Tensile Fracture of Graphite/Epoxy", TELAC Report 82-4, Massachusetts Institute of Technology, April, 1982.

19. R.N. Yancey and K.T. Kim, "Thickness Effects on the Failure of Notched Graphite/Epoxy Laminates", TELAC Report 86-24, Massachusetts Institute of Technology, December, 1986.

20. S.W. Tsai and E.M. Wu, "A Generalized Theory for Strength of Anisotropic Materials", *Journal of Composite Materials*, Vol. 5, 1971, pp. 58-80.

21. G.M. Sadlo and S. L. Brown, "The Contribution of Angle Ply Splits to Delamination Initiation, Growth, and Final Failure in Composites", TELAC Report 87-20, Massachusetts Institute of Technology, May, 1987.

22. R.D. Jamison, "The Role of Microdamage in Tensile Failure of Graphite/Epoxy Laminates", *Composite Science and Technology*, Vol. 24, 1985, pp. 83-99.

APPENDIX A: LIST OF REPORTS GENERATED

The following is a list of the reports which have been generated under this contract effort. Most of these were referenced in the main body of the report and are contained in the Reference section. However, they are again listed here for convenience.

P.A. Lagace and J.C. Brewer, "Quadratic Stress Criterion for Initiation of Delamination", *Journal of Composite Materials*, Vol. 22, December, 1988, pp. 1141-1155 (available as TELAC Report 86-7).

P.A. Lagace and A.J. Vizzini, "The Sandwich Column as a Compressive Characterization Specimen for Thin Laminates", *Composite Materials: Testing and Design (8th Conference), ASTM STP 972*, 1988, pp. 143-160 (available as TELAC Report 86-20).

R.N. Yancey and K.T. Kim, "Thickness Effects on the Failure of Notched Graphite/Epoxy Laminates", TELAC Report 86-24, December, 1986.

P.A. Lagace and J.C. Brewer, "Studies of Delamination Growth and Final Failure under Tensile Loading" presented at Sixth International Conference on Composite Materials, London, England, July, 1987 (available as TELAC Report 87-3).

A.J. Vizzini and P.A. Lagace, "An Elastic Foundation Model to Predict the Growth of Delaminations", *Proceedings of the AIAA/ASME/ASCE/AHS 28th Structures, Structural Dynamics and Materials Conference*, Monterey, California, April, 1987, pp. 776-782 (available as TELAC Report 87-8).

R.K. Cannon, "The Effects of Ply Dropoffs on the Tensile Behavior of Graphite/Epoxy Laminates", TELAC Report 87-12, S.M. Thesis, May, 1987.

K. Scribner and T. Wilson, "Delamination of Graphite/Epoxy Laminates under Compressive Loading", TELAC Report 87-19, December, 1987.

G.M. Sadlo and S. L. Brown, "The Contribution of Angle Ply Splits to Delamination Initiation, Growth, and Final Failure in Composites", TELAC Report 87-20, May, 1987.

J.C. Brewer, "Failure of Graphite/Epoxy Induced by Delamination", TELAC Report 88-6, Ph.D. Thesis, May, 1988.

P.A. Lagace and R.K. Cannon, "Effects of Ply Dropoffs on the Tensile Behavior of Graphite/Epoxy Laminates", *Proceedings of the 4th Japan-U.S. Conference on Composite Materials*, Washington, D.C., June, 1988, pp. 242-252 (available as TELAC Report 88-7).

From: Proceedings of the AIAA/ASME/ASCE/AHS 28th Structures, Structural Dynamics and Materials Conference, Monterey, California, April, 1987, pp.776-782.

87-0879

AN ELASTIC FOUNDATION MODEL TO PREDICT THE GROWTH OF DELAMINATIONS

Anthony J. Vizzini* and Paul A. Lagace**
Technology Laboratory for Advanced Composites
Massachusetts Institute of Technology
Cambridge, MA 02139

Abstract

A study was conducted to determine the growth characteristics of through-the-width delaminations in laminates under uniaxial compression. Twenty-five sandwich columns were manufactured and tested in uniaxial compression. Teflon inserts were used to cause through-the-width delaminations in one of the two facesheets of each specimen. The buckling and subsequent growth of the delaminations were monitored via strain gages data and edge replications. A delamination growth criterion based on a strength of materials approach is proposed. This allows the incorporation of the behavior of the interply matrix region modeled as an elastic foundation. There is a good correlation between the point at which delamination growth was observed and that predicted by the growth model using a simple linear buckling solution.

Nomenclature

A_1	amplitude of buckling mode
c_1	effective fixity coefficient
E	longitudinal modulus of delaminated sublaminate
E_f	modulus of the elastic foundation
f	foundation stiffness parameter
h	sublaminate thickness
I	moment of inertia
G_I	strain energy release rate in mode I
L	sublaminate length
l_u	unsupported (delamination) length
l_u/h	sublaminate slenderness ratio
P_{cr}	critical buckling load
t_f	foundation (interply matrix layer) thickness
t_f/h	foundation-sublaminate thickness ratio
w	out-of-plane deflection
w_{ave}	average deflection
w_c	center deflection
w_{cr}	critical center deflection
x	longitudinal coordinate
Z^{s1}	interlaminar shear strength in the 1-Z plane
Z^{s2}	interlaminar shear strength in the 2-Z plane
Z^t	through-the-thickness strength
σ_{1z}	interlaminar shear stress
σ_{2z}	interlaminar shear stress
σ_{zz}	interlaminar normal stress
σ	average stress
$[\ ]$	indicates sublaminate stacking sequence

* currently Assistant Professor of Aerospace Engineering, Composites Research Laboratories, University of Maryland, College Park, MD, Member AIAA
** Associate Professor of Aeronautics and Astronautics, Member AIAA

Introduction

The understanding of the behavior of delaminations in laminated structures is paramount to the design process of composite components. Delaminations arising from initial imperfections or in-service damage can greatly affect the stiffness and strength of the component. Even in the case of undelaminated structures, delaminations can arise from naturally occurring manufacturing voids and buckling can occur at the ply level leading to gross delamination and failure[1]. The same phenomenon can occur due to events such as impact[2].

The buckling and subsequent growth of delaminated sublaminates can be a controlling factor in the compressive behavior of a component. Two different approaches can be applied in determining the point at which growth will occur. Often the growth of a delamination is predicted to occur whenever the strain energy release rate for a given delamination geometry and material system is greater than the energy required to create an additional amount of surface area thus extending the delamination[3-6]. A strength of materials approach predicts delamination growth to occur whenever the interlaminar stresses in the vicinity of the delamination exceed the strength of the interface[7,8]. In the former method, the release rate is calculated and the required energy is experimentally measured; and in the latter method the state of stress is determined and the interface strength is experimentally measured.

In this study, 25 sandwich column specimens with six-ply facesheets were tested in uniaxial compression in order to observe the buckling and the growth of delaminated sublaminates. Delaminations were placed in one of the two facesheets via a teflon fabric insert. The buckling and subsequent growth of the sublaminate were monitored with strain gages and edge replications. The normal interlaminar stresses in the vicinity of the delamination, which are used in the growth criterion, are calculated based on a one-dimensional linear-elastic model of the delamination geometry.

Elastic Foundation Model

A thin interply resin layer is created during the process of the cure cycle in laminated composites[9]. This thin layer acts as an elastic foundation and thus constrains the deflection of the plies[1]. Thus, a laminate consisting of several plies can be modeled as a series of plates constrained to each other via this elastic foundation. It is this elastic foundation model which is used to study the buckling and growth behavior of delaminations of laminated structures in this study.

Upon the introduction of a delamination, a section of the elastic foundation is considered to have failed. This results in an unsupported region which is defined as a delaminated sublaminate and is free to buckle under compressive load. Generally, the boundary condition at the tip of the delamination is assumed to be clamped in order to determine the buckling behavior of the sublaminate[9,10]. However, this is not an accurate representation of the constraint imposed by the interply matrix region, i.e. the elastic foundation. In actuality, more than just the unsupported portion of the sublaminate buckles. Indeed, regions near the delamination tips also experience out-of-plane deflections which give rise to interlaminar normal stresses within the matrix layer. It is these stresses which lead directly to the failure of the matrix layer and thus the growth of the delamination. Clamped boundary conditions automatically set the deflections within the supported region to zero, and thus interlaminar normal stresses are removed directly.

Proposed Growth Model

The proposed growth criterion is based on a strength of materials approach. In essence, if the stresses are large enough to cause the interply matrix layer to fail, then growth of the delamination will occur. The general technique is to determine the interlaminar strains and thus the interlaminar stresses within the matrix layer.

The key assumption in the proposed growth criterion is that the matrix layer will fracture causing growth of the delamination when the averaged interlaminar normal stress in the interply matrix region reaches a critical value. This is an extension of the Quadratic Delamination Criterion (QDC)[3] originally developed to predict the initiation of free-edge delamination. The QDC predicts delamination initiation to occur whenever

$$\left(\frac{\langle\bar{\sigma}_{ZZ}\rangle}{Z^t}\right)^2 + \left(\frac{\bar{\sigma}_{1Z}}{Z^{S1}}\right)^2 + \left(\frac{\bar{\sigma}_{ZZ}}{Z^{S2}}\right)^2 = 1 \qquad (1)$$

where Z^t is the through-the-thickness strength, Z^{S1} is the interlaminar shear strength in the 1-Z plane, and Z^{S2} is the interlaminar shear strength in the 2-Z plane. The bar over the stresses indicates that this is an average of the interlaminar stresses over a given boundary layer. Compressive interlaminar normal stresses are ignored since it is postulated that they do not contribute to the delamination process on a first-order basis and this is indicated by the brackets around σ_{ZZ}.

In the current proposed criterion, the interlaminar shear stresses are ignored since their values are expected to be small for thin one-dimensional sublaminates and, more importantly, delamination growth is expected to be dominated by the interlaminar normal stress since in other studies G_I is the controlling parameter for thin through-the-width delaminated sublaminates[11,12]. Thus, the value of the average stress is compared to the through-the-thickness strength of the material, Z^t, to determine if fracture is likely to occur.

When buckling occurs, the deflection of the sublaminate near the delamination tips with respect to the remaining intact plies corresponds to strains within the interply matrix region. These strains are directly proportional to the interlaminar state of stress. Therefore, the average stress within the interply matrix region can be found by averaging the deflection over a given distance from the delamination tip; dividing by the thickness of the interply matrix region to give the average strain; and then multiplying this result by the modulus of the matrix region (the elastic foundation modulus) to give the average stress:

$$\bar{\sigma}_{ZZ} = E_f \frac{1}{t_f} w_{ave} \qquad (2)$$

where w_{ave} is the average deflection, t_f is the thickness of the interply matrix region, and E_f is the modulus of the matrix region. As in Eq. (1), only positive deflections, and thus positive stresses, are averaged. A buckled shape is critical when the associated average stress is equal to the through-the-thickness tensile strength, Z^t, of the material.

The averaging dimension was chosen to be 0.178 mm since this has been shown to be the averaging distance necessary to determine the initiation of delamination at a free edge for AS4/3501-6[3]. Furthermore, the through-the-thickness strength used for AS4/3501-6 is 43 MPa which has been obtained via direct measurements[13]. Both the averaging distance and the through-the-thickness strength are material values and do not vary from laminate to laminate.

Thus, the growth model is dependent only on material constants. All that is required is to determine the interlaminar state of stress or, in this case, of the deflections of the elastic foundation. This can be done be a number of methods.

Solution for Buckling Shape

A one-dimensional analysis was developed and utilized to determine the significant parameters and the extent to which the clamped boundary conditions could be moved towards the delamination without effecting its buckling behavior[14]. This indicates how much of the foundation must be included in the analysis. This same analysis produced the initial buckled shape of the delaminated sublaminate and the surrounding region. Although the analysis is a simple solution of the buckling problem, it provides a first-order approximation of the buckled shape.

The delamination sublaminate is modeled as a clamped beam supported near the boundaries by an elastic foundation and unsupported in the center as shown in Figure 1. The unsupported region corresponds to the delamination and the foundation to the interply matrix region. Thus, the bifurcation load and the initial buckled deflection with respect to any given point of the delaminated sublaminate and the surrounding area can be determined.

From the original parametric study, the governing nondimensional parameter in the solution of the bifurcation buckling load and shape is defined as the foundation stiffness parameter, f:

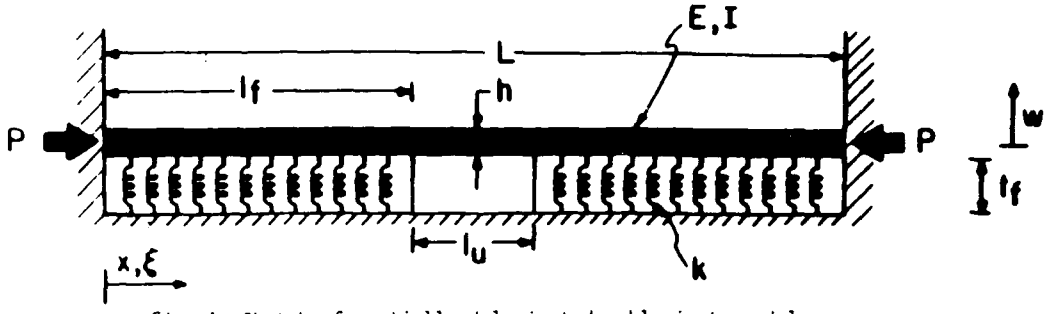

Fig. 1 Sketch of partially delaminated sublaminate model.

$$f = 12\left(\frac{E_f}{E}\right)\left(\frac{l_u}{h}\right)^4\left(\frac{t_f}{h}\right)^{-1} \qquad (3)$$

where E_f is the foundation stiffness; E is the longitudinal modulus of the unsupported beam; the sublaminate slenderness ratio, l_u/h, is the ratio of the delamination length to the sublaminate thickness; and the interply thickness ratio, t_f/h, is the ratio of the foundation thickness to the sublaminate thickness.

Two important values derived from the solution of the one-dimensional problem are the effective fixity coefficient and the normalized deflections at the delamination tip. The effective fixity coefficient, c', is found from the buckling load using the classical Euler equation based on the unsupported length.

$$c' = \frac{P_{cr}}{EI\pi^2/l_u^2} \qquad (4)$$

where I is the moment of inertia of the beam.

To determine the bifurcation point and the initial buckled shape, a Rayleigh-Ritz energy method is used. Mode shapes are assumed in order to determine the total potential energy given by the sum of the bending energy in the sublaminate and the spring energy in the elastic foundation minus the work done by the applied loads at the ends. The potential energy is then minimized with respect to the amplitudes of the individual mode shapes and the buckling load, the eigenvalue, and the buckled shape, the eigenvector, are determined.

In this analysis the assumed shapes are the symmetric cosines given by

$$w(x) = \sum_{i=1}^{N} A_i\{\cos[(2i-2)\pi x/L] - \cos[(2i)\pi x/L]\} \qquad (5)$$

where A_i are the amplitudes of the individual modes and L is the length of the sublaminate which includes the delaminated and the constrained regions. Since this analysis results in only the relative magnitudes of A_i, actual physical deflections are not available. However, the deflection at any point can be found relative to any reference point on the buckled sublaminate. The reference point used to determine the interlaminar normal stress in Eq. 2 is the center of the delaminated sublaminate. Thus Eq. 2 can be rewritten as

$$\sigma_{zz} = w_c E_f \frac{1}{E_f}\left(\frac{w_{ave}}{w_c}\right) \qquad (6)$$

where w_c is the center deflection. When the interlaminar normal stress is equal to the through-the-thickness strength of the material, Z^t, then the corresponding center deflection is the critical center deflection, w_{cr}, at which point the delamination will grow.

The analysis was implemented on a DEC VAX/780 in compilable Basic-Plus-2. The first 20 symmetric cosine modes were used in the assumed shape of w. The bifurcation point is determined and the critical center deflection is calculated. This was done for a {0} sublaminate made from AS4/3501-6 with a delamination length from 5 to 20 mm. For larger delamination lengths, the program produced erroneous values due to roundoff error.

Experimental Program

A total of 25 sandwich column specimens with six-ply facesheets were manufactured and tested. The facesheets all had a $[0/\pm60]_s$ layup and were manufactured from AS4/3501-6 graphite/epoxy in a standard cure cycle of one hour at 116°C and two hours at 177°C under 0.59 MPa pressure and a full vacuum. All laminates were postcured in an oven at 177°C for eight hours. The specimens were formed by bonding two facesheets to a three-part aluminum honeycomb core to achieve the configuration shown in Figure 2. This was done using American Cyanamid FM-123-2 film adhesive in a two hour cure at 107°C and 0.28 MPa pressure. Loading tabs were subsequently applied to the specimen. The resulting specimen provides a large test section, 50 mm x 200 mm, and has been shown to be successful[5] for compressive stress-strain and fracture data[5]. Through-the-width delaminations were placed in one of the facesheets by placing a rectangular 0.08 mm-thick teflon-coated fabric at the first ply interface during the lamination process. This results in a {0} and a {60/-60/-60/60/0} sublaminate. The size of the initial delamination was 50 mm (the width of the specimen) by the desired length. In this study five different delamination lengths were chosen: 3.2, 6.4, 8.9, 12.7, and 18.0 mm. Five specimens of each of the five delamination lengths were tested.

Two of the five specimens in each specimen group were randomly chosen and gaged with three longitudinal gages, two EA-06-125AD-120 and one

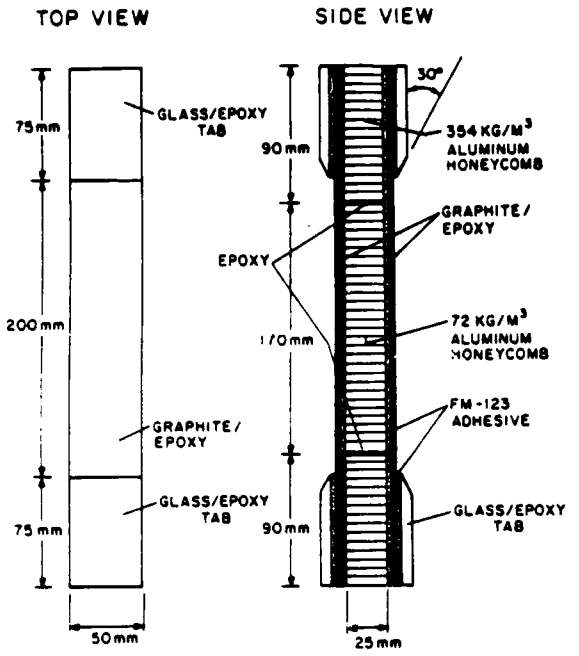

Fig. 2 Physical characteristics of the sandwich column specimen.

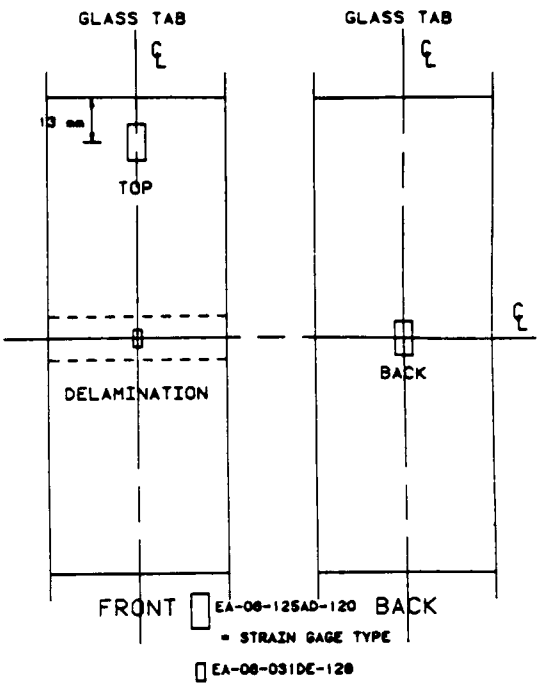

Fig. 3 Diagram indicating the locations of the delamination gage, the back gage, and the top gage.

EA-06-031DE-120. The locations of the three gages were chosen to be at key points in order to observe the effects of the buckling and growth of the delaminated sublaminate on the local and global behavior of the specimen. These locations are shown in Figure 3. The longitudinal gage on the back facesheet and the top longitudinal gage on the front facesheet monitor the global effect of the buckling and growth of the delamination by measuring the local modulus throughout the test. The gage over the delamination monitors the buckling of the sublaminate through strain reversal and the growth of the delamination through strain relaxation. A small gage was used in order to minimize the effect of the gage on the buckling and growth of the delaminated sublaminate. These two specimens provided an indication of when the delamination buckles and grows.

The remaining three specimens in each group were prepared for edge replication. The edges were milled smooth during the manufacturing process using a water-cooled diamond-encrusted wheel so that the facesheets and honeycomb core were of the same widths. This prevents the honeycomb from interfering with the edge replication. One edge of the top facesheet, which contains the implanted teflon insert, was polished in order to provide a smooth surface for the edge replication. The polishing was done with a felt bob soaked in a colloidal solution formed by two parts water and one part Kapolite-SF, a fine abrasive with an average particle size of 0.7 microns. The edge was cleaned with water.

An initial replication is taken of the column specimen along the smooth edge prior to loading. The specimen is clamped outside of the testing machine so that it is in its free-hanging state. The smooth edge is cleaned with a piece of acetone-soaked cheese cloth and allowed to dry. A piece of 25 mm-wide acetate film approximately 100 mm long is placed against the smooth edge. Acetone is applied near the top of the tape using a squeeze bottle and allowed to flow down the edge of the specimen. The tape is pressed against the edge using a rounded instrument. After the tape has dried, it is carefully removed and the edge is once again cleaned with acetone in order to remove any residue left by the tape. The tape is then placed between two pieces of glass and examined using a microscope. Any minor or global surface flaws along the replicated edge will appear in the acetate tape.

Replications are taken in the same manner during the test after the machine has been stopped. A replication was taken at about 75% of the load at which the initial delamination was expected to grow as determined from the specimens with a strain gage over the delamination. Additional replications were taken whe never growth was observed to have occurred. Growth was judged to occur whenever the delamination length appeared longer or whenever an audible click was heard. In these cases the loading ramp of the testing machine was halted and the load reduced by 10% to prevent further growth from occurring during the replication process. When the delamination grew to about 25 mm in length, the acetone would collect at the bottom of the delamination and would ruin the edge replication. Thus, replications were generally not performed above this length. After this point, the specimens were loaded in compression until failure at which point they were photographed and removed from the

testing machine. All testing was conducted with an MTS 810 testing machine with hydraulic grips. The tests were conducted in stroke control with a stroke rate of 1.09 mm per minute which is approximately equivalent to 5400 microstrain per minute in the test section. Data was taken automatically at 0.25 or 0.50 second intervals.

Results

The results of the analysis consist of the bifurcation load and the buckled shape. Only the shape of the buckled sublaminate and its surroundings is known, not the actual magnitude of the deflections for any given load in the post buckling regime since the analysis is a linear bifurcation model. For this study it is assumed that this shape is maintained throughout the entire post buckling region. Thus, the deflection of the sublaminate is simply the bifurcation shape multiplied by a scalar. The interlaminar normal stresses in the interply matrix layer, which are calculated from the out-of-plane deflections, are therefore proportional to the center deflection, w_c, of the delaminated sublaminate.

The deflections of the interply matrix layer based on the buckling model for an 8 mm-long AS4/3501-6 {0} sublaminate are shown in Figure 4 as an example of the output from the analysis. The deflections are normalized with respect to the center deflection. The distance along the x-axis is measured from a location away from the delamination. Thus, the delamination begins in this figure at 1 mm, and the region over which the deflections are averaged is 0.822 to 1.000 mm. In applying the failure criterion, part of the deflection within this averaging region is negative and, therefore, not included in the average.

The edge replications taken of the specimens prior to and during the loading provide a permanent record of the growth of the delaminations. Under the microscope, several points of interest could be seen clearly. In all cases, the delamination tips were observable. This usually coincided with the tip of the opening. Often, white lines indicating a possible delamination front which remained closed at the time of the replication were also observed.

Key measurements were made of each replication. These include the location of the left and right delamination tips and the maximum height of the buckled sublaminate. The height was defined to be the distance from the bottom of the buckled sublaminate to the top of the remaining intact plies of the laminate. The presence of the teflon fabric in the edge replications was discounted. Thus, the height is equal to the out-of-plane deflection of the sublaminate.

Using the one-dimensional linear buckling analysis, the critical center "height" at which growth of the delamination initiates is predicted. This height is compared to the measured heights from the replication data. These are plotted versus the delamination length in Figure 5. The prediction only extends to 20 mm since above this point, the computer program produces erroneous values due to roundoff error. The dotted line represents an extrapolation of the predicted values based on the linear regression of values from 17 mm to 20 mm. The experimental values indicate a linear behavior, and thus the line of best fit is included in the figure as the dashed line.

Discussion

The key concept throughout this study in terms of delamination buckling and growth is the ability of the interply matrix region to act as an elastic foundation. From this concept, the model of a sublaminate restrained by an elastic foundation was introduced. A delamination between the sublaminate and the remaining intact plies is represented by the removal of this elastic foundation.

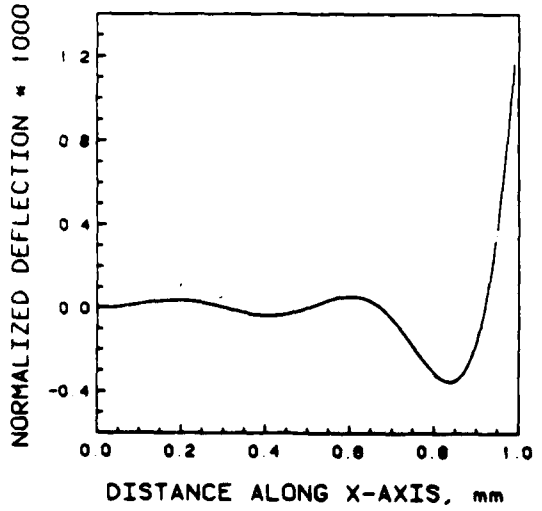

Fig. 4 Normalized out-of-plane deflections in the region of the elastic foundation for an 8 mm delamination.

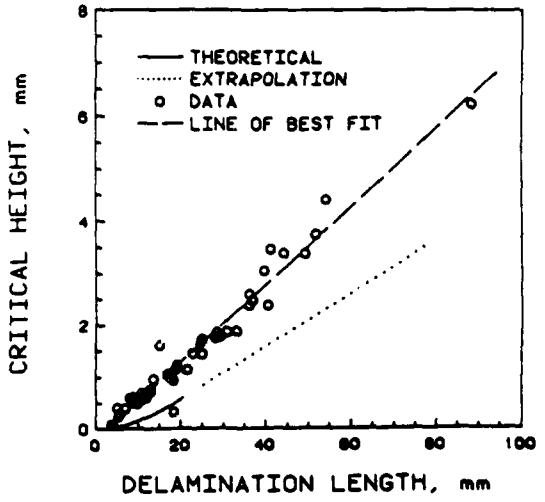

Fig. 5 Measured maximum heights and predicted critical heights for a 0^0 sublaminate versus delamination length.

Thus, no assumption is made of the constraint at the tip of the delamination, and out-of-plane deflections are free to occur in the region of the sublaminate constrained by the elastic medium.

It should be noted that the model is a representation of the physical interface between the plies. In practice, the properties of this interface, modulus and geometry, are not uniform throughout the laminate. This model, therefore, represents the interface on an "average", and the effects of eccentricities such as varying interply thickness, inclusions, and fiber "wandering" are not included.

The inclusion of the interply matrix layer acting as an elastic foundation has a great effect in determining the growth point and growth behavior of delaminated sublaminates. When the boundary conditions at the delamination tip are assumed to be clamped, the normal deflections are assumed to be zero. Analyses which assume clamped boundary conditions cannot be used directly to determine the stresses within the matrix layer, and thus cannot be used to determine growth from a strength of materials approach. By including the effect of the foundation and increasing the region which is allowed to deflect and buckle beyond the delaminated sublaminate, the state of interlaminar stress around a delamination can be determined.

There is a general correlation between the data and the prediction in Figure 5. Although the values differ by as much as a factor of two, there are similar trends. One important reminder is that the linear model assumes that the initial buckled shape at the point of bifurcation is maintained into the post buckling region. In actuality, the shape of the buckled sublaminate and thus the ratios between the center deflection and the deflections at locations in the sublaminate will vary as additional load is applied past the buckling point. Also the value for the interply thickness ratio, t_f/h, is only an estimate and was not measured in the context of this study. What is important to note is that this rather simple one-dimensional linear-elastic model yields stresses which predict growth initiation well within the same order of magnitude as is observed.

One limitation of this solution is that the growth point cannot be determined in terms of the applied load. Since postbuckling deflections cannot be determined by the linear buckling model, the applied load cannot be associated to a given buckled deflection. The growth point can only be predicted by a critical center deflection. This limitation is caused by the method used to determine the deflections near the delamination tip and not by the model of the elastic foundation. A nonlinear postbuckling analysis would predict the deflections in the foundation for a given applied load. Any improvement in predicting the deflections of the interply matrix region will result in a better prediction of the growth point and thus, give further evidence of the applicability of the foundation model on delamination growth.

Summary

This basic model represents a working basis form which to build a methodology to predict the growth of delamination due to sublaminate buckling using the strength of materials approach. The concept of the interply matrix layer acting as an elastic foundation has been the only addition to an otherwise simple handling of the buckling of a delamination. This basic formulation has shown merit in determining the point of the growth in terms of a critical center deflection. Additional refinements such as the extension to two dimensions and the encompassment of general nonlinear behavior and the post buckling region would greatly enhance this initial analysis. Considerations of initial deflections and other eccentricities would, again, further this analysis.

Acknowledgements

This work was supported by the Air Force Office of Scientific Research under Contract number F49620-83-K-0015 and Grant No. AFOSR-85-0206.

References

1. Vizzini, A.J. and Lagace, P.A., "The Role of Ply Buckling in the Compressive Failure of Graphite/Epoxy Tubes," AIAA Journal, Vol. 23, No. 11, November 1985, pp. 1791-1797.

2. Williams, J.G. and Rhodes, M.D., "The Effect of Resin on the Impact Damage Tolerance of Graphite/Epoxy Laminates," NASA Technical Memorandum 83213, October 1981.

3. O'Brien, T.K., "Interlaminar Fracture of Composites," NASA Technical Memorandum 85768, June 1984.

4. Webster, J.D., "Flaw Criticality of Circular Disbond Defects in Compressive Laminates," 1980-1981 Interim Report, NSG 1034, Center for Composite Materials, University of Delaware, Newark, Delaware, 1982.

5. Bottege, W.J. and Maewal, A., "Some Aspects of Delamination Buckling and Growth in Layered Plates," Proceedings of ASME Winter Meeting, November 1983, pp. 179-186.

6. Chai, H. and Babcock, C.D., "Two Dimensional Modelling of Compressive Failure in Delaminated Laminates," Journal of Composite Materials, Vol. 19, January 1985, pp. 67-98.

7. Kim, R.Y. and Soni, S.R., "Experimental and Analytical Studies on the Onset of Delamination in Laminated Composites," Journal of Composite Materials, Vol. 18, January 1984, pp. 70-80.

8. Brewer, J.C. and Lagace, P.A., "Quadratic Stress Criterion for Initiation of Delamination," submitted to Journal of Composite Materials.

Paul A. Lagace[1] *and Anthony J. Vizzini*[2]

The Sandwich Column as a Compressive Characterization Specimen for Thin Laminates

REFERENCE: Lagace, P. A. and Vizzini, A. J., **"The Sandwich Column as a Compressive Characterization Specimen for Thin Laminates,"** *Composite Materials: Testing and Design (Eighth Conference), ASTM STP 972*, J. D. Whitcomb, Ed., American Society for Testing and Materials, Philadelphia, 1988, pp. 143-160.

ABSTRACT: A study was conducted to evaluate the reliability of a sandwich column specimen for uniaxial compressive tests. Both stress strain and failure behavior were observed, and comparisons were made with predictions from existing techniques. The properties of the aluminum honeycomb core were also measured and included in the analysis to show its limited effects on the overall behavior of the specimen. Control tests were performed on specimens with aluminum facesheets to further quantify the effect of the honeycomb core on the overall behavior of the structure. The main battery of tests was conducted with graphite/epoxy facesheets of $[0_{12}]$, $[+\theta/0]_s$, and $[0/\pm\theta]$, configurations. The general excellent correlations between the observed moduli and Poisson's ratios and predicted values indicate that the specimen provides true stress-strain behavior. Moreover, consistent failure modes within the test section including both in-plane failure and ply buckling or delamination failure followed by in-plane failure indicate that the specimen is valid for failure behavior data.

KEY WORDS: compression, composites, test methods, sandwich column, graphite/epoxy, mechanical properties, failure

The development of a reliable compression specimen for thin laminated plates has been a key issue in determining the overall compressive behavior, that is, both stress-strain and fracture/failure, of composite materials. No specimen type to date has proven to be effective for general thin laminates. Current specimen configurations either cannot be used with a thin laminate with an arbitrary layup or impose an artificial constraint on the test article thereby restricting certain valid failure modes.

Specimens which depend on a fixture such as the IITRI test fixture [1] or the other recommended by the ASTM Standard Test Method for Compressive Properties of Unidirectional or Crossply Fiber-Resin Composites [D 3410-75 (1982)], although reliable, can be used only with relatively thick specimens (one to several millimetres thick) in order to preclude global Euler buckling. Furthermore, the resulting test section is small. This limits the usefulness of the specimen for other test programs such as monitoring damage growth under cyclic loads.

Other specimens which do incorporate thin laminates as the test article prevent legitimate failure modes by imposing artificial boundary conditions. Supporting jigs, while preventing overall buckling (as is their purpose), prevent the legitimate local failure of ply buckling [2]. The test section in sandwich beams is placed in compression via a four-point load application

[1]Associate professor, Technology Laboratory for Advanced Composites, Department of Aeronautics and Astronautics, Massachusetts Institute of Technology, Cambridge, MA 02139.

[2]Currently, assistant professor, Department of Aerospace Engineering, University of Maryland, College Park, MD 20742.

3]. This load application results in a moment couple which imposes a curvature in the test ection along with the compressive load. However, it is this curvature which can prevent ply buckling or delamination failure [4].

In this study, a uniaxially-loaded sandwich column was further developed and used to investiate the compressive behavior of graphite/epoxy laminates. The specimen is a refinement of ne used in a study by Lagace and Nolet [5]. Both stress-strain and failure behavior were observed and correlated to existing elastic and failure predictions. The honeycomb substructure as individually tested and evaluated to better quantify the behavior of the specimen.

pecimen Description

The uniaxial column specimen used throughout this study is composed of two 350-mm by 50-m graphite/epoxy facesheets bonded to a three-part honeycomb core with film adhesive as hown in Fig. 1. The three-part honeycomb core is manufactured from two 63-mm by 88-mm heavyweight" (354 kg/m^3) and one 63-mm by 175-mm "lightweight" (72 kg/m^3) aluminum oneycomb manufactured by American Cyanamid. All of the honeycomb sections are 25 mm hick. The substructure is fabricated by glueing the three pieces together using a room temperare epoxy.

Experimentally, it has been noted that the orientation of the lightweight honeycomb is impornt in the stress-strain behavior of the column [6]. The lightweight honeycomb is aligned so hat the ribbon direction coincides with the direction of negative strain.

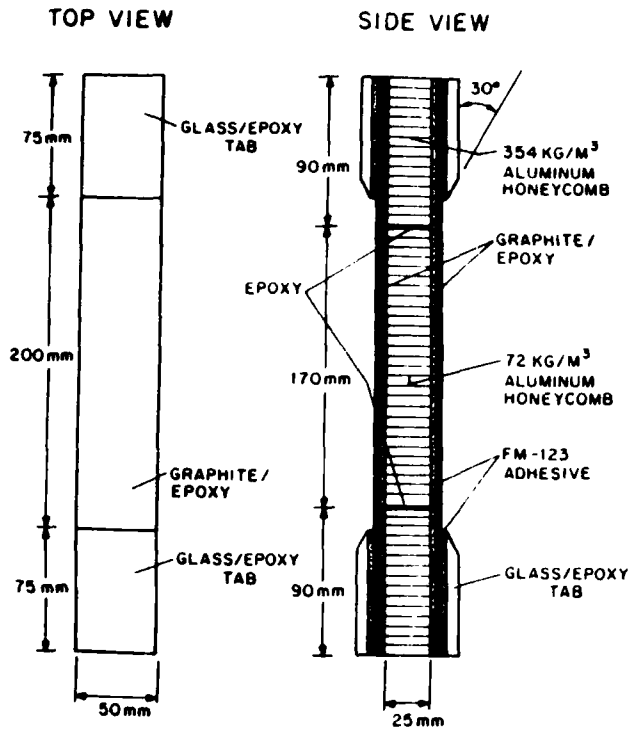

FIG. 1—*Physical characteristics of the sandwich column specimen.*

The column is formed by bonding the two identical facesheets to the honeycomb substructure with FM-123 film adhesive (from American Cyanamid). Care is taken to guarantee that the resulting beam is itself symmetric about its centerline. The bond is achieved in two hours at 108°C under 0.28 MPa pressure. The bond assembly is bagged and vented to atmosphere so that the individual honeycomb cells would be at atmospheric pressure after the bond. Cells at a lower pressure than atmospheric will result in a crushing of the honeycomb, whereas cells at a higher pressure will result in a bad bond. A second bonding cure is performed in order to bond beveled fiberglass loading tabs to the structure. These tabs are of the same proportions and basic configuration as those for the ASTM Standard Test Method for Tensile Behavior of Fiber-Resin Composites (D 3039-76). This bond was carried out in the same manner as the first, with the assembly again bagged and vented to atmosphere.

One of the advantages of the specimen is that it is of the same configuration as the ASTM tensile coupon. Load is introduced via hydraulic grips. Thus, the specimen can be used in tension-compression cyclic loadings. The heavyweight aluminum section of the substructure can withstand approximately 3.5 MPa of grip pressure for load introduction. For greater grip pressures, solid aluminum with the same dimensions is substituted for the "heavyweight" aluminum honeycomb. It should be noted that in this work, it was necessary to use solid aluminum for the $[0_n]$ specimens.

Honeycomb Tests

A total of 72 honeycomb specimens were manufactured and tested in order to determine the elastic properties of the honeycomb. Three different densities of aluminum honeycomb were used, "lightweight" (72 kg/m^3), "mediumweight" (194 kg/m^3), and "heavyweight" (354 kg/m^3). The honeycomb is manufactured from 5052 aluminum with a 3.175-mm cell and supplied by American Cyanamid. Tension specimens were 350 mm long by 50 mm or 100 mm wide. Glass tabs were bonded across the entire width at both ends of a specimen and drilled. The specimen was hung on a fixture and mass was added to a basket in increments of 0.2 to 2.2 kg for the lightweight depending on specimen width, 4.4 kg for the mediumweight, and 11 kg for the heavyweight honeycomb. Compressive specimens were 300 mm long by 50 mm or 100 mm wide. A piece of fiberglass was epoxied to the top and bottom of these specimens, and load was introduced by weights placed on the top of the specimen. The specimen was inside of a restraining jig which prevented overall column buckling. On both types of specimens, fabricated aluminum channels were glued to a reference cell on each side of the specimen in order to facilitate the measurement of transverse strain. Both tension and compression specimens are shown in Fig. 2 in their respective test setups.

For each specimen width, three specimens were manufactured with the ribbon direction coincidental with the loading direction and three with the ribbon direction perpendicular to the loading direction (nonribbon). This entire test matrix is summarized in Table 1. Dial gages were used in all of the tests in order to measure the longitudinal and transverse elongation. In both types of tests, two dial gages were used to measure the transverse elongation, one on each side of the specimen. In tension, longitudinal elongation was measured by one gage located beneath the applied weight. In compression, two gages were used, one on either side of the loading bar. The placement of the dial gages was such that small unconstrained rotations would not affect the measurements.

The results of the honeycomb tests are in terms of the two elastic moduli, E_l and E_T, and the two Poisson's ratios, ν_{LT} and ν_{TL}, for each of the two widths for both tension and compression. These results are summarized in Table 2. No results are available for the heavyweight honeycomb compressive specimens since the loads required for measurable elongation were too great for reliable use of the compression jig. It is important to note that the loads applied were kept low in order to keep the average longitudinal strain below 4%.

The difference between the modulus in the ribbon and nonribbon directions is attributed to

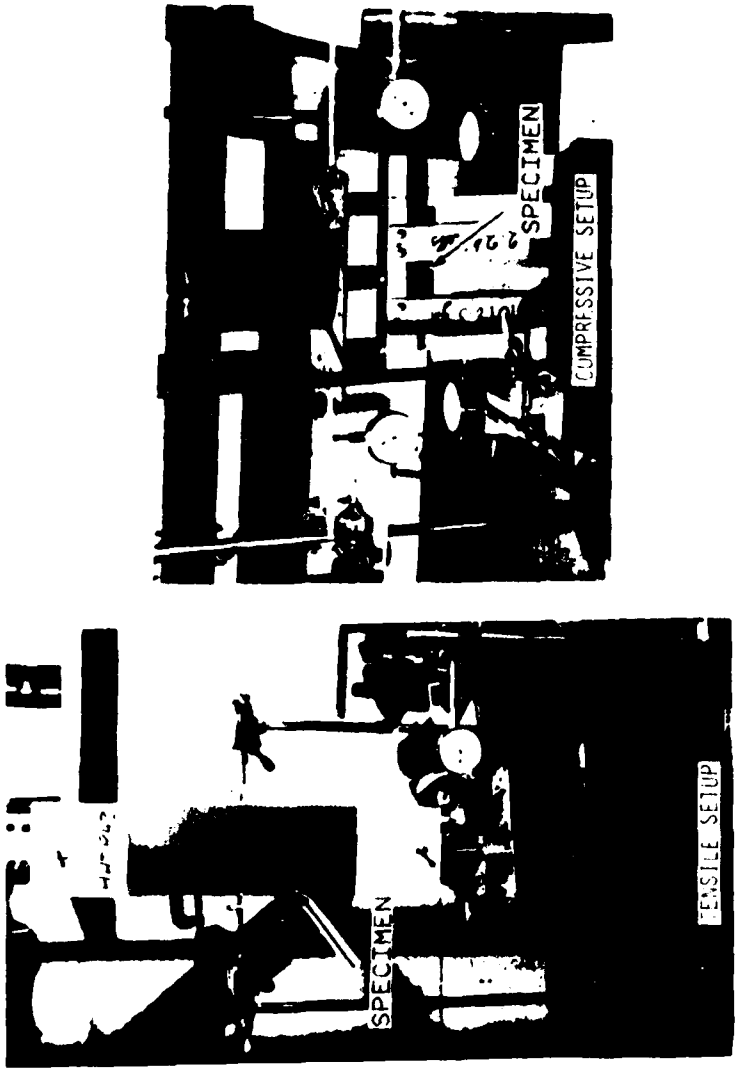

FIG. 2—*Setups for tension and compression honeycomb tests.*

TABLE 1—*Test matrix for honeycomb specimens.*

Specimen Type	Ribbon Direction 50-mm width	Ribbon Direction 100-mm width	Nonribbon Direction 50-mm width	Nonribbon Direction 100-mm width
		LIGHTWEIGHT (72 KG/M^3)		
Tension	3[a]	3	3	3
Compression	3	3	3	3
		MEDIUMWEIGHT (194 KG/M^3)		
Tension	3	3	3	3
Compression	3	3	3	3
		HEAVYWEIGHT (354 KG/M^3)		
Tension	3	3	3	3
Compression	3	3	3	3

[a]Number of specimens tested.

TABLE 2—*Honeycomb test results.*

Specimen Type	width, mm	E_L, MPa	E_T, MPa	ν_{LT}	ν_{TL}
Lightweight tension[a]	50	1.09	0.319	1.48	0.548
	100	1.07	0.376	1.67	0.568
Lightweight compression[a]	50	1.08	0.165	2.65	0.361
	100	1.02	0.164	2.16	0.449
Mediumweight tension[b]	50	10.8	2.92	1.84	0.480
	100	11.3	2.92	2.12	0.444
Mediumweight compression[b]	50	5.82	1.78	1.16	0.370
	100	3.80	1.95	0.598	0.409
Heavyweight tension[c]	50	48.4	27.2	1.22	0.564
	100	30.5	18.1	0.932	0.402

[a]72 kg/m^3.
[b]194 kg/m^3.
[c]354 kg/m^3.

the orthotropic nature of the honeycomb. The slight differences between the values for the 50-mm- and 100-mm-wide specimens are due to the inability to properly load the 100-mm-wide specimen in some cases. Therefore, the results from the 50-mm-wide specimens are used in the following assessment of the effect of the honeycomb core on the overall behavior of the specimen since the composite specimen is 50 mm wide.

Assessment of Effect of Honeycomb Core

An assessment of the effect of the lightweight honeycomb on the stress-strain behavior of the entire specimen is made by utilizing classical laminated plate theory. If the elastic properties of the lightweight honeycomb are included as part of the laminated plate, the effective moduli and Poisson's ratios for specimens with the two different orientations of honeycomb core (ribbon

and nonribbon) can be calculated. The effective values can be compared to a similar column with a core which carries no load; that is, the moduli of the core are zero. Three graphite/epoxy layups were chosen for this analytical evaluation: $[0_{12}]$, load in the fiber direction; $[90_{12}]$, load perpendicular to the fiber direction; and $[0/\pm 60]_s$, quasi-isotropic. The values of the longitudinal modulus based on the overall thickness and the Poisson's ratio are given for each of the three layups in Table 3 for the three possible core configurations: ribbon, nonribbon, and no-load. In this analysis, the film adhesive layer was considered to be a perfect bond and load transfer mechanism. The graphite/epoxy properties used for these calculations are listed in the first column of Table 6.

This analysis indicates that the stress-strain behavior of the laminate is negligibly affected by the presence of the honeycomb substructure, as is evidenced by the values in Table 3. In order to illustrate any difference in the calculated elastic properties of the various sandwich columns with the three different types of cores, it is necessary to carry out the calculations to two or three decimal places. This can be seen in Table 3. These results would indicate that for the range of strains generally considered, the presence of the lightweight honeycomb core will have no discernible effect on the stress-strain behavior of the composite facesheets and the overall structure.

In order to further assess the effects of the honeycomb core, two sandwich column specimens, as well as one coupon, were manufactured with aluminum facesheets, strain gaged, and tested. The facesheets and coupon were cut in the same orientation from a single piece of 0.80-mm-thick 5052 aluminum. The lightweight honeycomb was oriented in the ribbon direction in one column and in the nonribbon direction in the other column. Both columns were twice loaded in compression, unloaded, and ungripped. Then the columns were loaded in compression, unloaded, loaded in tension, unloaded, and ungripped. The tensile coupon was twice loaded in tension and unloaded. Load and strain data were taken along all loading and unloading segments. A summary of the stress-strain results is provided in Table 4. In all cases, the column specimens exhibited the same modulus during the tension load segment as in the previous compression unload segment, and these results are thus reported in the same column.

The aluminum/aluminum specimens indicate that the lightweight honeycomb has little, if any, effect on the overall stress-strain behavior of the aluminum facesheets. In spite of the small number of aluminum/aluminum specimens, the repeatability of the tests and the fact that the

TABLE 3—*Calculated effect of honeycomb substructure on elastic constants.*

Layup	Loading	Core		
		Ribbon	Nonribbon	No-load
$[0]_{12}$	tension	14.612[a] (0.28081)	14.610 (0.28036)	14.610 (0.28000)
	compression	14.600 (0.27615)	14.610 (0.27866)	14.610 (0.28000)
$[0/\pm 60]_s$	tension	3.0824 (0.29791)	3.0806 (0.29773)	3.0802 (0.29761)
	compression	3.0699 (0.29619)	3.0802 (0.29719)	3.0802 (0.29761)
$[90]_{12}$	tension	1.1775 (0.022695)	1.1756 (0.022692)	1.1748 (0.022615)
	compression	1.1625 (0.022269)	1.1731 (0.022286)	1.1748 (0.022615)

[a]Longitudinal modulus, GPa (Poisson's ratio).

TABLE 4—*Results of aluminum specimens.*

Specimen Type	Test Type		
	Compressive Load	Compressive Unload/Tensile Load	Tensile Load
Column (ribbon)	73.7[a] (0.338)	73.8 (0.335)	74.6 (0.350)
Column (nonribbon)	69.8 (0.327)	72.1 (0.339)	71.0 (0.373)
Coupon	... ...	73.0 (0.338)	72.7 (0.346)

[a]Longitudinal modulus, GPa (Poisson's ratio).

measured moduli are very close to the actual value of 71.5 GPa for 5052 aluminum indicate that the sandwich column specimen allows for true measurement of elastic properties. However, despite the above calculations and these experimental assessments which indicate no effect of the orientation of the lightweight honeycomb, results which are more consistent with previous results and predictions have been achieved for compression when the honeycomb is oriented in the ribbon direction [6].

In light of these latter observations, further tests should be conducted to better quantify and understand the exact effects of the aluminum honeycomb core in the overall behavior of the specimen.

Graphite/Epoxy Specimen Tests

A total of 140 column specimens with six, ten, or twelve-ply graphite/epoxy facesheets were manufactured and tested. Of the 140 specimens, 95 were manufactured using AS1/3501-6 and 45 using AS4/3501-6. The layups utilized are $[\Theta_n]$, $[\pm\Theta/0]_s$, and $[0/\pm\Theta]_s$ with lamination angles, Θ, of 0, 15, 30, 45, 60, 75, 90 deg. This entire test program is summarized in Table 5. The stacking sequences and lamination angles were chosen to correspond with existing tensile data and to provide a data base for any further work in compression.

The graphite/epoxy facesheets were manufactured using standard procedures. The material

TABLE 5—*Test matrix for graphite/epoxy specimens.*

Material	Layup	Lamination Angle, deg						
		0	15	30	45	60	75	90
AS1/3501-6	$[0]_{12}$	5[a]	5	5	5	5	5	5
	$[\pm\Theta/0]_s$	...	5	5	5	5	5	5
	$[0/\pm\Theta]_s$	...	5	5	5	5	5	5
AS4/3501-6	$[0]_{10}$	5	...	...	...	...	...	...
	$[0]_{12}$	...	...	...	...	...	...	5
	$[\pm\Theta/0]_s$	...	...	5	5	5	...	...
	$[0/\pm\Theta]_s$	...	...	5	5	5	...	5

[a]Number of specimens tested.

is supplied as a preimpregnated 305-mm-wide tape, cut into plies, laid up into a 305-mm by 350-mm laminate, and placed on a flat aluminum cure plate. The cure takes place in an autoclave and follows the manufacturer's recommended cycle of one hour at 116°C and two hours at 177°C with 0.59 MPa pressure and a full vacuum (762 mm Hg) applied throughout. All laminates were post-cured at 177°C in an oven for eight hours. The laminates were machined into the desired sized facesheets, each laminate yielding five facesheets. The average measured per ply thickness was 0.134 mm with a coefficient of variation of 4.7%. The nominal value of the ply thickness, 0.134 mm, was used in the calculations of stress.

The facesheets were manufactured into columns by the previously described process. The completed column specimens were gaged with two longitudinal and one transverse 120-Ω gages (Micro Measurement type EA06-125AD-120). The longitudinal gages were placed in the center of the test section, one on each facesheet, in order to determine the moduli of both of the two individual graphite/epoxy facesheets as well as the overall specimen modulus (the average of the two facesheet values). In addition, this arrangement allows a check for the presence of any bending. The transverse gage was placed along the centerline, 13 mm above the longitudinal gage on the designated top facesheet. The transverse gage and the corresponding longitudinal gage were used to determine the Poisson's ratio of the specimen.

All of the specimens were tested on an MTS 810 machine equipped with hydraulic grips. The ends of the column were gripped and the specimen then loaded at a constant stroke rate of 1 mm/min, which is equivalent to a strain rate of approximately 5000 microstrain/min. The maximum load was determined for each specimen, and strain gage and load data were taken automatically at 0.5-s intervals with the use of a PDP-11/34 computer. Any noises indicative of damage were noted during the test. Photographs were taken of the failed specimen.

The longitudinal moduli and the Poisson's ratios of the specimens were determined with the aid of a program known as LIN6 [7], which determines best-fit linear regions of a data set. The stress was found by dividing the applied load by the nominal area (the sum of the measured widths of the two facesheets times the nominal thickness). Moduli were determined for each longitudinal gage and also for the average of the two gages. Poisson's ratios were determined from the transverse gage and the corresponding longitudinal gage.

Basic Ply Properties

The elastic properties of a unidirectional ply are determined from uniaxial compression and tension tests along the fiber direction and perpendicular to it (E_L, E_T, ν_{LT}, ν_{TL}) as well as from shear tests (G_{LT}). The basic ply elastic constants which were measured in this investigation are compared against previously reported values in Table 6. For AS1/3501-6, no delineation is made between tensile and compressive behavior for the previously reported values of elastic constants. Different tensile and compressive values are reported for the AS4/3501-6 material [8] except for the case of the Poisson's ratios. The Poisson's ratios are stated without a reference to the sense of the loading and without the statistics of the data variation provided with the other elastic constants. The same value is thus listed in tension and compression for the previously reported Poisson's ratios in Table 6. Furthermore, it is unknown what specimen was used to obtain the compressive data in Ref 8.

In general, there is good agreement between the previously reported and the measured values of the longitudinal and transverse moduli and the minor Poisson's ratios. There is a slight difference between the moduli measured in tension and those measured in compression. This difference between tensile and compressive values has been previously noted by Tennyson [10] and Jones [11].

However, the relatively large difference in the major Poisson's ratio between tension and compression is unexplained. It is unlikely that this difference is accounted for in terms of the overall behavior of the specimen since the difference in the Poisson's ratios measured in the aluminum/aluminum honeycomb specimens was negligible. However, the aluminum facesheets are isotropic, whereas unidirectional composite facesheets have a high degree of orthotropy. This discrepancy remains unexplained. It should be noted that the values obtained in this study for the AS4/3501-6 material do not satisfy reciprocity. Thus, it is suggested that further measurements be made to better quantify these discrepancies.

Several of the basic ply ultimate strengths were also measured. Five strengths characterize the behavior of a ply:

X^t = longitudinal tensile ultimate,
X^c = longitudinal compressive ultimate,
Y^t = transverse tensile ultimate,
Y^c = transverse compressive ultimate, and
S = shear ultimate.

Previously reported values are compared with those measured here in Table 7. Good agreement is seen in all of the AS4/3501-6 values and in the transverse values of AS1/3501-6. The value of the longitudinal compressive ultimate for AS1/3501-6 as provided by Ref 9 is suspect. The only difference between the two material systems is the fiber. For the AS1 system, the previously reported longitudinal ultimates are about the same regardless of the load direction; whereas, there is a large difference between the values for the AS4 system. The current work suggests that this difference does exist.

TABLE 6—*Basic ply elastic properties of materials used.*

	AS1/3501-6		AS4/3501-6		
	Tension, Ref 9	Compression, Measured	Tension, Ref 8	Compression, Ref 8	Compression, Measured
E_L, GPa	130.0	127.1	142.7	139.3	133.8
E_T, GPa	10.5	"	9.65	"	11.7
ν_{LT}	0.28	0.38	0.30	0.30	0.41
ν_{TL}	0.023	"	0.024	0.024	0.019
G_{LT}, GPa	6.0	"	"	"	"

"Not determined in this investigation.
"Not provided.

TABLE 7—*Basic ply strengths of materials used.*

	AS1/3501-6		AS4/3501-6	
	Ref 9	Measured	Ref 8	Measured
X^t, MPa	1661	"	2156	2356[b]
X^c, MPa	−1698	−1186	1560	1468
Y^t, MPa	53.9	"	54.1	49.4[b]
Y^c, MPa	−221	−236	"	−186
S, MPa	105	"	"	"

"Not determined in this investigation.
[b]Ref 12.
"Not provided.

General Laminate Behavior

Stress-Strain

As previously discussed, a longitudinal gage was placed on each facesheet of the sandwich specimen in order to better assess the reliability of the test method. A comparison of these readings will indicate whether any global bending/buckling is present in the test specimens. In specimens which did not delaminate prior to final failure, the strain gages provided data up to the point of failure. In Fig. 3, the two stress-strain curves from these gages are shown for a AS4/3501-6 $[\pm 60/0]_s$ specimen. The stress and all of the strain values have been multiplied by -1 in order to place the origin at the bottom left corner of the plot. These back-to-back longitudinal gages show very similar behavior and thus the lack of any bending component. However, some results do show some slight difference between the two gages, indicating that some bending is present. The difference in the two strains never exceeds 3% of their average, which indicates that the bending component is indeed small. These slight deviations can be attributed to geometric eccentricities due to different facesheet widths, different adhesive thicknesses, and slight variations in the moduli of the facesheets.

The averages and extremes of the experimentally determined longitudinal modulus and Poisson's ratio of all the specimens are plotted in Figs. 4 and 5 for AS1/3501-6 $[\theta_{12}]$ laminates, Figs. 6 and 7 for AS1/3501-6 $[\pm\theta/0]_s$ and $[0/\pm\theta]_s$ laminates, and Figs. 8 and 9 for AS4/3501-6 $[\pm\theta/0]_s$ and $[0/\pm\theta]_s$ laminates. Since in-plane elastic constants are independent of stacking sequence, the $[\pm\theta/0]_s$ and $[0/\pm\theta]_s$ data are pooled. The predictions obtained from classical laminated plate theory using the measured elastic constants in compression for the unidirectional ply (as listed in Table 6) are also provided. If a value was not measured herein or available, then a previously reported value was used. For example, 10.5 GPa was used for the transverse modulus of the AS1/3501-6, and 6.0 GPa was used in all cases for the shear modulus. Generally, excellent agreement is seen between the experimental and theoretical values of the elastic constants with low coefficients of variation. This indicates that the specimens produce repeatable and acceptable stress-strain results.

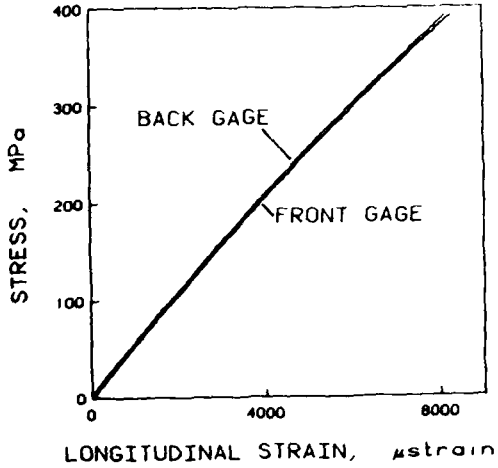

FIG. 3—*Typical compressive stress-strain plot of back-to-back longitudinal gages on a graphite/epoxy sandwich column specimen.*

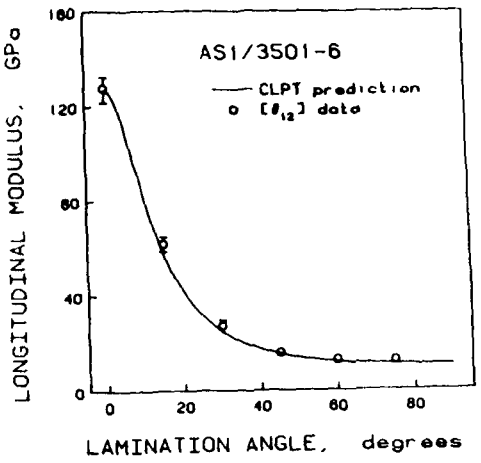

FIG. 4—*Experimental and calculated longitudinal moduli for AS1/3501-6 $[\theta_{12}]$ specimens versus lamination angle.*

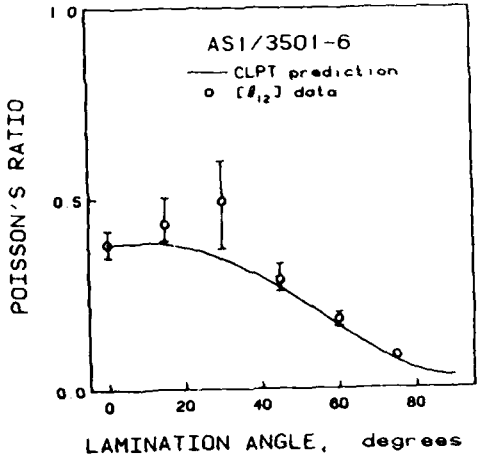

FIG. 5—*Experimental and calculated Poisson's ratios for AS1/3501-6 $[\theta_{12}]$ specimens versus lamination angle.*

Failure Stresses and Modes

In determining the maximum load-carrying capability of a specimen, care was taken not to halt the test prematurely due to slight decreases in the load. Local failures such as ply buckling and ply delamination can reduce the load slightly [2]. Generally, failure was judged to occur when either or both of the facesheets fractured resulting in a load reduction of at least 40%.

The failure stresses were averaged and are plotted in Fig. 10 for AS1/3501-6 $[\theta_{12}]$ laminates, Fig. 11 for AS1/3501-6 $[+\theta/0]_s$ and $[0/+\theta]_s$ laminates, and Fig. 12 for AS4/3501-6 $[\pm\theta/0]_s$

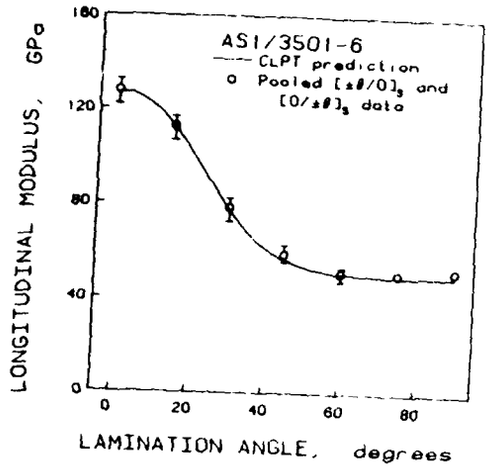

FIG. 6—*Experimental and calculated longitudinal moduli for pooled AS1/3501-6 [±Θ/0]s and [0/±Θ]s specimens versus lamination angle.*

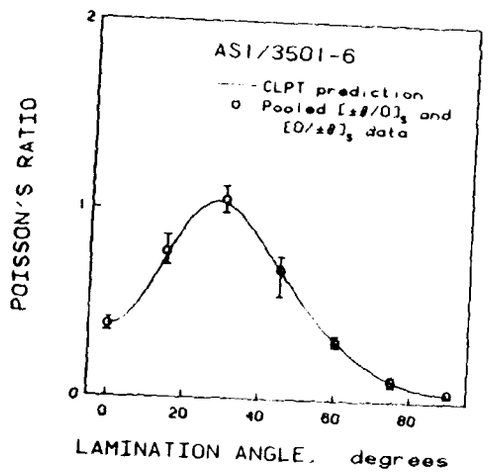

FIG. 7—*Experimental and calculated Poisson's ratios for pooled AS1/3501-6 [±Θ/0]s and [0/±Θ]s specimens versus lamination angle.*

and $[0/\pm\Theta]_s$ laminates. Predicted in-plane fracture stresses are also shown. These were determined in three ways. The first two methods involve the stress interaction criterion of Tsai and Wu [*13*]. The third method involves a maximum stress criterion.

The stress interaction criterion is a curve fit of experimental data to a quadratic polynomial. The two-dimensional tensorial form of the equation indicates that a unidirectional ply will fail when

$$F_{1111}\sigma_{11}^{(\theta)2} + 2F_{1122}\sigma_{11}^{(\theta)}\sigma_{22}^{(\theta)} + F_{2222}\sigma_{22}^{(\theta)2} + 4F_{1212}\sigma_{12}^{(\theta)2} + F_{11}\sigma_{11}^{(\theta)} + F_{22}\sigma_{22}^{(\theta)} = 1 \qquad (1)$$

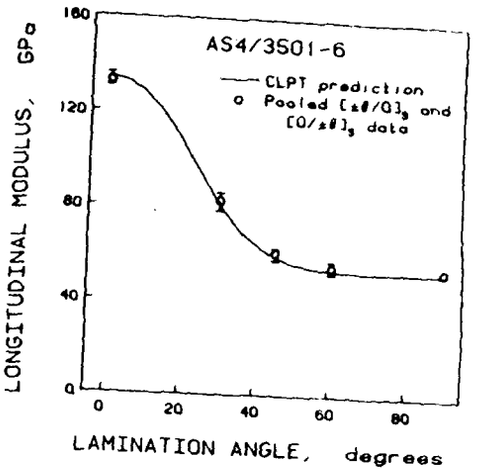

FIG. 8—*Experimental and calculated longitudinal moduli for pooled AS4/3501-6 [±Θ/0]s and [0/±Θ]s specimens versus lamination angle.*

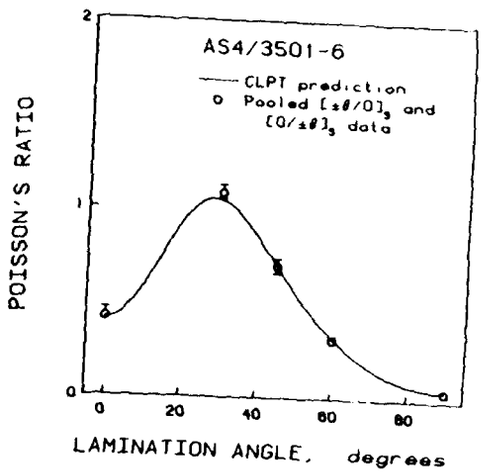

FIG. 9—*Experimental and calculated Poisson's ratios for pooled AS4/3501-6 [±Θ/0]s and [0/±Θ]s specimens versus lamination angle.*

where the $\sigma_{ij}^{(\theta)}$ are the ply stresses in the Θ, ply as referenced to the ply axes. Five of the six strength parameters (F_{1111}, F_{2222}, F_{11}, F_{22}, F_{1212}) are obtained by using the five basic strengths of a single ply of the material: longitudinal tension, longitudinal compression, transverse tension, transverse compression, and shear. The sixth constant, F_{1122}, is the interaction term. It has been suggested [*14*] that this be set by likening the Tsai-Wu criterion to the Mises-Hencky criterion for isotropic materials. This gives the equation

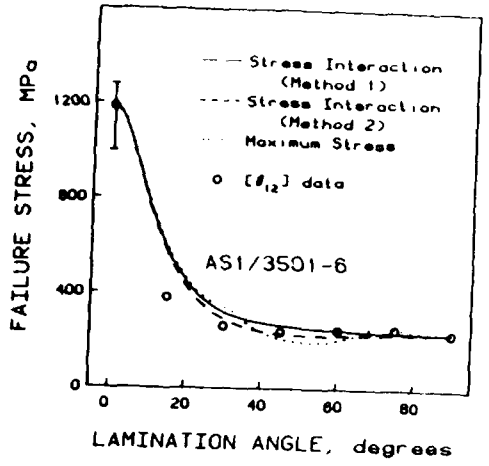

FIG. 10—*Experimental and predicted compressive failure stresses for AS1/3501-6 $[\theta_{12}]$ specimens versus lamination angle.*

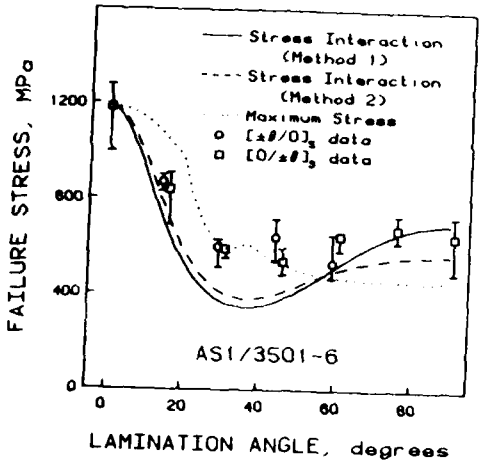

FIG. 11—*Experimental and predicted compressive failure stresses for AS1/3501-6 $[\pm\Theta/0]_s$ and $[0/\pm\Theta]_s$ specimens versus lamination angle.*

$$F_{1122} = -\frac{1}{2}(F_{1111}F_{2222})^{1/2} \tag{2}$$

for the interaction term. It has also been suggested that when the primary loading is compressive, the value of the interaction term be set to zero [15]. This is the second interaction criterion plotted in Figs. 11 and 12.

The maximum stress criterion is also a curve fit of experimental data. Here, failure of a unidirectional ply is predicted to occur at any one of three equalities:

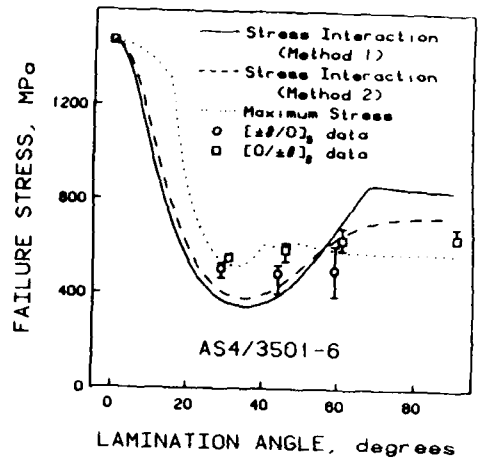

FIG. 12—*Experimental and predicted compressive failure stresses for AS4/3501-6 $[\pm\Theta/0]_s$ and $[0/\pm\Theta]_s$ specimens versus lamination angle.*

$$1 = \begin{cases} \dfrac{\sigma_{11}^{(i)}}{X^t} & \text{if } \sigma_{11} > 0 \\ \dfrac{\sigma_{11}^{(i)}}{X^c} & \text{if } \sigma_{11} < 0 \end{cases} \tag{3a}$$

$$1 = \begin{cases} \dfrac{\sigma_{22}^{(i)}}{Y^t} & \text{if } \sigma_{22} > 0 \\ \dfrac{\sigma_{22}^{(i)}}{Y^c} & \text{if } \sigma_{22} < 0 \end{cases} \tag{3b}$$

$$1 = \left| \frac{\sigma_{12}^{(i)}}{S} \right| \tag{3c}$$

These failure criteria are applied using the ply stresses in ply axes on a ply-by-ply basis. The ply stresses are calculated from classical laminated plate theory and the basic unidirectional ply properties of the material. In this study, laminate failure will be assumed to occur when the first ply is calculated to fail.

In general, good agreement is seen between the experimental and theoretical values, with the maximum stress criterion appearing to be the best fit to the experimental data.

The observed failure modes are consistent within a given layup and include several types of valid failure mechanisms. The unidirectional specimens failed as a result of in-plane fracture with considerable splitting. The $[\pm\Theta/0]_s$ laminates failed primarily as a result of in-plane fracture with "cracks" oriented in the layup angle (splitting of two plies and fiber fracture in four) occurring in some cases for Θ equal to 15 and 45 deg and in all cases for Θ equal to 30 deg. The $[0/\pm\Theta]_s$ laminates ultimately failed as a result of in-plane fracture. Again, "cracks" occurred for Θ equal to 30 and 45 deg. Ply buckling and delamination of the outermost 0-deg ply occurred prior to failure in most of the $[0/\pm\Theta]_s$ specimens with Θ greater than 45 deg. Specimens

FIG. 13—*Representative photographs of various failure modes in graphite/epoxy sandwich columns: (a) in-plane fiber fracture, (b) in-plane splitting and concurrent fiber fracture, and (c) ply buckling with in-plane fracture.*

with a lamination angle of either 60 or 75 deg produced the most delamination prior to final failure. Photographs of typical in-plane fracture, in-plane "cracks," and ply buckling with subsequent in-plane fracture are presented in Fig. 13.

Summary

A sandwich column specimen, utilizing a core of aluminum honeycomb and composite test laminates as facesheets, has been proposed as a compressive characterization specimen for composite laminates, especially for relatively thin laminates. The experimental results indicate that the stress-strain behavior of the specimens correlates well with that predicted by classical laminated plate theory, and repeatable results are achieved. Measurement of the honeycomb properties and subsequent analysis indicates that the presence of the core would have a negligible effect on the behavior of the specimen. In general, this is evidenced by the experimental results for the graphite/epoxy specimens. The graphite/epoxy tests utilizing this specimen also produced valid compressive and fracture/failure data. The modes of damage which have been reported to occur under compressive load are allowed by this specimen. Those modes observed in these specimens include in-plane fracture, in-plane splitting, free-edge delamination, and ply or sublaminate buckling. Therefore, the specimen provides a realistic test of the material.

The uniaxial column specimen is thus a valid compression characterization specimen for thin laminates and should also have applications to thick laminates. This specimen has additional advantages as well. Due to its large unconstrained test section, it is ideal for monitoring damage growth and is therefore useful in cyclic testing. Furthermore, since load is transferred via hydraulic grips and the basic configuration of the specimen is similar to that of a standard tensile coupon, tension-compression cyclic tests can also be conducted using this specimen.

Acknowledgments

This work was supported by the Air Force Office of Scientific Research under Contract No. AFOSR-85-0206. Major David Glasgow was the contract monitor.

References

[1] Hofer, K. E., Jr. and Rao, P. N., "A New Static Compression Fixture for Advanced Composite Materials," *Journal of Testing and Evaluation*, Vol. 5, No. 4, July 1977, pp. 278–283.

[2] Vizzini, A. J. and Lagace, P. A., "The Role of Ply Buckling in the Compressive Failure of Graphite/Epoxy Tubes," *AIAA Journal*, Vol. 23, 1985, pp. 1791–1797.

[3] Shuart, M. J., "An Evaluation of the Sandwich Beam Compression Test Method for Composites," *Test Methods and Design Allowables for Fibrous Materials, ASTM STP 734*, American Society for Testing and Materials, Philadelphia, pp. 152–165.

[4] Chatterjee, S. N., Pindera, M. J., Pipes, R. B., and Dick, B., "Composite Defect Significance," Report No. NADC-81034-60, Material Sciences Corp., Spring House, PA, Nov. 1982.

[5] Lagace, P. A. and Nolet, S. C., "The Effect of Ply Thickness on Longitudinal Splitting and Delamination in Graphite/Epoxy under Compressive Cyclic Load," *Composite Materials: Fatigue and Fracture, ASTM STP 907*, American Society for Testing and Materials, Philadelphia, 1986, pp. 335–360.

[6] Nolet, S. C., "The Effect of Ply Thickness on the Initiation and Growth of Delamination in Graphite/Epoxy Laminates with Holes under Compressive Cyclic Loading," Technology Laboratory for Advanced Composites Report 84-1, Massachusetts Institute of Technology, Cambridge, MA, Jan. 1984.

[7] Vizzini, A. J. and Lagace, P. A., "TELAC Software Manual," Technology Laboratory for Advanced Composites Report 84-14, Massachusetts Institute of Technology, Cambridge, MA, Sept. 1984.

[8] "Magnamite AS4/3501-6 Graphite Prepreg Tape and Fabric Module," internal report, Hercules Corp., Magna, UT.

[9] Lagace, P. A., "Static Tensile Fracture of Graphite/Epoxy," Technology Laboratory for Advanced Composites Report 82-4, Massachusetts Institute of Technology, Cambridge, MA, April 1982.

[10] Tennyson, R. C., "Buckling of Laminated Composite Cylinders: A Review," *Composites*, Jan. 1975, pp. 17–24.

[11] Jones, R. M., "Buckling of Circular Cylindrical Shells with Different Moduli in Tension and Compression," USAF Report No. SAMSO-TR-70-55, U.S. Air Force, Dec. 1969.
[12] Vizzini, A. J. and Archard, K. F., "Characterization of AS4/3501-6 Graphite/Epoxy," Technology Laboratory for Advanced Composites, Massachusetts Institute of Technology, Cambridge, MA, in preparation.
[13] Tsai, S. W. and Wu, E. M., "A General Theory of Strength for Anisotropic Materials," *Journal of Composite Materials*, Vol. 5, Jan. 1971, pp. 58-80.
[14] Tsai, S. W. and Hahn, H. T., *Introduction to Composite Materials*, Technomic, Westport, CT, 1980.
[15] Tennyson, R. C., Elliot, G., Mabson, G. E., and Tratt, M., "Failure Analysis for Composite Laminates," *Proceedings*, the AIAA/ASME/ASCE/AHS 25th Structures, Structural Dynamics, and Materials Conference, American Institute of Aeronautics and Astronautics, New York, May 1984, pp. 74-84.

from: Proceedings of the Fourth Japan-U.S. Conference on Composite Materials, Washington, D.C., June, 1988, pp. 242-252.

Effects of Ply Dropoffs on the Tensile Behavior of Graphite/Epoxy Laminates

PAUL A. LAGACE*
Technology Laboratory for Advanced Composites
Massachusetts Institute of Technology
Cambridge, MA 02139

RAYMOND K. CANNON**
United States Air Force Academy
Colorado Springs, Colorado

ABSTRACT

The effects of ply dropoffs on the stress-strain behavior, fracture strength and fracture modes of graphite/epoxy laminates in tension were investigated. Test variables include the number, order, angular orientation, and effective ply thickness of the dropped plies. Seven different layups with ply dropoffs were manufactured and tested to failure in uniaxial tension. Flat laminates with similar layups were also constructed and tested to serve as a base. The stress-strain behavior of the ply dropoff specimens was closely approximated by those of the flat specimens having the same layups as the dropped and undropped sections. The failure stresses and modes of the ply dropoff laminates were similar to those of the flat laminates having the same layup as the dropped section of the ply dropoff laminate. Only the order of the ply dropoffs appeared to have any affect as laminates with all plies dropped adjacent to each other tended to delaminate away from the rest of the laminate in the undropped section. However, failure stresses were still unaffected.

INTRODUCTION

In order to make a structural configuration efficient, the thickness of the structure is often tapered as the requirements to carry load decrease. In structures made of composite materials, this is accomplished by terminating, or "dropping off", individual plies. These ply dropoffs are essentially a discontinuity which acts as a stress riser both in the plane and out of the plane, even with strictly in-plane loading.

Relatively little work has been done to study the effects of ply dropoffs, and much of this has been design-specific [1,2,3]. Recently, more fundamental studies of ply dropoffs in composite laminates have been undertaken. Analytical work [4,5] has indicated that stress concentrations do arise in the vicinity of the ply dropoff and that interlaminar stresses, which can cause delamination, also occur. The specific configuration of the ply dropoff, and the "resin pocket" created during the manufacturing procedure, has been shown to play an important role in determining the local stress field [5]. Some experimental work has also been accomplished, but this has generally dealt with compressive loading [6]. Curry, Johnson, and Starnes [7] have conducted work both in tension and compression and have shown that the configuration was more sensitive to compressive loading in terms of reduction in load-carrying capability. Nevertheless, a

*Associate Professor of Aeronautics and Astronautics, TECHNOLOGY LABORATORY FOR ADVANCED COMPOSITES, Massachusetts Institute of Technology, Cambridge, MA 02139

**currently at United States Air Force Academy, Colorado Springs, Colorado

reduction in load-carrying capability was also observed for tensile loading.

The current study concentrates on tensile loading. This is done in order to separate global structural effects, such as buckling, from the local effects on the stress field which the dropoff configuration causes. In this way, the effects of ply dropoffs on stress-strain behavior, fracture modes, and fracture strength can be experimentally isolated and studied.

EXPERIMENTAL METHODOLOGY

Test Program

A number of factors were isolated and studied by varying the layups considered in this work. These factors include the number of plies dropped off, the orientation of the plies dropped off, the arrangement of the dropped plies within the laminate, and the effective ply thickness. This led to five different classes of ply dropoffs being considered in order to isolate these factors. These classes are (1) a single 0° ply dropped off; (2) two 0° plies dropped off symmetrically; (3) angle plies (±45°,±15°) dropped off symmetrically; (4) 0° and angle plies dropped off symmetrically; and (5) an entire symmetric sublaminate ($[\pm 45/0]_S$) dropped off. The seven test laminates, divided into these categories, are listed in Table 1.

TABLE 1 - SUMMARY OF TEST LAMINATES

Laminate[a]	Undropped Section	Dropped Section
$[\pm 45/0_D/0/-+45]_T$	$[\pm 45/0]_S$	$[\pm 45/0/-+45]_T$
$[\pm 45_2/0/0_D]_S$	$[\pm 45_2/0_2]_S$	$[\pm 45_2/0]_S$
$[+45/+45_D/-45/-45_D/0/0_D]_S$	$[\pm 45_2/0_2]_S$	$[\pm 45/0]_S$
$[\pm 45/\pm 45_D/0_2]_S$	$[\pm (45)_2/0_2]_S$	$[\pm 45/0_2]_S$
$[+15/+15_D/-15/-15_D/0/0_D]_S$	$[\pm 15_2/0_2]_S$	$[\pm 15/0]_S$
$[\pm 45/\pm 45_D/0/0_D]_S$	$[(\pm 45)_2/0_2]_S$	$[\pm 45/0]_S$
$[\pm 45/0/(\pm 45/0)_D]_S$	$[\pm 45/0]_{2S}$	$[\pm 45/0]_S$

[a] subscript 'D' indicates ply dropped off at centerline.

The majority of the laminates were based on the $[\pm 45/0]_s$ stacking sequence configuration. This is a relatively well understood layup which does not delaminate due to free edge effects [8]. Thus, the effects of the ply dropoffs can be isolated from those of the free edge. No 90° plies were included in order to reduce the likelihood of transverse crack formation before the effects of the ply dropoff become substantial. An alternative layup using ±15° plies rather than the ±45° plies was chosen specifically for its tendency to delaminate at the free edge [8]. This allowed for comparison between laminates with a tendency toward in-plane and out-of-plane failure, and the effects of ply dropoffs on each.

The basic tensile coupon shown in Fig. 1 was utilized for all experiments. In specimens with ply dropoffs, the appropriate plies were terminated at the specimen midline as indicated. These plies are notated by a subscript 'D' in Table 1. The specimen is thus divided into "undropped" and "dropped" sections. In addition to the ply dropoff configurations, flat laminates (without ply dropoffs) were studied. The configurations of these laminates are the same as the various configurations of the undropped and dropped sections of the ply dropoff laminates as noted in Table 1. Five replicates of each laminate in Table 1 were manufactured and tested. Hercules AS4/3501-6 graphite/epoxy was used throughout.

All plies were dropped off internally. That is the plies which are dropped off have covering contoured plies over them such that the dropped ply is not exposed. This was done for realism as most structural designs using ply dropoffs have internal ply dropoffs. Furthermore, most of the specimens with ply dropoffs were constructed with one side flat as would be

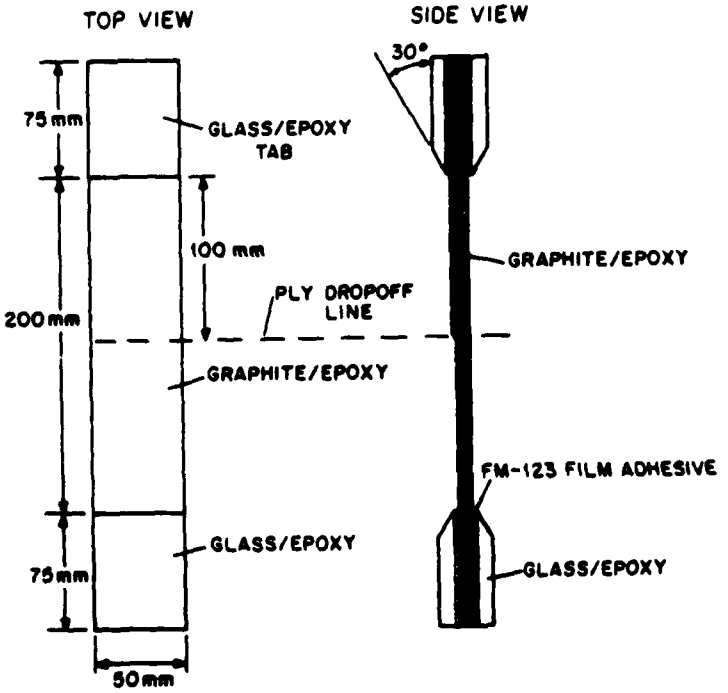

Figure 1 Configuration of coupon specimen indicating ply dropoffs.

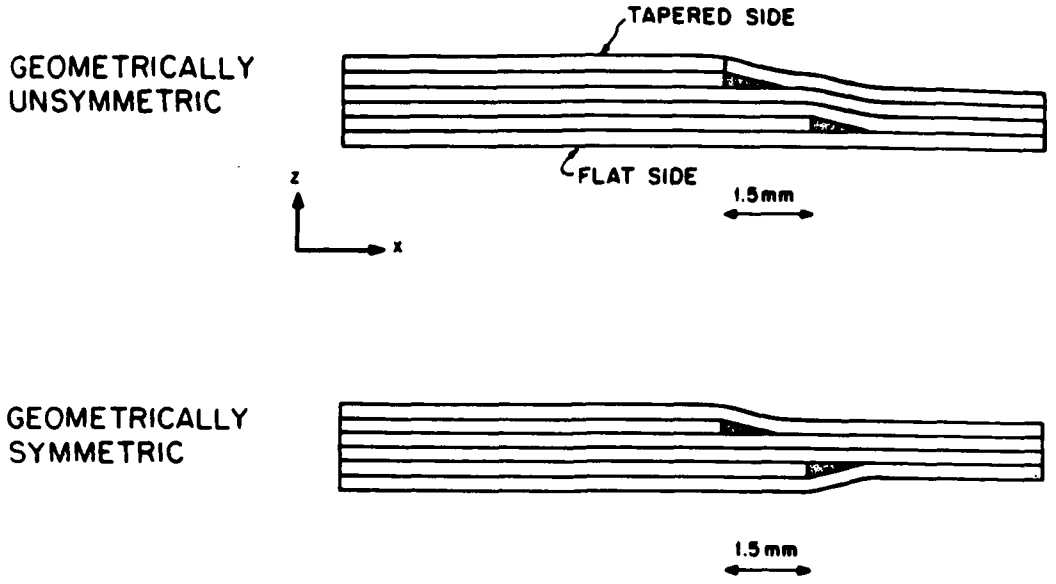

Figure 2 Illustration of layup configuration for specimens with ply dropoffs: **(top)** done in a geometrically unsymmetric manner; and **(bottom)** done in a geometrically symmetric manner.

done in actual applications. The other side is not flat due to the ply dropoffs. The plies laid up on top of the terminating plies curve over the ply dropoff and then become flat again over the dropped section of the coupon. Although the specimens are laid up symmetrically, with both the dropped and undropped sections having symmetric layups, the entire specimen is not geometrically symmetric as the midplanes of the dropped and undropped sections do not coincide. Thicker loading tabs were used on the dropped end of the specimen to minimize loading eccentricity. Nevertheless, some bending is likely to be induced. In order to separate out this influence, the $[\pm 15/0]_s$ type specimens with dropoffs were layed up in a geometrically symmetric manner as compared to the geometrically unsymmetric manner as illustrated in Fig. 2.

Manufacture and Testing

Special care was taken in manufacturing the specimens with ply dropoffs. A preliminary study was conducted to determine the best means to drop off the plies without causing voids at the ply dropoffs. This study showed that plies should be dropped off with a spacing of 1.5 mm (for a 0.134 mm thick ply) and that overlaid plies should carefully conform to the dropped area. This was accomplished with a plastic smoothing tool. Specific procedures are summarized in Reference 9.

All curing was accomplished in an autoclave according to the manufacturer's schedule. This involves 1 hour at 116°C and 2 hours at 177°C with 0.59 MPa pressure and a full vacuum applied throughout. No top caul plate was used since the upper surface is not flat. These laminates were postcured at 177°C in an oven for 8 hours. Individual coupons were cut from each cured panel with a water-cooled diamond wheel cutter. Glass/epoxy loading tabs were bonded onto each end of the specimen with

American Cyanamid FM-123-2 film adhesive resulting in the specimen shown in Fig. 1. A thicker tab was used on the end with the ply dropped off in order to compensate for the reduced thickness.

All specimens were instrumented with strain gages to determine longitudinal strain. For the specimens without ply dropoffs, one gage was centered on the test section. For the coupons with ply dropoffs, four strain gages were used. Back to back gages were centered on both the dropped and undropped halves of the coupon 50 mm from the dropoff line as shown in Fig. 3. The back to back gages were used to detect any bending which might occur in the coupons with ply dropoffs. In addition, four specimens were outfitted with photoelastic coating in order to observe the strain gradient in the vicinity of the ply dropoff.

The coupon tests were conducted using an MTS 810 testing machine equipped with hydraulic grips. These monotonic-to-failure tests were done under stroke control at a rate of 1 mm per minute which gives a strain rate of approximately 5000 microstrain per minute over the 200 mm test section. Strain and load data were taken automatically by computer. In the tests with photoelastic coatings, the test was halted at discrete intervals to take photographs of the specimen.

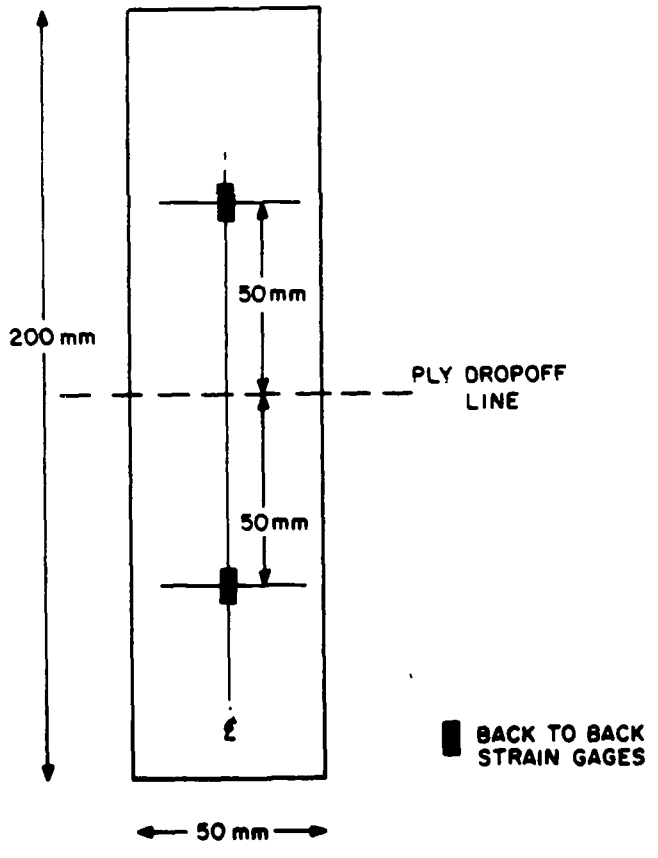

Figure 3 Location of back to back strain gages on specimens with ply dropoffs.

FAILURE ANALYSIS

The failure stresses of the laminates were predicted using an in-plane failure criterion, namely the Maximum Stress Criterion. The stresses in the laminate are considered on a ply by ply basis as referenced to the fiber direction in the ith ply. For the AS4/3501-6 material utilized, this criterion can be expressed as:

$$-1468 \text{ MPa} \leq \sigma_{11}^{(i)} \leq 2356 \text{ MPa}$$

$$-186 \text{ MPa} \leq \sigma_{22}^{(i)} \leq 49.4 \text{ MPa}$$

$$-105 \text{ MPa} \leq \sigma_{12}^{(i)} \leq 105 \text{ MPa}$$

For the flat laminates, these ply stresses were calculated using classical laminated plate theory. However, for the laminates with ply dropoffs, bending stresses will arise as noted earlier. An analysis was developed, based on the energy method, to determine the deflections and thus strains and stresses due to this bending. The details of this analysis are provided in Reference 9. These stresses were used with those resulting from the stretching to determine the failure stresses of laminates with ply dropoffs.

For these laminates with ply dropoffs, the in-plane failure strength (designated as first ply failure in all cases) of each section of the laminate (dropped and undropped) was calculated using this technique. Since the two sections of the laminates are of different thicknesses, the failure load of the laminate was determined as the minimum of the failure load of the two sections calculated using the individual nominal thicknesses of the two sections. The local effects of the ply dropoffs were not taken into account either in terms of in-plane stress concentrations or interlaminar stresses which arise.

RESULTS AND DISCUSSION

Stress-Strain Behavior

The ply dropoffs did not have a significant effect on the global stress-strain behavior of the specimens. The analysis of Reference 9 indicated that bending effects would die out, to 1% of their maximum effect, within 25 to 70 mm of the ply dropoff line depending on the layup. The strain gages, located 50 mm from the ply dropoff line, did not show any discernible bending in any of the specimens as any strain differences between the front to back gages on the dropped and undropped sections of the ply dropoff laminates did not provide any consistent or significant indication of curvature. Furthermore, the moduli measured with the strain data from these gages corresponded with those predicted using laminated plate theory and the basic ply properties.

The tests of laminates with photoelastic coatings also showed that the region where strain deviated from the far-field value was restricted to within approximately 50 mm of the ply dropoff line. In addition, the strain was consistent across the width of the specimen.

Fracture Stresses

The average fracture loads of all the laminates are listed in Table 2 along with the corresponding average stresses in the dropped and undropped

sections of the laminates. The data in the table are best examined by comparing the failure load of a specimen with a ply dropoff to the corresponding flat laminates of the dropped and undropped sections. Observations of the failure modes indicate that failure always occurs in the dropped section, thus the failure load of the corresponding laminate with the stacking sequence of the dropped section is most important.

TABLE 2 - SUMMARY OF FRACTURE LOADS AND STRESSES

Laminate	Maximum Load, kN	Fracture Stress[a], MPa	
		Undropped Section	Dropped Section
$[\pm 45/0_D/0/-+45]_T$	18.1 (3.1%)[b]	451	541
$[\pm 45_2/0/0_D]_S$	28.9 (18.8%)	359	431
$[+45/+45_D/-45/-45_D/0/0_D]_S$	29.0 (10.3%)	361	722
$[\pm 45/\pm 45_D/0_2]_S$	64.4 (4.2%)	801	1202
$[+15/+15_D/-15/-15_D/0/0_D]_S$	37.6 (2.8%)	468	935
$[\pm 45/\pm 45_D/0/0_D]_S$	32.2 (13.6%)	401	801
$[\pm 45/0/(\pm 45/0)_D]_S$	29.8 (9.6%)	371	741
$[\pm 45/0]_S$	32.3 (12.3%)	804	
$[\pm 45/0/-+45]_S$	18.4 (9.9%)	548	
$[\pm 45_2/0_2]_S$	64.2 (6.2%)	799	
$[\pm 45_2/0]_S$	33.8 (5.4%)	505	
$[\pm 15_2/0_2]_S$	57.2 (7.5%)	712	
$[\pm 15/0]_S$	35.3 (1.6%)	878	
$[(\pm 45)_2/0_2]_S$	63.0 (6.9%)	783	
$[\pm 45/0_2]_S$	59.5 (6.5%)	1110	
$[\pm 45/0]_{2S}$	70.4 (1.4%)	876	

[a] Stress based on thickness of dropped or undropped section.

[b] Numbers in parentheses are coefficients of variation.

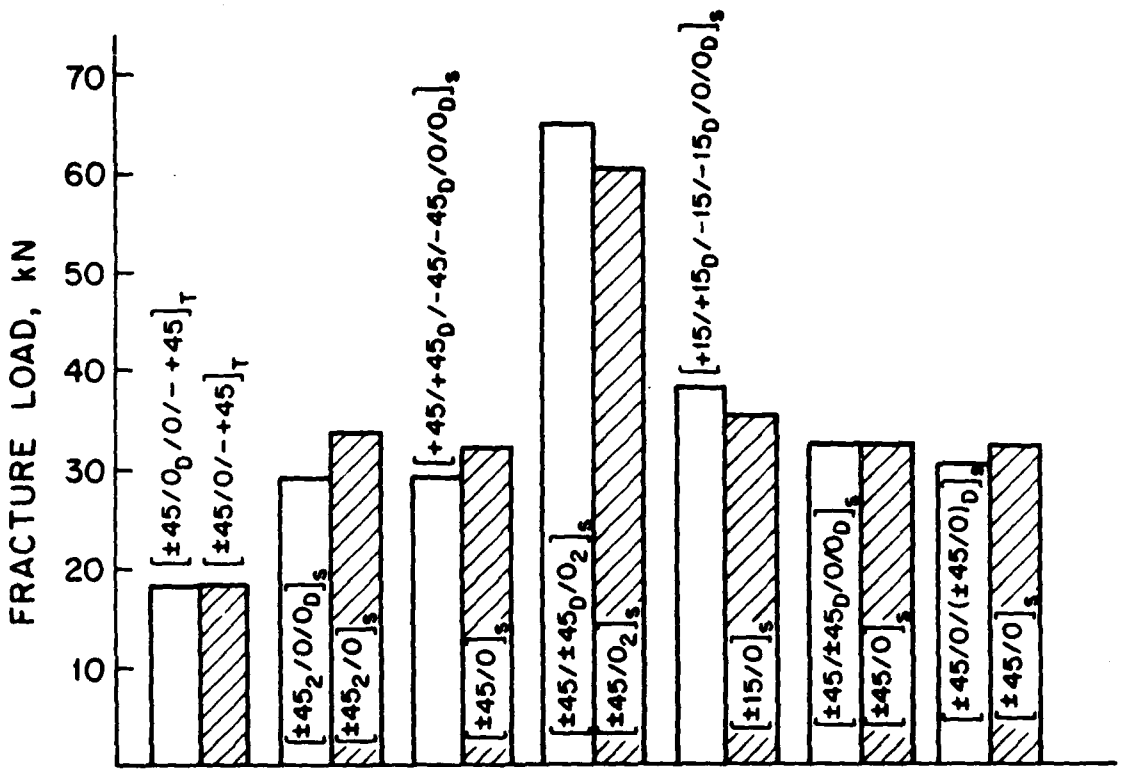

Figure 4 Bargraph representation of fracture loads comparing ply dropoff specimen with flat specimen configuration of section with ply dropoffs.

To better illustrate this comparison, the failure load of the dropped laminate and the corresponding flat laminate with the undropped section layup is shown in bargraph format for all laminates in Fig. 4. It is clear that in all cases, the ply dropoff has not affected the ultimate load-carrying capability of the basic laminate. The ultimate load-carrying capability can thus be calculated from the fracture stresses of the basic layup of each section and determining the minimum load-carrying capability of the two sections.

The predicted failure stresses, as normalized to the thickness of the dropped section, are shown in Table 3 along with the experimental failure stresses. Two predictions are shown, one using only the stresses from laminated plate theory, the second incorporating the stresses calculated from the bending which arises due to the geometric unsymmetry. It is clear that incorporating the stresses due to bending causes a very conservative estimate of the failure stress while the predictions using solely the stresses due to stretching provides a good estimate. This indicates that a better analysis of the local stress gradients should be undertaken, but also indicates that these local stress concentrations may not play a significant role in global fracture.

It is further noted that the ply dropoff laminate which was geometrically symmetric, $[+15/+15_D/-15/-15_D/0/0_D]_S$, did not show any changes in fracture behavior from the base laminates as was the case for those laminates which were geometrically unsymmetric. This occurred despite the fact that no bending was observed in the former while bending

TABLE 3 - PREDICTED FRACTURE STRESSES[a] FOR PLY DROPOFF LAMINATES

Laminate	Predicted Fracture Stress, MPa		Experimental Fracture Stress, MPa
	Method A[b]	Method B[c]	
$[\pm 45/0_D/0/-+45]_T$	464	252	541
$[\pm 45_2/0/0_D]_S$	464	239	431
$[+45/+45_D/-45/-45_D/0/0_D]_S$	638	364	722
$[\pm 45/\pm 45_D/0_2]_S$	866	439	1202
$[+15/-15_D/-15/-15_D/0/0_D]_S$	2105	d	935
$[\pm 45/\pm 45_D/0/0_D]_S$	638	364	801
$[\pm 45/0/(\pm 45/0)_D]_S$	638	371	741

[a] Based on thickness of dropped section.

[b] Bending effect not included.

[c] Bending effect included.

[d] No bending since layup was done geometrically symmetric.

was observed in the vicinity of the ply dropoff in the other six laminates. Thus, the role of this local bending appears to be of negligible significance.

Fracture Modes

The presence of the ply dropoffs did not appear to have an effect on the failure modes in all but one case. Failure in the laminates with ply dropoffs generally originated at the area of the ply dropoff and extended into the dropped section of the laminate. In some cases, damage was observed in the undropped section. In these cases, calculations show that the stresses were nearly critical in this section when failure occurred. Failure modes of the ply dropoff laminates generally approximated that of the flat specimen with a layup equal to that of the dropped section of the laminate. Most notably, in-plane failure occurred in those laminate in which in-plane failure was observed to occur in the base flat laminates and out-of-plane failure occurred in the $[+15/+15_D/-15/-15_D/0/0_D]_S$ laminate where out-of-plane (delamination) failure was observed to occur in the base laminate: $[\pm 15/0]_S$.

The one exception noted is the $[\pm 45/0/(\pm 45/0)_D]_S$ laminate which failed with considerable delamination as the sublaminate consisting of the inner six dropped plies would normally delaminate away from the rest of the

undropped sections and then in-plane fracture would occur. The basic flat laminates, $[\pm 45/0]_{2S}$ and $[\pm 45/0]_{S}$, both failed in an in-plane mode. A possible cause of this difference in failure modes is that this laminate is laid up with all of the plies dropped off consecutively as a single sublaminate for a total of six consecutive ply dropoffs. It appears that dropping these plies off all at once rather than spreading them throughout the laminate is more delamination critical. It is important to note that the failure stress of the $[\pm 45/0/(\pm 45/0)_{D}]_{S}$ laminate was only about 8% lower than that of the flat laminate modeling the dropped section. Thus, there is essentially no strength reduction when considering normal data scatter. So, although delamination does appear at these ply dropoffs, it did not appear to alter the final fracture stress.

SUMMARY

The tests conducted indicate that the presence of ply dropoffs has little effect on the tensile global stress-strain or fracture behavior of graphite/epoxy laminates when compared to the base laminate behavior of the "undropped" and "dropped" sections of the laminate configuration. Only in the case where several plies were dropped off consecutively was the failure mode affected in that delamination occurred where it normally would not in flat laminates. However, even in this case the ultimate load-carrying capability was insignificantly affected.

It would appear from this study that any adverse affect of a ply dropoff in tension can be mitigated by carefully constructing the ply dropoffs to avoid consecutive abrupt terminations. This does not, however, indicate that the structural affect of ply dropoffs, such as in the compressive response, can be mitigated in the same manner. Designers should thus distribute the termination of several plies through the thickness of the laminate rather than dropping these off at one location. The fact that the termination of several plies at one location did induce delamination indicates that the specifics of the dropoff geometry and the manufacturing procedure can be key to damage development and should be carefully studied in terms of damage progression under cyclic load and in terms of contribution to overall instability and final failure under compressive loads.

ACKNOWLEDGEMENTS

This work was sponsored by the Air Force Office of Scientific Research under Grant Number AFOSR-85-0206.

REFERENCES

1. Grimes, G.C., and Dusablon, E.G., "Study of Compressive Properties of Graphite/Epoxy Composites with Discontinuities", Composite Materials: Testing and Design, ASTM STP 787, American Society for Testing and Materials, 1982, pp. 513-538.

2. Grimes, G.C., Adams, D.F., and Dusablon, E.G., "The Effects of Discontinuities on Compression Fatigue Properties of Advanced Composites", Northrop Technical Report NOR-80-158, Northrop Corporation, Hawthorne, CA, October, 1980.

3. Adams, D.F., Ramkumar, R.L., and Walrath, D.E., "Analysis of Porous Laminates in the Presence of Ply Drop-offs and Fastener Holes", Northrop Technical Report NOR 84-113, Northrop Corporation, Hawthorne, CA, May, 1984.

4. Wu, C.M.L., and Webber, J.P.H., "Analysis of Tapered (in Steps) Laminated Plates Under Uniform Inplane Load", Composite Structures, Vol. 5, 1986, pp. 87-100.

5. Kemp, B.L., and Johnson, E.R., "Response and Failure Analysis of a Graphite-Epoxy Laminate Containing Terminating Internal Plies", AIAA Paper 85-0608, 1985.

6. DiNardo, M.T., and Lagace, P.A., "Buckling and Postbuckling of Laminated Composite Plates with Ply Dropoffs", Proceedings of the AIAA/ASME/ASCE/AHS 28th Structures, Structural Dynamics and Materials Conference, Monterey, CA, April, 1987.

7. Curry, J.M., Johnson, E.R., and Starnes, J.H., Jr., "Effect of Dropped Plies on the Strength of Graphite-Epoxy Laminates", Proceedings of the AIAA/ASME/ASCE/AHS 28th Structures, Structural Dynamics and Materials Conference, Monterey, CA, April, 1987.

8. Lagace, P.A., Brewer, J.C., and Kassapoglou, C., "The Effect of Thickness on Interlaminar Stresses and Delamination", Journal of Composites Technology & Research, Fall, 1987, pp. 81-87.

9. Cannon, R.K., "The Effects of Ply Dropoffs on the Tensile Behavior of Graphite/Epoxy Laminates", TELAC Report 87-12, Massachusetts Institute of Technology, Cambridge, MA, May, 1987.